JAERI-M
90-236

EVALUATION REPORT ON SCTF CORE-II TEST S2-08
(EFFECT OF CORE INLET SUBCOOLING ON THERMAL-HYDRAULIC BEHAVIOR INCLUDING TWO-DIMENSIONAL BEHAVIOR IN PRESSURE VESSEL DURING REFLOOD IN PWR-LOCA)

January 1991

Akira OHNUKI, Takamichi IWAMURA, Yutaka ABE
Hiromichi ADACHI* and Yoshio MURAO

日本原子力研究所
Japan Atomic Energy Research Institute

JAERI-Mレポートは，日本原子力研究所が不定期に公刊している研究報告書です。
入手の問合わせは，日本原子力研究所技術情報部情報資料課（〒319-11茨城県那珂郡東海村）あて，お申しこしください。なお，このほかに財団法人原子力弘済会資料センター（〒319-11 茨城県那珂郡東海村日本原子力研究所内）で複写による実費頒布をおこなっております。

JAERI-M reports are issued irregularly.
Inquiries about availability of the reports should be addressed to Information Division Department of Technical Information, Japan Atomic Energy Research Institute, Tokai-mura, Naka-gun, Ibaraki-ken 319-11, Japan.

編集兼発行　日本原子力研究所
印　　刷　いばらき印刷㈱

Evaluation Report on SCTF Core-II Test S2-08 (Effect of Core Inlet Subcooling on Thermal-Hydraulic Behavior Including Two-Dimensional Behavior in Pressure Vessel During Reflood in PWR-LOCA)

Akira OHNUKI, Takamichi IWAMURA, Yutaka ABE
Hiromichi ADACHI* and Yoshio MURAO

Department of Reactor Engineering
Tokai Research Establishment
Japan Atomic Energy Research Institute
Tokai-mura, Naka-gun, Ibaraki-ken

(Received December 19, 1990)

During reflood in a PWR-LOCA, the degree of subcooling at core inlet of ECC water injected into cold legs is affected by the degree of condensation of steam in cold legs, the degree of heat release from downcomer wall and the temperature difference of remaining water in the lower plenum. The different degree of the subcooling might affect the thermal-hydraulic behaviors including two-dimensional behaviors in pressure vessel in terms of the different height of boiling initiation point.

The present report investigates the effects of the difference of the core inlet subcooling on the thermal-hydraulic behaviors including two-dimensional behaviors in the pressure vessel in the Slab Core Test Facility (SCTF) Core-II tests under gravity feed mode. The following test results are examined: Tests S2-02 (Reference test) and Test S2-08 (High subcooling test). The degree of the difference of the subcooling between the two tests was about 20 to 35 K in the LPCI period.

The following conclusions were obtained from this study:

(1) Higher the subcooling gave larger amount of water accumulation in the core and gave better core cooling. These tendencies were also

---

* Yamagata University

recognized in comparisons under the same distance from the quench front. Since the same tendencies can be predicted in the analyses with REFLA code because of the lower steam generation rate below quench front in the high subcooling test, the differences in the tests are supposed to be caused by the same reason.

(2) Higher the subcooling gave larger amount of water accumulation in upper plenum. The carry-over liquid mass into hot leg became smaller in the later period in the higher subcooling test. These differences for carry-over and de-entrainment characteristics can be explained by the differences of quench velocity and of steam mass flow rate generated in the core.

(3) No significant influence of the different degree of the subcooling was observed on the two-dimensional thermal-hydraulic behaviors in the pressure vessel. Namely, radial differences of sectional void fraction, heat transfer coefficient and the pressure among bundles at the same elevation were almost the same amount for the two tests. Radial differences of liquid levels in the upper plenum was also almost the same amount for the two tests.

Keywords: Reactor Safety, PWR-LOCA, Two-Phase Flow, Reflood, SCTF, Subcooling, Two-Dimensional Thermal-Hydraulics, Heat Transfer, Quench, Void Fraction

JAERI－M　90－236

SCTF第2次炉心試験S 2 － 08評価報告書
（圧力容器内における二次元挙動を含むPWR再冠水時熱水力学的挙動に対する炉心入口サブクール度の効果）

日本原子力研究所東海研究所原子炉工学部
大貫　晃・岩村　公道・阿部　豊
安達　公道*・村尾　良夫

（1990年12月19日受理）

PWR－LOCA時再冠水過程では，コールドレグに注入されたECC水の炉心入口でのサブクール度はコールドレグでの凝縮の程度，ダウンカク壁からの入熱の程度及び下部プレナム残存水の水温の違いにより変化する。サブクール度の違いにより炉心内での沸騰開始点の高さが変わり，圧力容器内における二次元挙動を含む熱水力学的挙動に影響を及ぼすことが考えられる。

本報告書では，SCTF第2次炉心重力冠水試験での圧力容器内における二次元挙動を含む熱水力学的挙動に対する炉心入口サブクール度の違いの効果を調べる。試験S 2 － 02（基準試験）及びS 2 － 08（高サブクール度試験）の結果を検討する。両試験でのサブクール度の違いはLPCI期において20から35K程度であった。

本研究から以下の結論が得られた。

(1) サブクール度が高いほど炉心内の蓄水量は多く炉心冷却は促進された。これらの傾向は同一のクエンチフロントからの距離で比較しても見られた。REFLAコードによる解析を行い，サブクール度が高い場合クエンチフロントより下で生成される蒸気流量が低くなり，試験と同様の傾向を予測できることを確認した。このことから，試験においても同様の原因でこれらの違いが生じたものと推定される。

(2) サブクール度が高いほど上部プレナム内の蓄水量は多くなった。ホットレグへのキャリーオーバ量はサブクール度が高いほど後半少なくなった。キャリーオーバやディエントレイメント特性に対するこれらの違いは，クエンチ速度及び発生蒸気量の違いにより説明できる。

(3) 圧力容器内における二次元熱水力学的挙動に及ぼすサブクール度の違いの効果はほとんどなかった。すなわち，ボイド率や熱伝達率の半径方向の差及び半径方向の差圧はサブクール度の違いによらずほぼ同程度であった。上部プレナム内の半径方向の液位分布に対してもサブクール度の違いの効果はほとんどなかった。

東海研究所：〒319－11　茨城県那珂郡東海村白方字白根 2 － 4
*　山形大学

Contents

1. Introduction 1
2. Facility and Test Description 3
2.1 Test Facility 3
2.2 Test Conditions and Procedure 3
3. Results and Discussion 5
3.1 Measured Boundary Conditions 5
3.2 Hydraulic Behavior in Pressure Vessel except Core 5
3.3 One-Dimensional Thermal-Hydraulic Behavior in Core 7
3.4 Two-Dimensional Thermal-Hydraulic Behavior in Core 9
4. Conclusion 12
Acknowledgment 13
References 13
Appendix Selected Data of Test S2-08 63

目　　次

1. 序　論 1
2. 試　験 3
2.1 試験装置 3
2.2 試験条件及び試験手順 3
3. 試験結果及び検討 5
3.1 測定された境界条件 5
3.2 炉心を除く圧力容器内水力学的挙動 5
3.3 炉心内１次元熱水力学的挙動 7
3.4 炉心内２次元熱水力学的挙動 9
4. 結　論 12
謝　辞 13
参考文献 13
付　録　試験Ｓ２－０８のデータ抄 63

1. Introduction

The test program of Slab Core Test Facility (SCTF) is a part of the large scale reflood test program in which the test program of Cylindrical Core Test Facility (CCTF) is also conducted. The principal purposes of both test programs are to clarify thermal-hydraulic behaviors in the primary coolant system of a pressurized water reactor (PWR) during a reflood phase of a large break loss-of-coolant accident (LOCA) and to demonstrate and quantify the safety margin of the emergency core coolant system (ECCS) against the accident. In the CCTF test program, major objective is to study system behaviors. On the other hand, major objective of the SCTF test is to study two-dimensional thermal-hydraulic behaviors in pressure vessel which has a core of electrically heated rod bundles with a full height, full radial width and single bundle along the azimuthal direction.

Many small scale reflood experiments have been performed in the past.[1] However, the two-dimensional behaviors have not been clarified because the flow area of the core was much smaller than that in an actual reactor. Therefore, effects of various test parameters on the two-dimensional reflooding phenomena have been studied in the SCTF test series[2]-[7] and the core radial power profile was revealed to be a dominant parameter for heat transfer enhancement in higher power bundles[6][7]. And it was reported in reference (7) that a larger cross flow between rod bundles was induced under steeper radial power profile. So the cross flow between bundles is important to investigate the heat transfer enhancement in the higher power bundles.

During the reflood in PWR-LOCA, the degree of subcooling at core inlet of ECC water injected into cold legs is affected by the degree of condensation of steam flowing through cold legs, the degree of heat release from downcomer wall and the difference of temperature of remaining water in lower plenum. The different degree of subcooling might affect the two-dimensional thermal-hydraulic behavior in the core due to the cross flow in terms of the different height of boiling initiation point.

Iwamura, et al. studied the effect of the subcooling on reflooding phenomena using the SCTF Core-I tests under forced feed mode[4] and however the two-dimensional thermal behaviors were not fully investigated especially on the heat transfer enhancement. And it is not clear whether the results can apply to the condition under gravity feed mode realized in an actual

reactor or not.

In the present report, the effects of the subcooling on the thermal-hydraulic behaviors including two-dimensional behaviors in the pressure vessel are investigated using the SCTF Core-II tests under gravity feed mode and the effects on the heat transfer enhancement in the core are clarified experimentally.

Tests investigated in this report are Tests S2-02 (Reference test) and S2-08 (High subcooling test). The selected data obtained in Test S2-08 are presented in Appendix.

2. Facility and Test Description

2.1 Test Facility

The SCTF was designed to properly simulate the two-dimensional thermal-hydraulic behaviors in pressure vessel during refill-reflood phase. The pressure vessel is slab geometry as shown in Fig. 2.1.1. Full scale radial and axial section of a reference PWR is provided using a simulated core with single bundle depth. The reference reactor is the Trojan reactor in the United States which is a four loop 3300MWt PWR. The simulated core consists of 8 bundles arranged in a row. On the other hand, simplified primary coolant loops are provided. Bird's-eye view of the pressure vessel and the coolant loop is shown in Fig. 2.1.2. The scaling of flow area and fluid volume of each component is in accordance with the core flow area scaling. The principal dimensions of the facility is shown in Table 2.1.1, and the comparison of dimensions between the SCTF and the referred PWR is shown in Table 2.1.2 and in Fig. 2.1.3.

Each bundle has 234 electrically heated rods and 22 non-heated rods. The arrangement of rod bundles is shown in Fig. 2.1.4. The dimensions of the heater rods are based on a 15×15 type fuel bundle and the heated length and the outer diameter of each heater rod are 3.66m and 10.7mm, respectively. The dimension, configuration and axial power distribution of each heater rod are shown in Fig. 2.1.5. The axial peaking factor is 1.4. The heater rods and non-heated rods are fixed at the top of the core allowing the rods to move downward when the thermal expansion occurs. For better simulation for flow resistance in the lower plenum the simulated rods do not penetrate through the bottom plate of the lower plenum.

The design of upper plenum internals is based on that of the new Westinghouse 17×17 array fuel assemblies. The internals consist of control rod guide tubes, support columns, orifice plates and open holes as shown in Fig. 2.1.6. The radius of each component is scaled down by factor 8/15 from that of an actual reactor.

More detailed information on the SCTF is available in reference (8).

2.2 Test Conditions and Procedure

Two gravity feed tests, Tests S2-02 and S2-08, were selected in this report to meet the objective in Introduction. In Test S2-02, ECC water was

injected into the lower plenum during accumulator (Acc) injection period and into the intact cold leg during low pressure coolant injection (LPCI) period. Therefore, ECC water temperature during LPCI period is expected to be heated up due to condensation of steam flowing through the intact cold leg in this test. On the other hand, ECC water was injected only into the lower plenum during whole transients in Test S2-08. By this method, the degree of core inlet subcooling was kept higher in Test S2-08 than that in Test S2-02. The other test conditions were almost the same between these two tests. Therefore, Test S2-02 is called as Reference test and Test S2-08 is called as High subcooling test in this report. Major specified test conditions are summarized in Table 2.2.1.

The test procedure for these two tests is as follows: After setting the initial conditions (pressure and saturation condition, etc.), core heating was initiated. When four thermocouple signals at the surface of cladding exceeded 1053K, the Acc injection into the lower plenum was initiated. The initial water level in the lower plenum was about 0.16m and about 0.2m below the bottom of heated part for Tests S2-02 and S2-08, respectively. The maximum cladding temperature at the reflood initiation was intended to be about 1072K for both tests. After keeping the core power constant for 40s from the injection start, the core power decay simulation was started from the value at 40s after shutdown of an actual reactor. The decay curve was based on the "1.02×(ANS standard + actinides)".

As described above, there are some differences except for the subcooling between the two tests such as the injection location and the initial water level in lower plenum. However, we consider that the effect of the core inlet subcooling can be investigated from the comparisons between the results of the two tests because the boundary conditions at core inlet except for the subcooling are almost the same between the two tests as discussed in the next chapter.

3. Results and Discussion

3.1 Measured Boundary Conditions

Figures 3.1.1 and 3.1.2 show the comparison of ECC mass flow rate and ECC water temperature measured at each injection port. In these figures, L.P. means the port at lower plenum and I.C.L means the port at intact cold leg. ECC mass flow rate and switching time from Acc injection to LPCI are almost the same for these two tests. ECC water temperature in the high subcooling test is lower than that in the reference test during whole transients.

Figure 3.1.3 shows the comparison of pressure at containment tank-Ⅱ. Pressure overshoot is recognized in the period between reflood initiation time and about 150s for both tests. In the other period, the pressure is kept at the set pressure 0.15 MPa. No significant difference is observed on the pressure between the two tests.

Figure 3.1.4 shows the comparison of heating power supplied to each bundle. Initial set value and the shape of transient for each bundle are almost the same between the two tests. As shown in this figure, the power is the highest in bundles 3 and 4 and the lowest in bundles 7 and 8 during whole transients.

Chronology of major events is summarized in Table 3.1.1

3.2 Hydraulic Behavior in Pressure Vessel except Core

In this section, mass flow rate and fluid subcooling at the core inlet and carry-over characteristics from the core to the upper plenum and from the upper plenum to steam/water separator are presented and discussed.

Figures 3.2.1(1), 3.2.1(2) and 3.2.2 show the comparison of core inlet mass flow rate and integrated mass into the core. These values were obtained by mass balance in the SCTF system. Basic equation for the mass balance is as follows:

Mass flow rate at the core inlet =

ECC mass flow rate + Condensation mass flow rate in the intact cold leg - Bypass mass flow rate from downcomer to containment tank-I - Accumulated mass flow rate in the downcomer, in the lower plenum and in the core baffle region.

Flooding velocity shown in Fig. 3.2.1(2) was calculated based on the core

flow area of 0.35m^2 shown in Table 2.1.1. Since this flow area is the maximum area as described in Table 2.1.1, effective flooding velocity might be higher than the value shown in Fig. 3.2.1(2). It is found from these figures that the difference of the mass flow rate is negligible small between the tests irrespective of the existence of the condensation in intact cold leg in the reference test during the LPCI period.

In order to make clear the effect of the condensation for the mass balance, the liquid level in the downcomer is compared in Fig. 3.2.3 and the integrated mass of the condensation in intact cold leg and of the bypass from the downcomer to the containment tank-I are compared in Fig.3.2.4. No significant difference is observed on the liquid level in the downcomer between the two tests. In the high subcooling test, condensation and bypass mass flow rates are almost zero value except for the initial period because of the lack of injection of ECC water into the intact cold leg. On the other hand, the condensation and the bypass are occurred continuously in the reference test and the amount of the bypass mass flow rate is almost the same as that of the condensation as shown in Fig. 3.2.4. Therefore, no increase of mass flow rate into the lower plenum due to the condensation is reasonable in the reference test because the same amount of the bypass mass flow rate is occurred from the downcomer to the containment tank-I.

Figures 3.2.5 and 3.2.6 show the comparison of core inlet fluid temperature and core inlet subcooling between the two tests. The temperature is lower and the subcooling is higher in the high subcooling test. The difference of the subcooling is about 20 to 35K in the LPCI period.

Figures 3.2.7 and 3.2.8 show the comparison of pressure at several locations in the pressure vessel. The pressures in the high subcooling test are slightly higher until about 200s and lower after that time. These differences were considered to be caused by the difference of steam mass flow rate generated in the core shown in Fig. 3.2.9. The steam mass flow rate was obtained by the measurement of venturies at loop. The tendency of difference of the steam mass flow rate is correspond to that recognized in the pressure transient.

Figures 3.2.10(1) through 3.2.10(4) show the comparison of liquid level in the upper plenum above each bundle. The accumulated mass in the upper plenum is getting larger in the high subcooling test. Radial difference of the liquid level (Liquid level above bundle 8 - liquid level above bundle 1) is also larger in the high subcooling test as shown in Fig. 3.2.11.

The amount of carry-over from the core is reported to be the function of the core inlet mass flow rate, the distance from the quench front to the core exit and the steam mass flow rate generated in the core.[9] Figures 3.2.12 through 3.2.14 show the comparison using the same distance from the quench front. The accumulated mass in upper plenum and the radial difference of liquid level are almost the same between the two tests in these comparisons except for the upper plenum mass in the region of the distance from quench front less than about 0.5m. Based on the results in Ref.(9), the remaining difference on the upper plenum mass was supposed to be caused by the difference of steam mass flow rate shown in Fig. 3.2.14.

Figures 3.2.15 through 3.2.18 show the comparison of carry-over liquid mass into the hot leg and into the steam/water separator. Those two values can be recognized to be the same in the region of the distance from the quench front more than about 1.5m and however become smaller in the high subcooling test in the region less than about 1.5m. This difference was considered to be caused by the smaller steam mass flow rate in the high subcooling test in that region shown in Fig. 3.2.14. The results in Figs. 3.2.12, 3.2.14, 3.2.16 and 3.2.18 indicate that the decrease of steam mass flow rate decreases the carry-over liquid mass into the hot leg and increases the de-entrained mass in the upper plenum.

3.3 One-Dimensional Thermal-Hydraulic Behavior in Core

In this section, one-dimensional water accumulation and heat transfer behaviors in the core are presented and discussed by examining the comparison plots in bundle 4 (Highest power bundle).

Figures 3.3.1 through 3.3.2(2) show the comparison of vertical differential pressures in bundle 4. The differential pressure for core full height is larger in the high subcooling test than that in the reference test during almost whole transients. This difference is mainly occurred in the lower half of the core as shown in Figs. 3.3.2(1) and (2). In the upper half of the core, no significant difference is observed until about 300s.

Figures 3.3.3(1) through 3.3.3(3) show the comparison of sectional void fractions in bundle 4 . These void fractions were calculated from sectional differential pressures by neglecting the effects of frictional and accelerational pressure drops. These comparisons indicate that the decreasing rate of void fraction is higher in the high subcooling test especially in the

lower half of the core. In the upper part of the core shown in Fig. 3.3.3(3), the difference of the void fraction is small until about 300s. These characteristics on the core water accumulation are correspond to the previous study in Ref. (4).

Figures 3.3.4(1) through 3.3.4(3) show the comparison of clad surface temperatures along center rod in bundle 4. The degree of heat transfer is higher in the high subcooling test. Turnaround temperature and quench time are lower and shorter in the high subcooling test, respectively. Quench envelope in bundle 4 is compared in Fig. 3.3.5. The difference on the quench time is larger in the upper part of the core than that in the lower part of the core. These characteristics of better core cooling in the high subcooling test are also recognized in the comparisons of heat transfer coefficients shown in Figs. 3.3.6(1) through 3.3.6(3).

Figures 3.3.7(1) through 3.3.7(4) show the comparison of the heat transfer coefficient using the same distance from quench front. The heat transfer coefficient is higher in the high subcooling test even in these plots although the difference is smaller than that in Figs. 3.3.6(1) through 3.3.6(3). The higher heat transfer at the same distance from the quench front was considered to be caused by the higher liquid fraction (1 - sectional void fraction) at the same distance from the quench front shown in Figs. 3.3.8(1) through 3.3.8(3) based on the heat transfer correlation for saturated film boiling developed by Murao[10]. The heat transfer correlation includes the term of liquid fraction and the correlation indicates that the higher liquid fraction gives the higher heat transfer coefficient due to thinner vapor film thickness.

In order to make clear the physical reason for establishing the higher liquid fraction in the higher subcooling test even at the same distance from quench front, the analyses were performed using REFLA-1D code[11][12] with the modification for effect of liquid flow rate on film boiling heat transfer by Ohnuki, et al.[13]. The accuracy of correlations in the code and of the code prediction has been verified with several small scale test data and also with the CCTF and the SCTF test data[13]-[15].

Figure 3.3.9 shows the comparison of the clad surface temperature between the data and the predictions with the REFLA code. The measured temperature was obtained by averaging the data of several thermocouples at 1.905m elevation in bundle 4. The REFLA code predicts the tendency of higher heat transfer in the high subcooling test although the difference be-

tween the two tests is underestimated.

Figure 3.3.10 shows the comparison of the following values predicted with the REFLA code using the same distance from quench front: heat transfer coefficient, liquid fraction and steam velocity. The REFLA code predicts the same tendency as in the data in the region of distance from quench front less than about 1.1m, the tendency that the heat transfer coefficient and the liquid fraction are higher in the high subcooling test even at the same distance from quench front. The tendency was caused by the lower steam velocity in the high subcooling test in the code shown in Fig. 3.3.10(c) because the void fraction correlation in the code depends on the steam velocity. This result is supposed to indicate that the higher liquid fraction in the high subcooling test is caused by the lower steam generation rate below the quench front due to the higher core inlet subcooling.

3.4 Two-Dimensional Thermal-Hydraulic Behavior in Core

In this section, two-dimensional thermal-hydraulic behaviors in the core are presented and discussed by comparing radial differences of the sectional void fraction, horizontal differential pressure and the radial difference of heat transfer coefficient.

Figure 3.4.1 shows the comparison of the radial difference of sectional void fraction in the core. In the lower half of the core, no significant difference is observed on the radial difference between the two tests and almost flat distribution is recognized even though the void fraction in bundle 8 at 1.365-1.905m section in the high subcooling test is higher after the quench of this section. In the upper half of the core, almost the flat distribution is also recognized for the two tests except in the period observed a higher void fraction in bundle 8. The degree of difference of void fraction between in bundles 2 and 4 and in bundle 8 is almost the same between the two tests although the time observed the difference is faster in the high subcooling test.

Figure 3.4.2 shows the comparison of horizontal differential pressure at 1.905m (almost middle elevation of the core) and 3.235m (upper part of the core) elevations. Plus sign of these differential pressures indicates that the pressure in bundle 1 or bundle 4 is higher than that in bundle 4 or bundle 8, respectively. And the direction of cross flow is supposed to be correspond to the sign. In the middle region of the core, the pressure is

higher in bundle 4 than that in bundle 8 until about the quench time of this region for the two tests and maximum plus value is almost the same between the two tests. The different changing time from plus to minus values between the two tests was considered to be caused by the different quench velocity because the horizontal differential pressure is almost the same at the same distance from the quench front as shown in Fig. 3.4.3(2). In the upper part of the core, the pressure in bundle 8 is getting higher with time and the initiation time of the higher pressure in bundle 8 is faster in the high subcooling test. The horizontal differential pressures in this region are affected by non-uniformity of liquid levels in the upper plenum as discussed in reference (7). The comparison is shown in Fig. 3.4.3(3). The time observed the higher pressure in bundle 8 in each test is well correspond to that initiated the non-uniform distribution of liquid levels in the upper plenum. Since this radial distribution of liquid levels is almost correlated by the same distance from the quench front as shown in Fig. 3.2.13, the difference of the horizontal differential pressure is smaller in the comparison of Fig. 3.4.3(1) using the same distance from the quench front.

Figures 3.4.4 (1) through 3.4.4(6) show the radial comparison of heat transfer coefficients at 1.38m, 1.905m and 2.33m elevations in each test. Although no significant difference is observed on the radial difference at 1.38m elevation and between bundles 2 and 4 at all elevations, the heat transfer coefficient in bundle 8 is slightly lower in a time period at 1.905m and 2.33m elevations for the two tests. The difference of heat transfer coefficients between the different power bundles are reported to become larger with increasing the radial power ratio.[6][7] This higher heat transfer in higher power bundle has a role to decrease the difference of quench velocity among different power bundles as shown in Fig. 3.4.5. The difference of quench time in each bundle is getting smaller along the axial direction.

In order to make clear the degree of the radial difference of heat transfer coefficients, the heat transfer coefficient is compared at the same distance from the quench front of each bundle in Figs. 3.4.6(1) through 3.4.6(6). And the amount of the radial difference between the maximum and the minimum heat transfer coefficients in each test is compared in Fig. 3.4.7. It is found from these figures that no significant differences are observed on the degree of the radial difference of heat transfer coeffi-

cients at the same distance from quench front. This result indicate that the two-dimensional heat transfer behavior such as heat transfer enhancement in higher power bundles is not affected by the different degree of the core inlet fluid subcooling within the test condition investigated in this study.

4. Conclusion

The present evaluation study on the SCTF tests revealed the following conclusions concerning the effects of the difference of the core inlet fluid subcooling on the thermal-hydraulic behaviors including two-dimensional behaviors in the pressure vessel during reflood under gravity feed mode. The degree of the difference of the core inlet subcooling between the two tests investigated in this report was about 20 to 35K in the LPCI period.

(1) Higher the subcooling gave larger amount of water accumulation in the core and gave better core cooling. These tendencies were also recognized in comparisons under the same distance from the quench front. Since the same tendencies can be predicted in the analyses with REFLA code because of the lower steam generation rate below quench front in the high subcooling test, the differences in the tests are supposed to be caused by the same reason.

(2) Higher the subcooling gave larger amount of water accumulation in the upper plenum. The carry-over liquid mass into the hot leg and into the steam/water separator became smaller in the later period in the higher subcooling test. These differences for carry-over and de-entrainment characteristics can be explained by the differences of quench velocity and of steam mass flow rate generated in the core.

(3) No significant influence of the different degree of the subcooling was observed on the two-dimensional thermal-hydraulic behaviors in the pressure vessel. Namely, radial differences of sectional void fraction, heat transfer coefficient and the pressure among bundles at the same elevation were almost the same amount for the two tests. Radial differences of liquid levels in the upper plenum was also almost the same amount for the two tests.

Acknowledgment

They would like to express their appreciation to Dr.M.Sobajima and to Messrs. T.Iguchi, T.Okubo, Drs. J.Sugimoto and H.Akimoto of CCTF analysis group for their useful discussions.

References

(1) For instance, L.E. Hochreiter, FLECHT SEASET Program Final Report, NUREG/CR-4167, (1985).

(2) H. Adachi, et al., System Pressure Effects on Reflooding Phenomena observed in the SCTF Core-I Forced Flooding Tests, JAERI-M 83-079, (1982).

(3) Y. Sudo, et al., Effect of Upper Plenum Water Accumulation on Reflooding Phenomena under Forced Flooding in SCTF Core-I Test, JAERI-M 83-114, (1983).

(4) T. Iwamura, et al., Effects of Core Inlet Water Subcooling on Reflooding Phenomena - SCTF Core-I Forced Feed Flooding Test -, JAERI-M 83-122, (1983).

(5) M. Sobajima, et al., Examination of Repeatability in Reflood Phenomena under Forced Flooding in SCTF Core-I Tests, JAERI-M 83-237, (1984).

(6) T. Iwamura, et al., Effects of Radial Core Power Profile on Core Thermo-Hydraulic Behavior during Reflood Phase in PWR-LOCA, J. Nucl. Sci. Tech., 20[9], 743-751, (1983).

(7) T. Iwamura, et al., Two-Dimensional Thermal-Hydraulic Behavior In Core In SCTF Core-II Cold Leg Injection Tests (Radial Power Profile Test Results), JAERI-M 85-106, (1985).

(8) H. Adachi, et al., Design of Slab Core Test Facility (SCTF) in Large Scale Reflood Test Program, Part I : Core-I, JAERI-M 83-080, (1983).

(9) A. Ohnuki and M. Sobajima, Mass Effluent Rate out of Core during Reflood, J. Nucl. Sci. Tech., 20[3], 267-269, (1983).

(10) Y. Murao and J. Sugimoto, Correlation of Heat Transfer Coefficient for Saturated Film Boiling during Reflood Phase Prior to Quenching, J. Nucl. Sci. Tech., 18[4], 275-284, (1981).

(11) Y. Murao, et al., REFLA-1D/MODE3 : A Computer Code for Reflood Thermo-Hydrodynamic Analysis during PWR-LOCA -User's Manual-, JAERI-M 84-243, (1985).

(12) T. Hojo, et al., User's Manual of the REFLA-1D/MODE4 Reflood Thermo-

Acknowledgment

They would like to express their appreciation to Dr.M.Sobajima and to Messrs. T.Iguchi, T.Okubo, Drs. J.Sugimoto and H.Akimoto of CCTF analysis group for their useful discussions.

References

(1) For instance, L.E. Hochreiter, FLECHT SEASET Program Final Report, NUREG/CR-4167, (1985).

(2) H. Adachi, et al., System Pressure Effects on Reflooding Phenomena observed in the SCTF Core-I Forced Flooding Tests, JAERI-M 83-079, (1982).

(3) Y. Sudo, et al., Effect of Upper Plenum Water Accumulation on Reflooding Phenomena under Forced Flooding in SCTF Core-I Test, JAERI-M 83-114, (1983).

(4) T. Iwamura, et al., Effects of Core Inlet Water Subcooling on Reflooding Phenomena - SCTF Core-I Forced Feed Flooding Test -, JAERI-M 83-122, (1983).

(5) M. Sobajima, et al., Examination of Repeatability in Reflood Phenomena under Forced Flooding in SCTF Core-I Tests, JAERI-M 83-237, (1984).

(6) T. Iwamura, et al., Effects of Radial Core Power Profile on Core Thermo-Hydraulic Behavior during Reflood Phase in PWR-LOCA, J. Nucl. Sci. Tech., 20[9], 743-751, (1983).

(7) T. Iwamura, et al., Two-Dimensional Thermal-Hydraulic Behavior In Core In SCTF Core-II Cold Leg Injection Tests (Radial Power Profile Test Results), JAERI-M 85-106, (1985).

(8) H. Adachi, et al., Design of Slab Core Test Facility (SCTF) in Large Scale Reflood Test Program, Part I : Core-I, JAERI-M 83-080, (1983).

(9) A. Ohnuki and M. Sobajima, Mass Effluent Rate out of Core during Reflood, J. Nucl. Sci. Tech., 20[3], 267-269, (1983).

(10) Y. Murao and J. Sugimoto, Correlation of Heat Transfer Coefficient for Saturated Film Boiling during Reflood Phase Prior to Quenching, J. Nucl. Sci. Tech., 18[4], 275-284, (1981).

(11) Y. Murao, et al., REFLA-1D/MODE3 : A Computer Code for Reflood Thermo-Hydrodynamic Analysis during PWR-LOCA -User's Manual-, JAERI-M 84-243, (1985).

(12) T. Hojo, et al., User's Manual of the REFLA-1D/MODE4 Reflood Thermo-

Hydrodynamic Analysis Code, JAERI-M 85-210, (1986) in Japanese.

(13) A. Ohnuki, et al., Effect of Liquid Flow Rate on Film Boiling Heat Transfer during Reflood in Rod Bundle, J. Nucl. Sci. Tech., 27[6], 535-546, (1990).

(14) T. Okubo and Y. Murao, Assessment of Core Thermo-Hydrodynamic Models of REFLA-1D with CCTF Data, JAERI-M 83-103, (1983).

(15) T. Iguchi and Y. Murao, Predictability of REFLA Core Model for SCTF Data, JAERI-M 87-163, (1987) in Japanese.

Table 2.1.1 Principal dimensions of SCTF core-II

1.	Core Dimension	
	(1) Quantity of Bundle	8 Bundles
	(2) Bundle Array	1 × 8
	(3) Bundle Pitch	230 mm
	(4) Rod Array in a Bundle	16 × 16
	(5) Rod Pitch in a Bundle	14.3 mm
	(6) Quantity of Heater Rod in a Bundle	234 rods
	(7) Quantity of Non-Heated Rod in a Bundle	22 rods
	(8) Total Quantity of Heater Rods	234×8=1872 rods
	(9) Total Quantity of Non-Heated Rods	22×8=176 rods
	(10) Effective Heated Length of Heater Rod	3660 mm
	(11) Diameter of Heater Rod	10.7 mm
	(12) Diameter of Non-Heated Rod	13.8 mm
2.	Flow Area & Fluid Volume	
	(1) Core Flow Area	0.259 m^2
	(2) Core Fluid Volume	0.92 m^3
	(3) Baffle Region Flow Area	0.10 m^2
	(4) Baffle Region Fluid Volume (nominal)	0.36 m^3
	(5) Effective Core Area Based on the Measured Level-Volume Relationship Including Gap between Core Barrel and Pressure Vessel Wall and Various Penetration Holes	0.35 m^2
	(6) Downcomer Flow Area	0.121 m^2
	(7) Upper Annulus Flow Area	0.158 m^2
	(8) Upper Plenum Horizontal Flow Area	0.525 m^2
	(9) Upper Plenum Fluid Volume	1.16 m^3
	(10) Upper Head Fluid Volume	0.86 m^3
	(11) Lower Plenum Fluid Volume	1.305 m^3
	(12) Steam Generator Inlet Plenum Simulator Flow Area	0.626 m^2
	(13) Steam Generator Inlet Plenum Simulator Fluid Volume	0.931 m^3

Table 2.1.1 (Continued)

(14) Steam Water Separator Fluid Volume	5.3	m^3
(15) Flow Area at the Top Plate of Steam Generator Inlet Plenum Simulator	0.195	m^2
(16) Hot Leg Flow Area	0.0826	m^2
(17) Intact Cold Leg Flow Area (Diameter = 297.9 mm)	0.0697	m^2
(18) Broken Cold Leg Flow Area (Diameter = 151.0 mm)	0.0179	m^2
(19) Containment Tank-I Fluid Volume	30	m^3
(20) Containment Tank-II Fluid Volume	50	m^3
3. Elevation & Height		
(1) Top Surface of Upper Core Support Plate (UCSP)	0	mm
(2) Bottom Surface of UCSP	- 76	mm
(3) Top of the Effective Heated Length of Heated Rod	- 393	mm
(4) Bottom of the Skirt in the Lower Plenum	-5270	mm
(5) Bottom of Intact Cold Leg	+ 724	mm
(6) Bottom of Hot Leg	+1050	mm
(7) Top of Upper Plenum	+2200	mm
(8) Bottom of Steam Generator Inlet Plenum Simulator	+1933	mm
(9) Centerline of Loop Seal Bottom	-2281	mm
(10) Bottom Surface of End Box	-185.1	mm
(11) Top of Upper Annulus of Downcomer	+2234	mm
(12) Height of Steam Generator Inlet Plenum Simulator	1595	mm
(13) Height of Loop Seal	3140	mm
(14) Inner Height of Hot Leg Pipe	737	mm
(15) Bottom of Lower Plenum	-5770	mm
(16) Top of Upper Head	+2887	mm

Table 2.1.2 Comparison of dimensions between SCTF and the reference PWR

Item	SCTF	PWR	Ratio (SCTF/PWR)
Quantity of Bundle	8	193	1/24.1
Number of Heater Rod	1872	39372	1/21.0
Number of Rods	2048	43425	1/21.2
Effective Length of Heater Rod (mm)	3660	3660	1/1
Rod Pitch (mm)	14.30	14.30	1/1
Diameter of Heater Rod (mm)	10.70	10.72	1/1
Diameter of Unheated Rod (mm)	13.80	13.87	1/1
Flow Area between Core Walls (m^2)	0.259	4.76	1/17.7
Effective Core Area Based on the Measured Level-Volume Relationship (m^2)	0.35	4.76	1/13.6
Fluid Volume of Core Enveloped by Honeycomb Insulators*	0.92	17.95	1/19.5
Fluid Volume of Lower Plenum (m^3)	1.305	29.62	1/22.7
Fluid Volume of Upper Head (m^3)	0.86	19.8	1/23.0
Baffle Region Flow Area (m^2)	0.10	1.76	1/17.6
Upper Plenum Fluid Volume (m^3)	1.16	23.8	1/20.5
Downcomer Flow Area (m^2)	0.121	2.47	1/20.4
UCSP Thickness (m)	76	76	1/1
Steam Generator Inlet Plenum Simulator Volume	0.931	4.25×4	1/18.3
Height of Steam Generator Inlet Plenum Simulator (m)	1.595	1.595	1/1
Flow Area at the Top Plate of Steam Generator Inlet Plenum Simulator (m^2)	0.19	4.0	1/21.2
Major Axis Length of Hot Leg Cross Section (mm)	737	736.6	1/1
Flow Area of Hot Leg (m^2) (4 Loops)	0.0826	1.704	1/20.6
Flow Area of Intact Loop (m^2) (3 Loops)	0.0696	1.149	1/16.5
Flow Area of Broken Cold Leg (m^2)	0.0179	0.383	1/21.4
* Fluid Volume of Core Including Gaps between Core Barrel and Pressure Vessel Wall (m^3)	1.74		

Table 2.2.1 Major specified test conditions

	High Subcooling Test (S2-08)	Reference Test (S2-02)
Initial system pressure (MPa)	0.15	0.15
Acc injection mass flow rate (kg/s)	20	19.4
LPCI injection mass flow rate (kg/s)	5.6	5.4
Acc injection port	Lower plenum	Lower plenum
LPCI injection port	Lower plenum	Intact cold leg
Acc water temperature (K)	340	353
LPCI water temperature (K)	340	341
Initial total core power (MW)	7.12	7.12
Power decay curve	(ANS+Actinide)×1.02 from 40s after scram	
Supplied power ratio		
Bundle 1 and 2	1.001	1.001
Bundle 3 and 4	1.065	1.065
Bundle 5 and 6	1.015	1.015
Bundle 7 and 8	0.919	0.919
Maximum core temp. at reflood initiation (K)	1072	1073

Table 3.1.1 Chronology of major events

	High Subcooling Test (S2-08)	Reference Test (S2-02)
	Time after flood(s)	
Core power "ON"	-148.0	-149.5
Acc injection initiation	-3.0	-3.5
Reflood initiation	0	0
Maximum containment tank II pressure	32.0 (0.17MPa)	30.5 (0.17MPa)
Core power decay initiation	37.0	36.5
Switching of ECC from Acc to LPCI	51.0	51.5
Maximum core pressure	52.0 (0.215MPa)	52.5 (0.215MPa)
Maximum core temperature	37.0 (1157K)	125.0 (1205K)
Whole core quenched	479.0	568.0

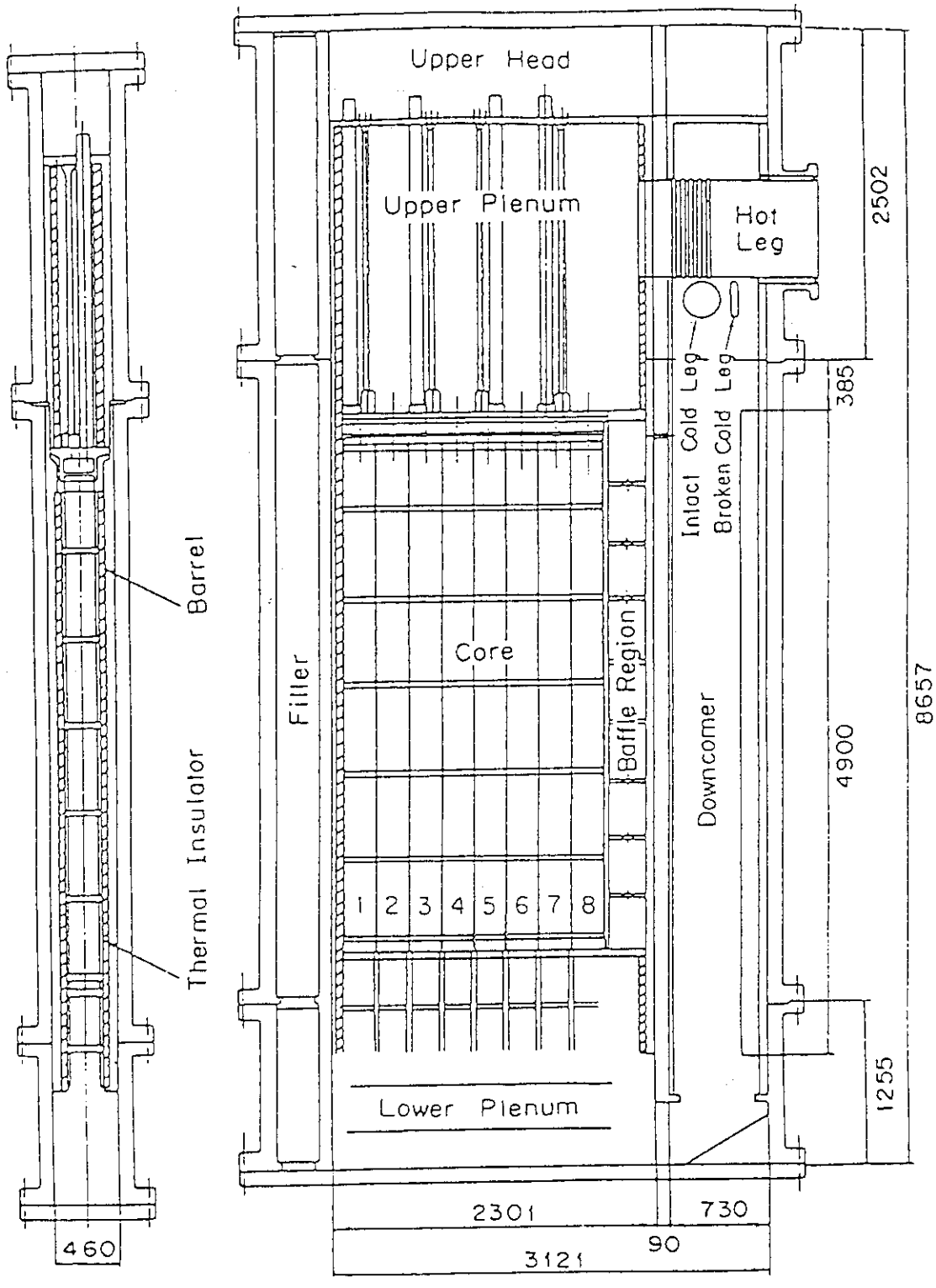

Fig.2.1.1 Vertical cross sections of pressure vessel

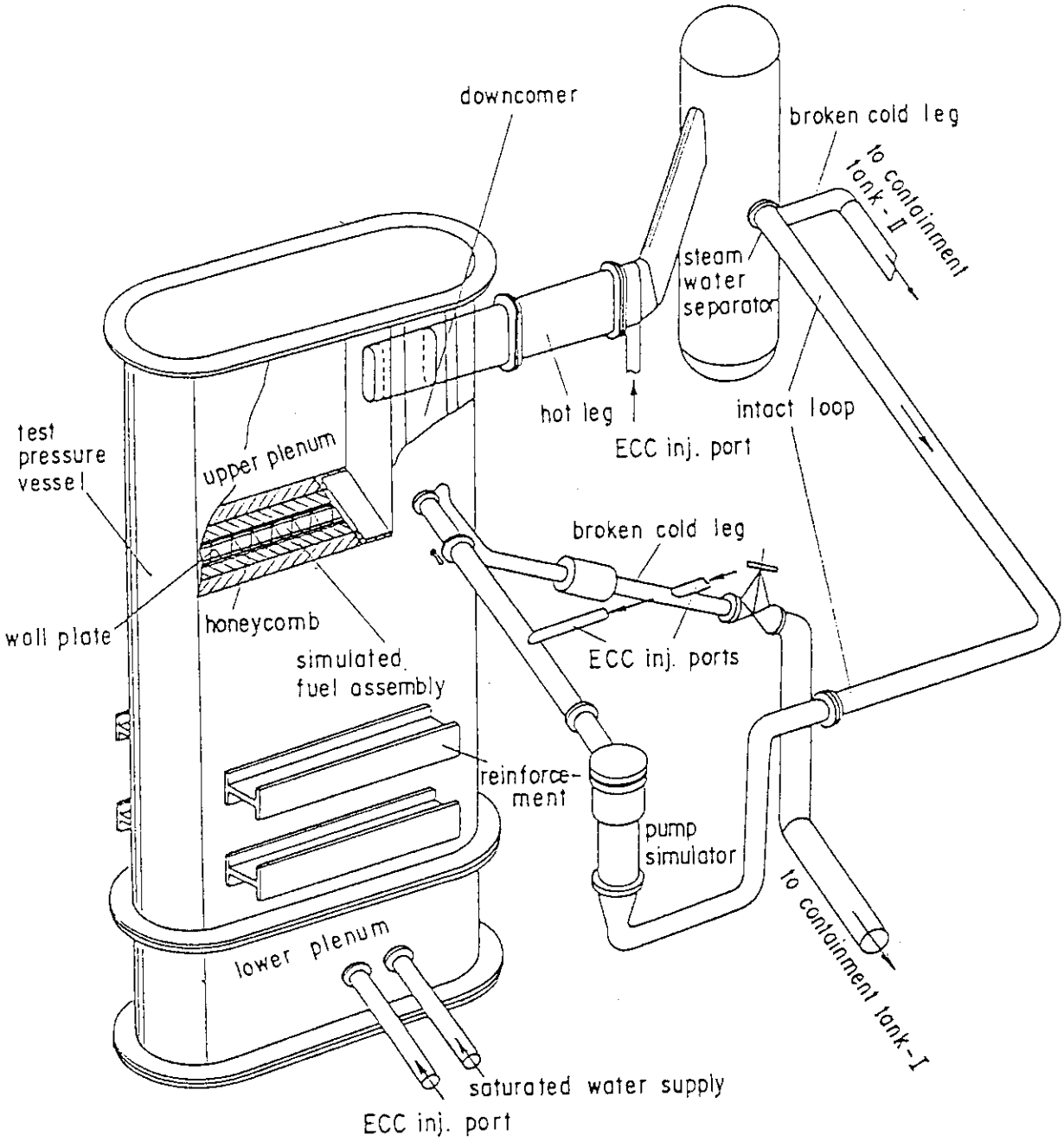

Fig.2.1.2 Bird's-eye view of SCTF

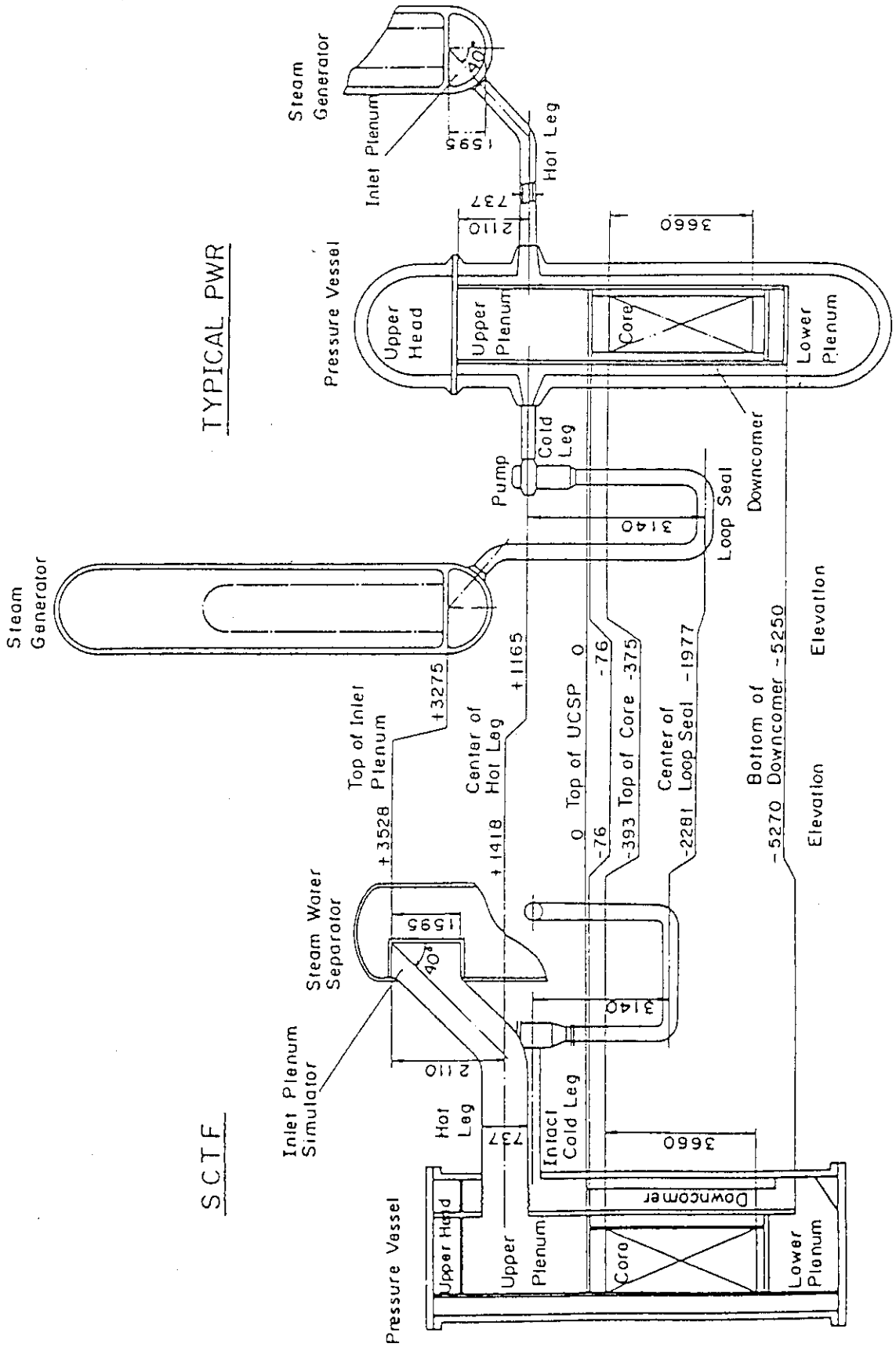

Fig.2.1.3 Comparison of dimensions between SCTF and the reference PWR

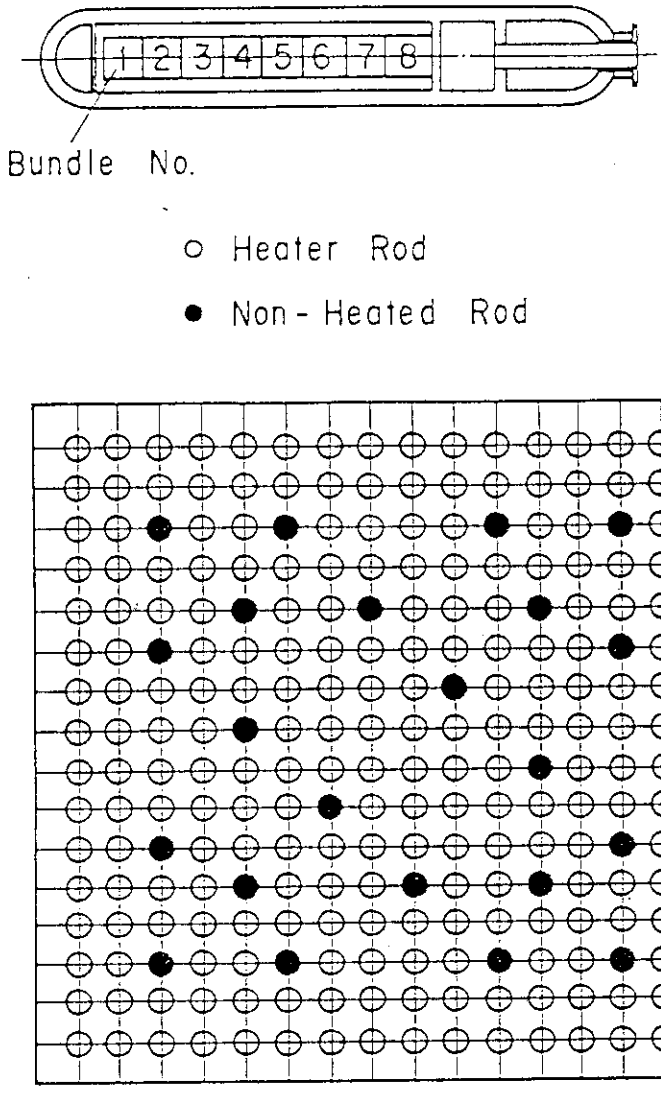

Fig.2.1.4 Arrangement of rod bundles

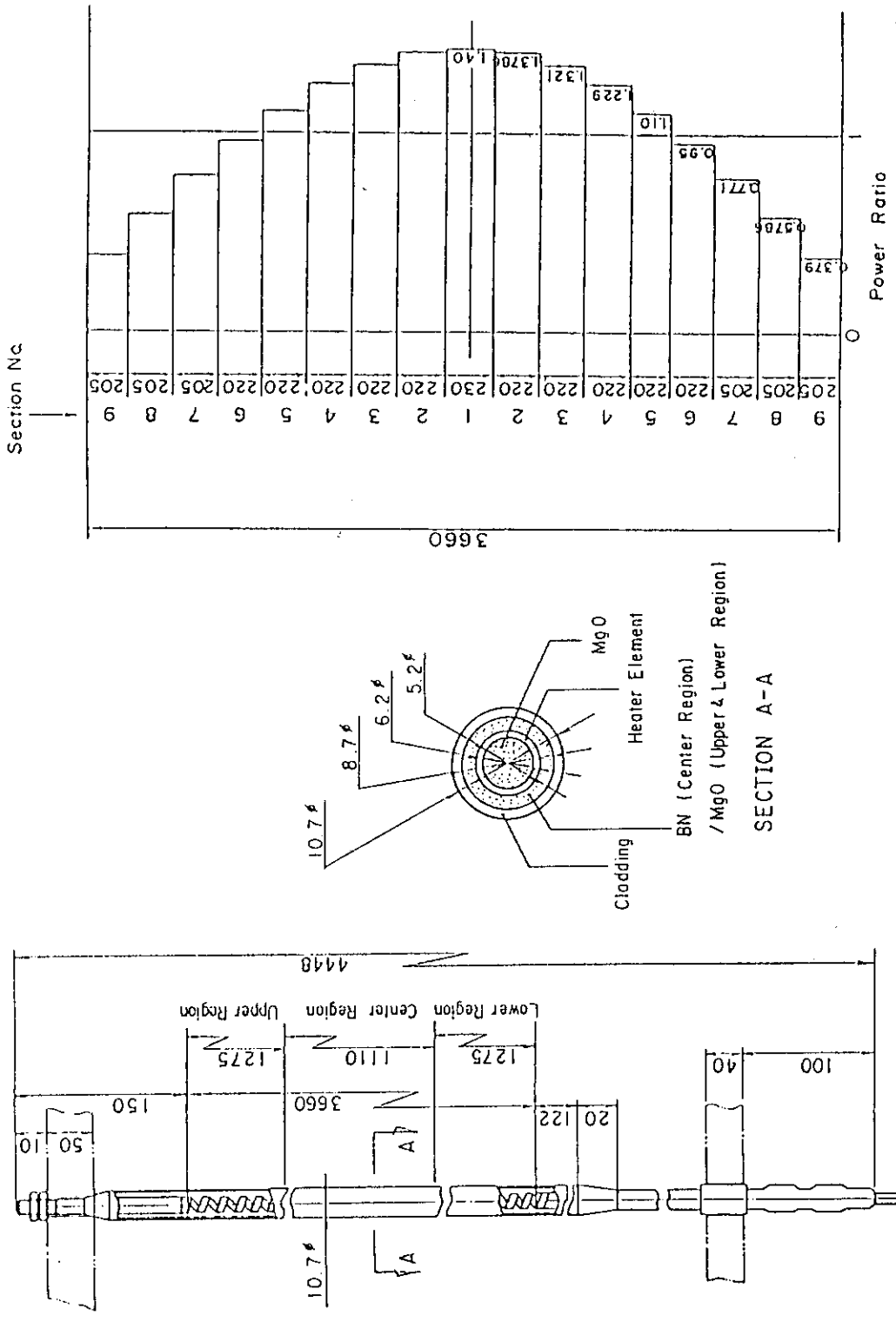

Fig.2.1.5 Dimension, configuration and axial power distribution of heater rods

Heater Rod

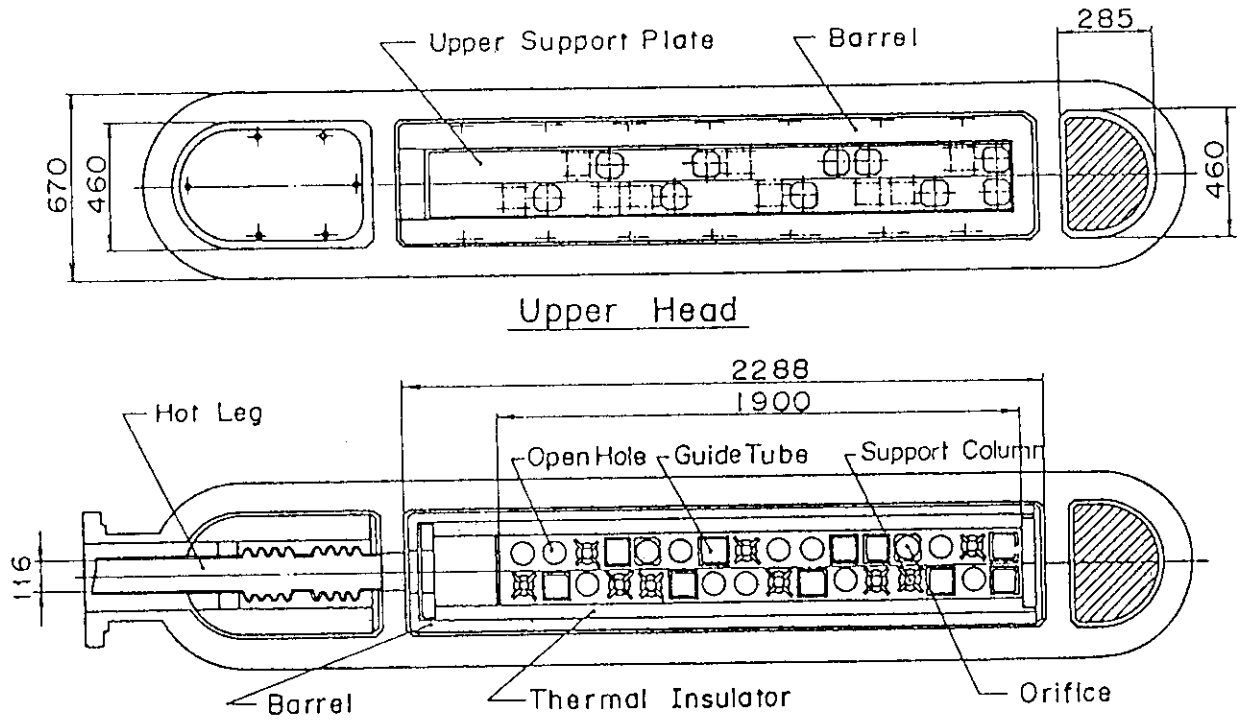

Fig.2.1.6 Horizontal cross sections in upper head and in upper plenum

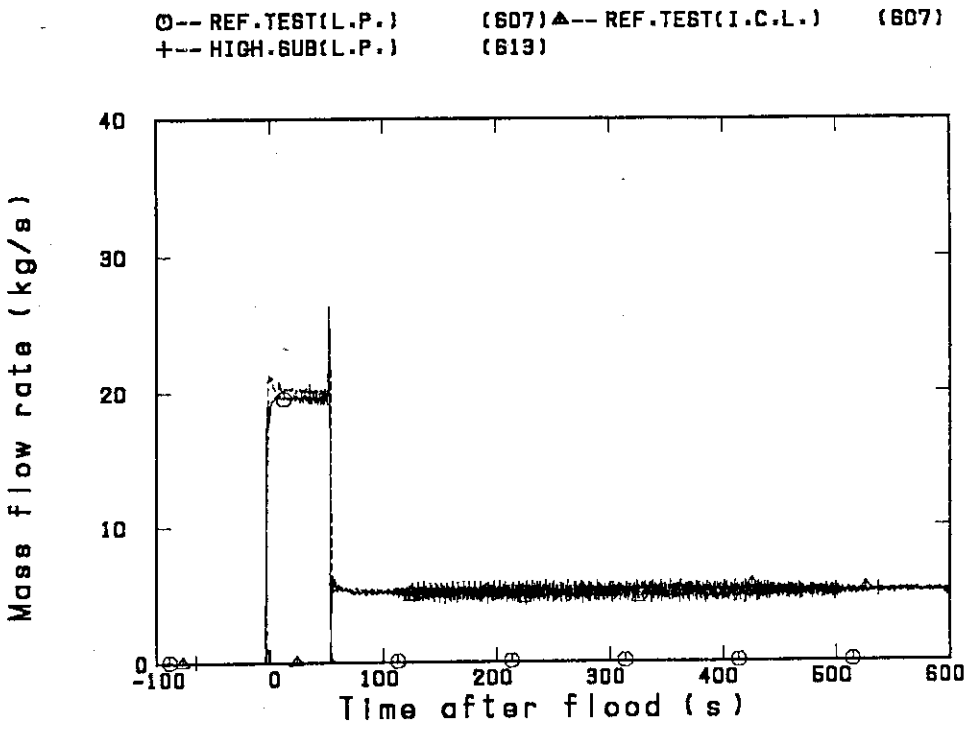

Fig.3.1.1 Comparison of ECC mass flow rate

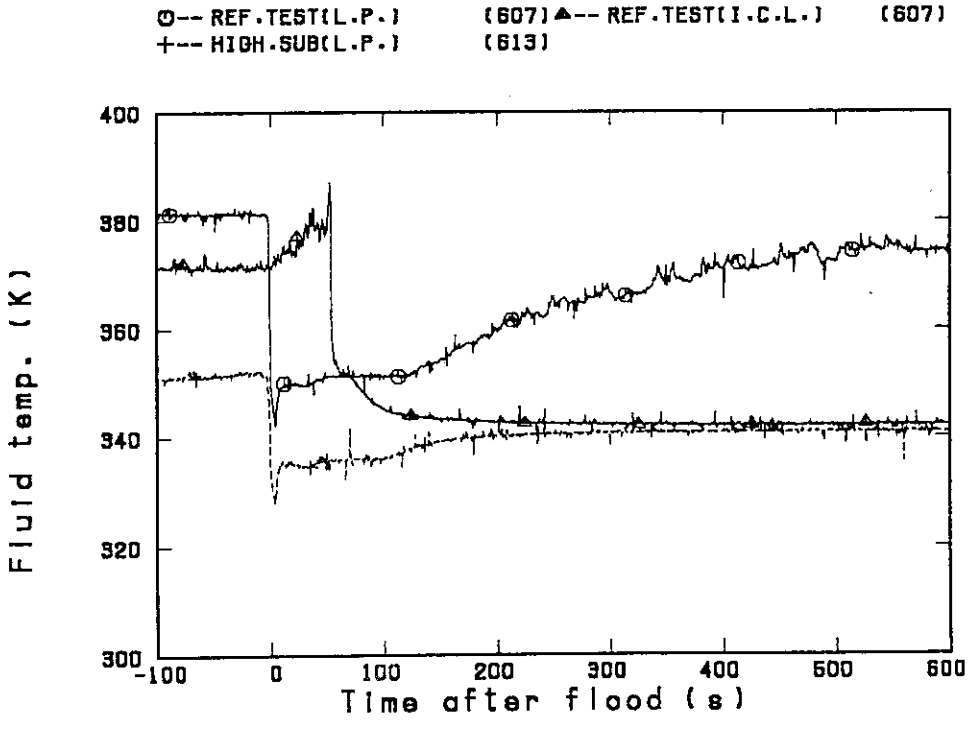

Fig.3.1.2 Comparison of ECC fluid temperature

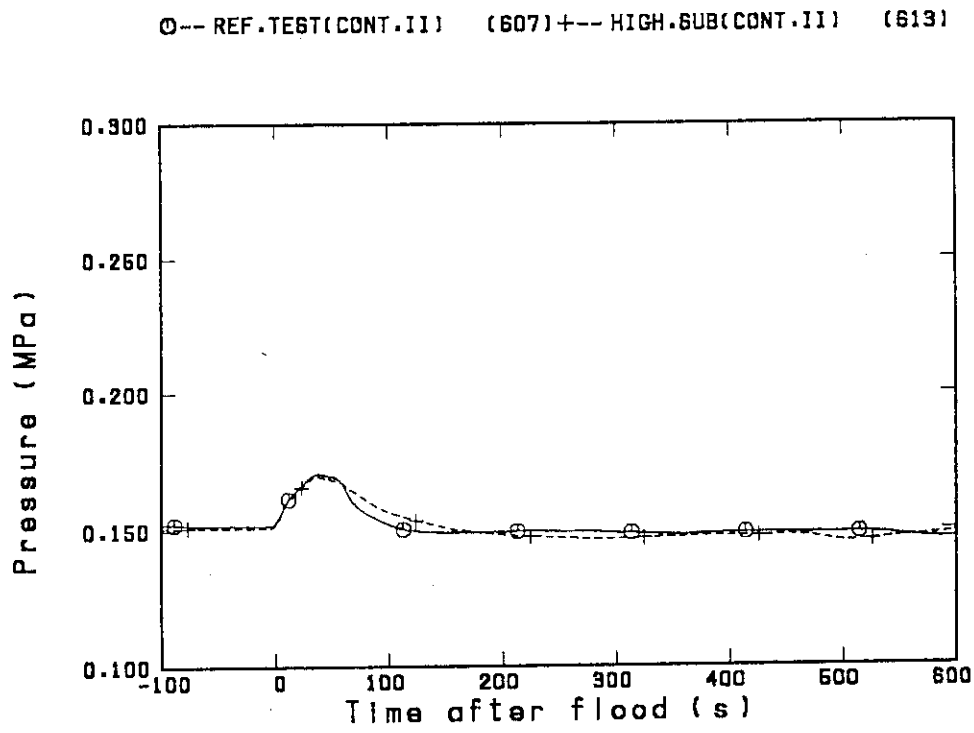

Fig.3.1.3 Comparison of pressure at containment tank-II

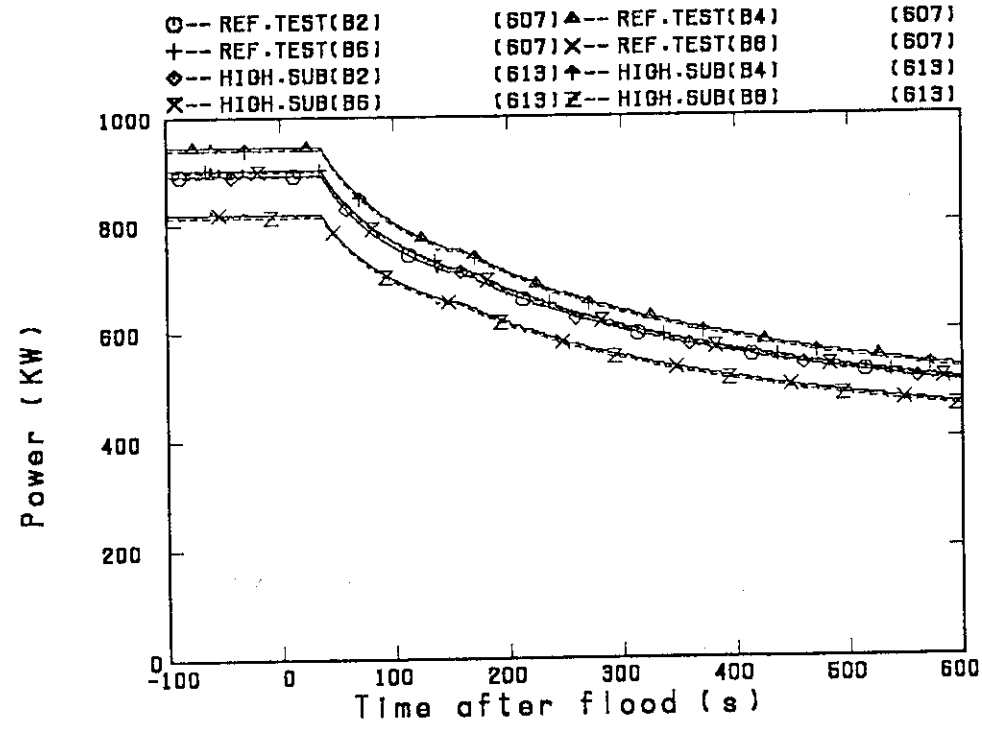

Fig.3.1.4 Comparison of power at bundles 2, 4, 6 and 8

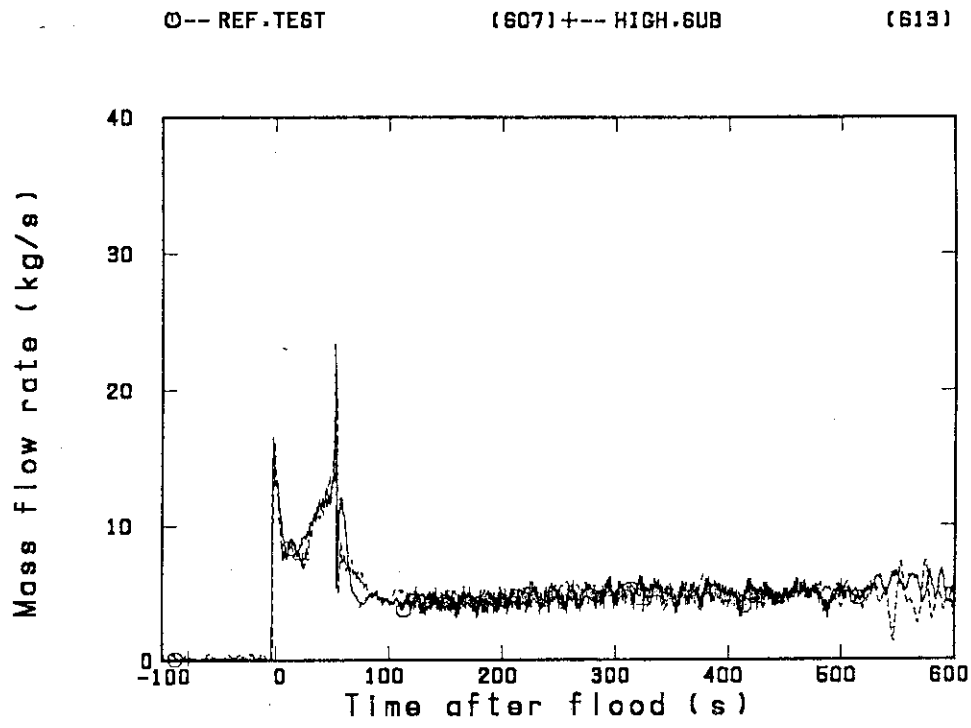

Fig.3.2.1(1) Comparison of core inlet mass flow rate

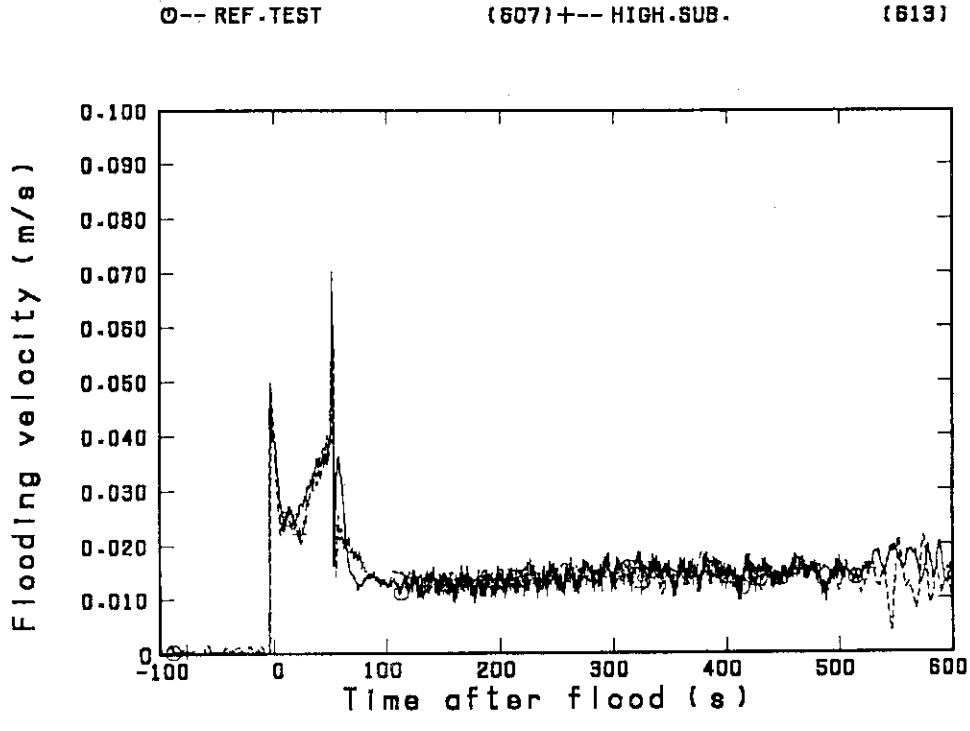

Fig.3.2.1(2) Comparison of core inlet flooding velocity

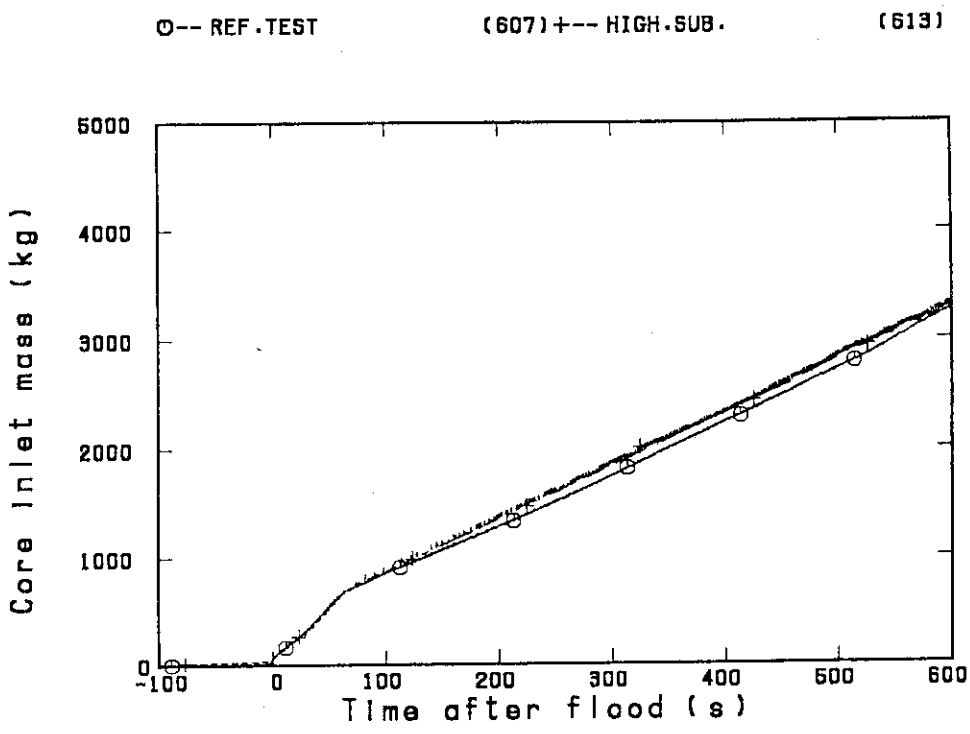

Fig.3.2.2 Comparison of integrated core inlet mass flow

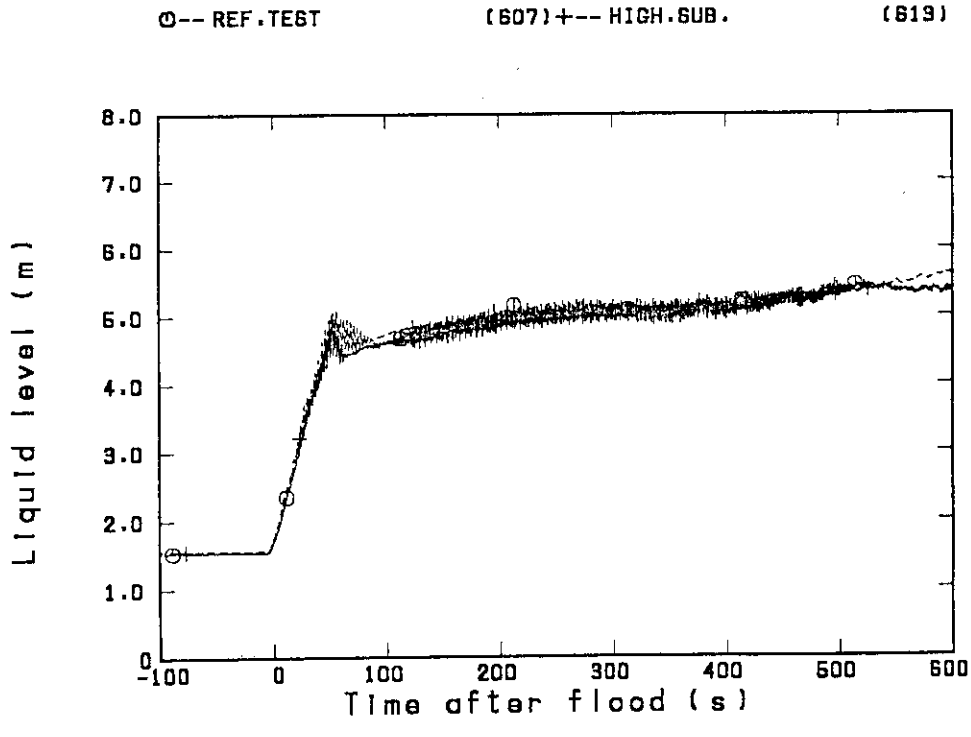

Fig.3.2.3 Comparison of liquid level in downcomer

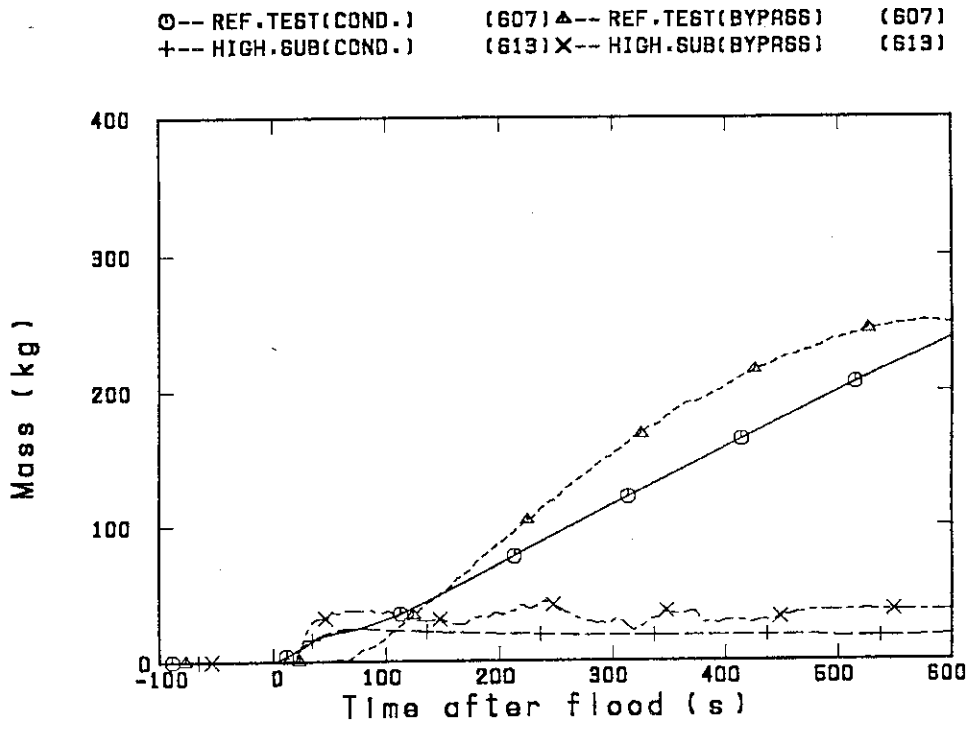

Fig.3.2.4 Comparison of condensation and bypass mass flow

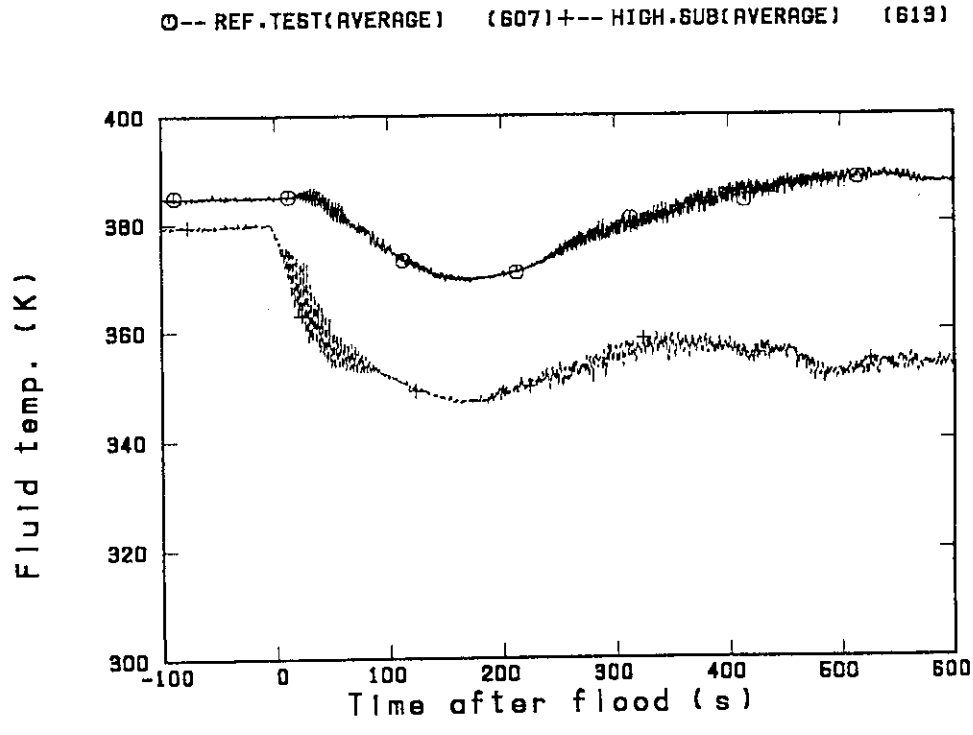

Fig.3.2.5 Comparison of core inlet fluid temperature

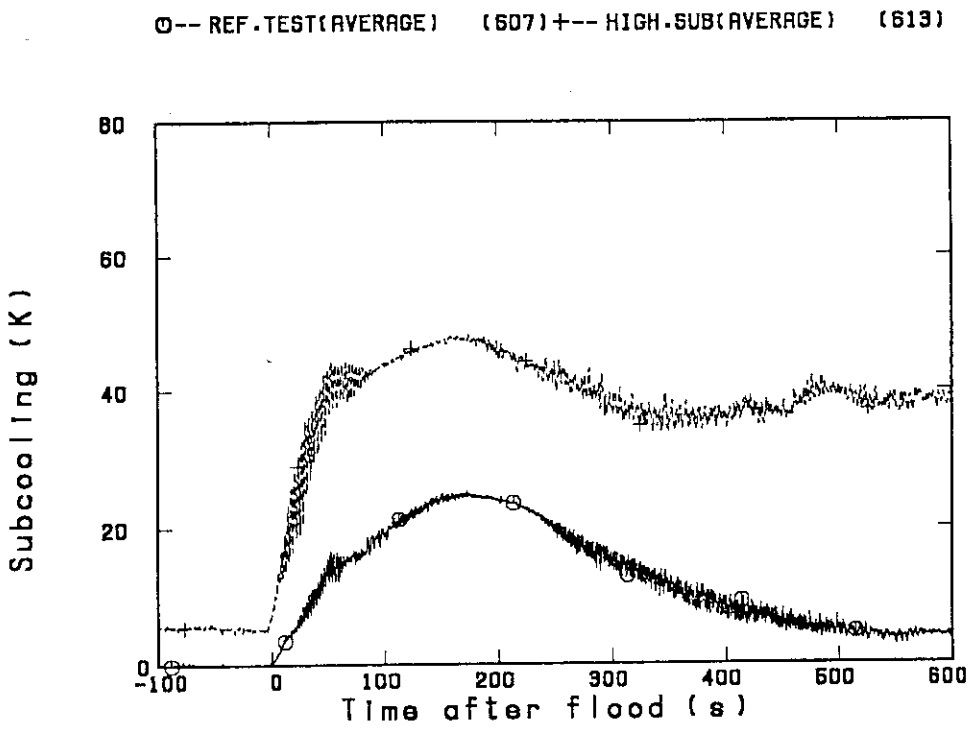

Fig.3.2.6 Comparison of core inlet subcooling

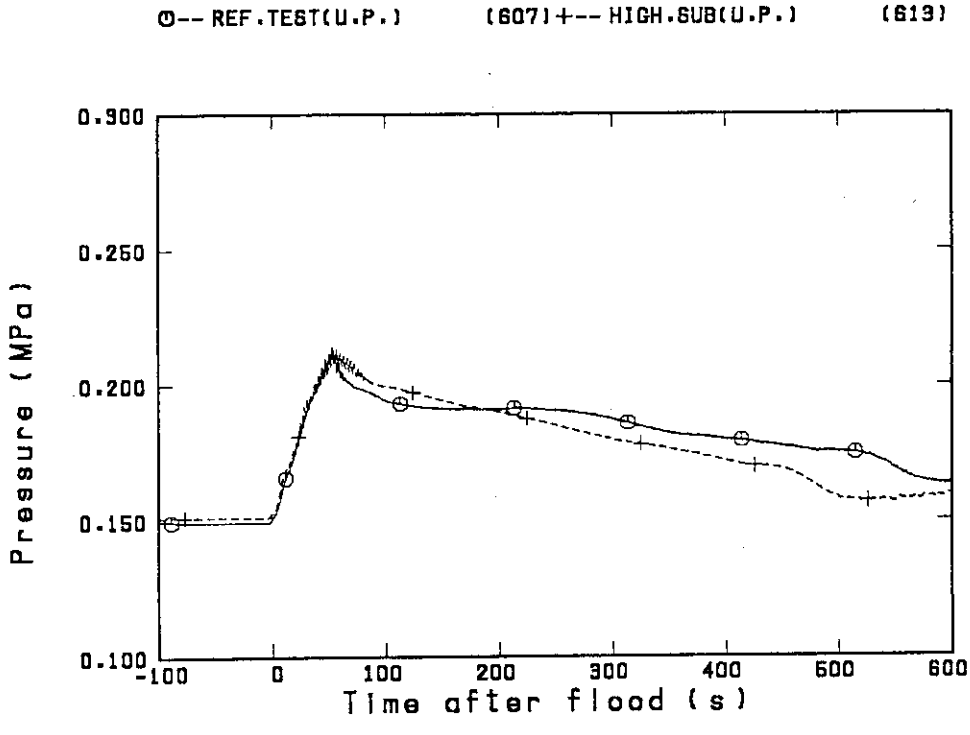

Fig.3.2.7 Comparison of pressure at upper plenum

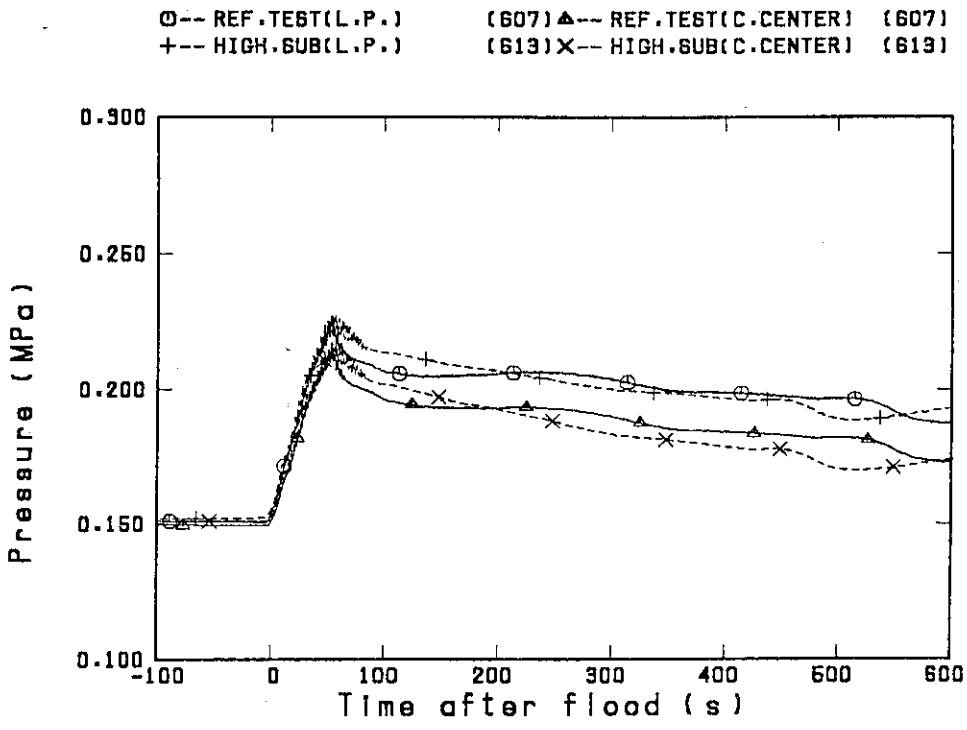

Fig.3.2.8 Comparison of pressure at lower plenum and at core center

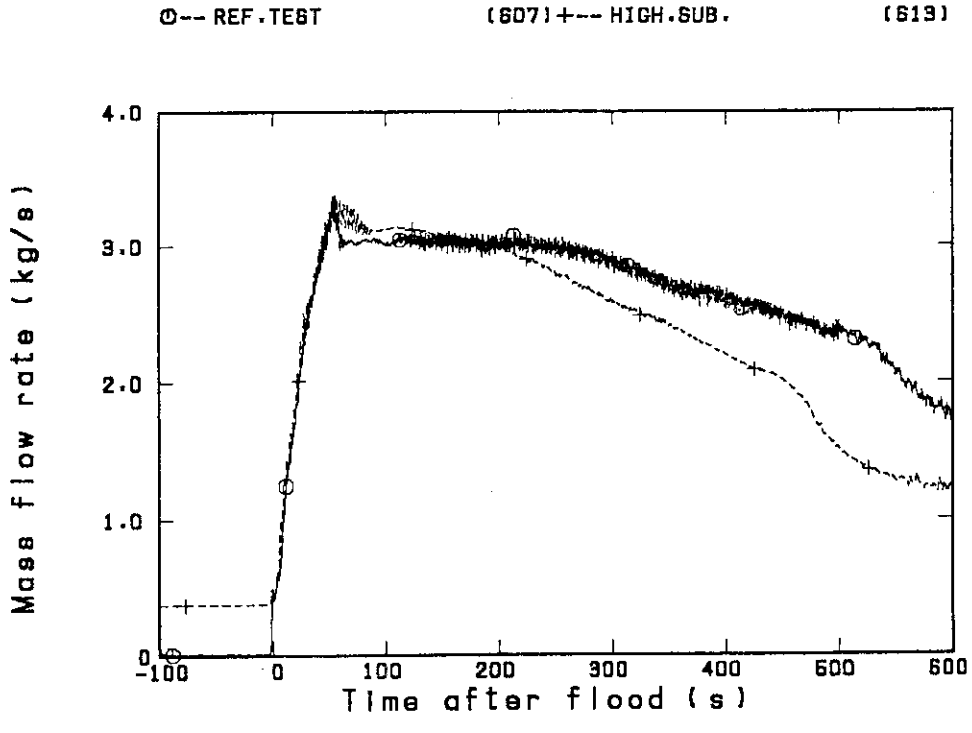

Fig.3.2.9 Comparison of steam mass flow rate generated in core

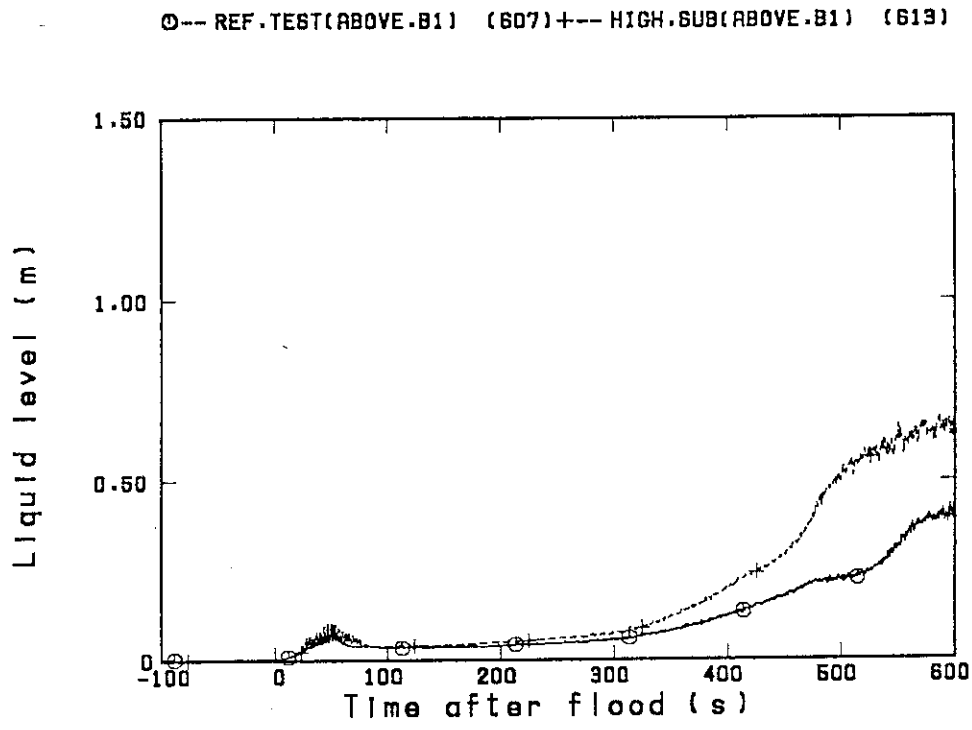

Fig.3.2.10(1) Comparison of liquid level in upper plenum above bundle 1

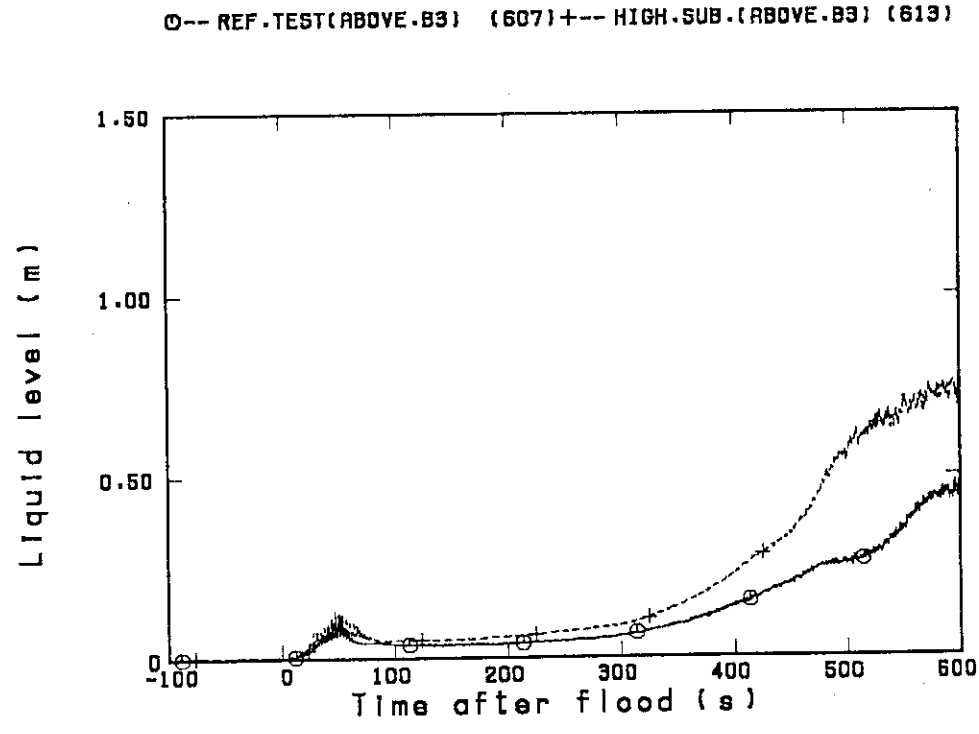

Fig.3.2.10(2) Comparison of liquid level in upper plenum above bundle 3

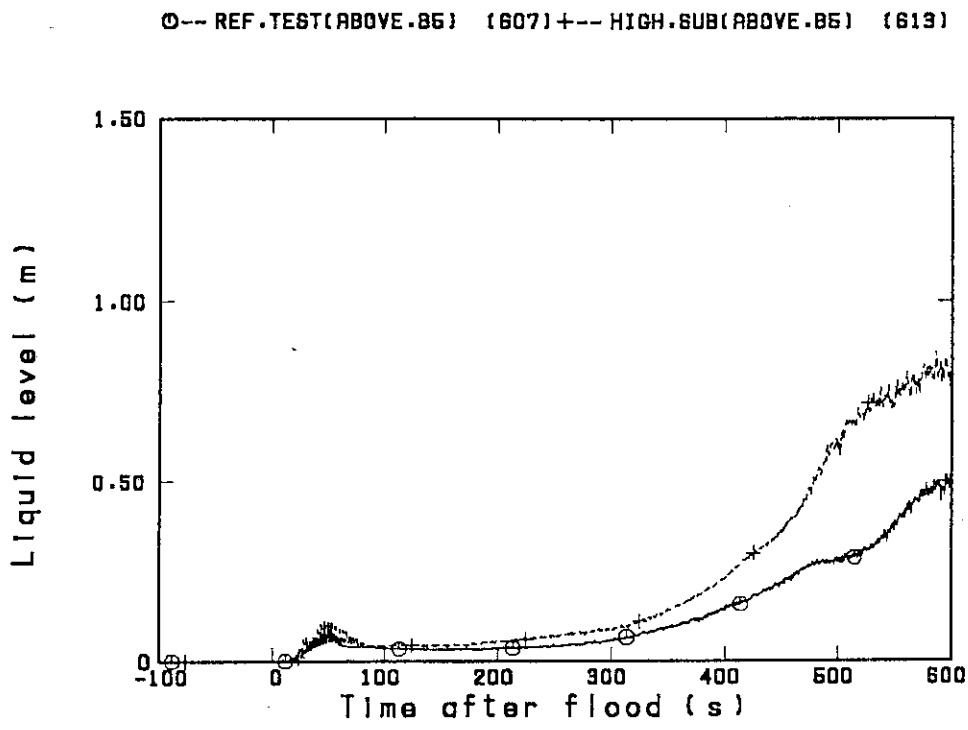

Fig.3.2.10(3) Comparison of liquid level in upper plenum above bundle 5

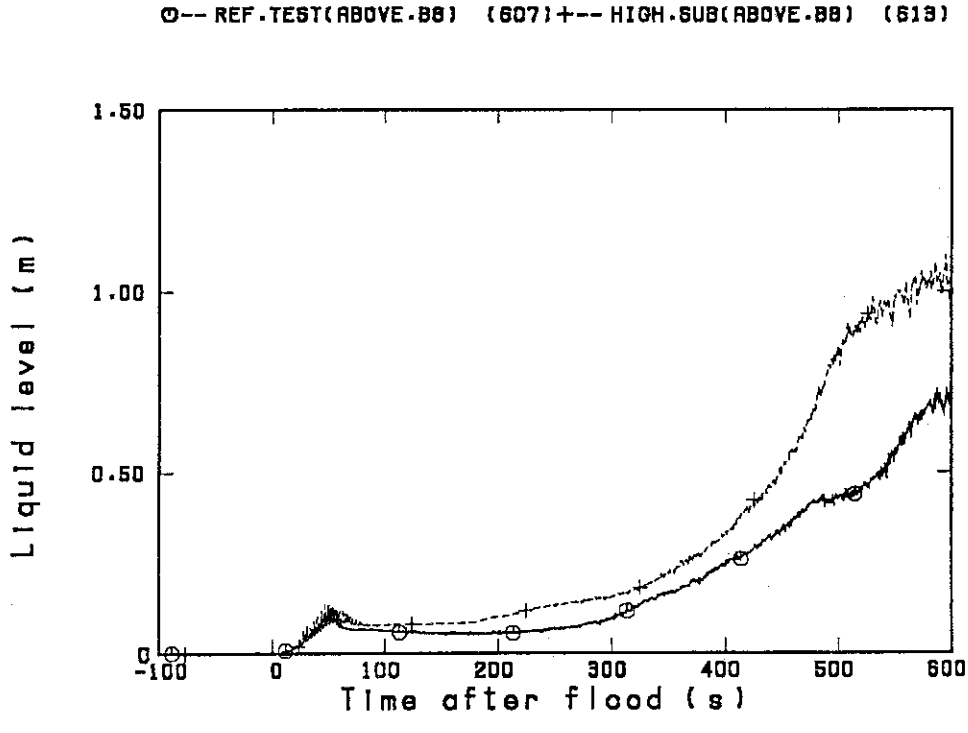

Fig.3.2.10(4) Comparison of liquid level in upper plenum above bundle 8

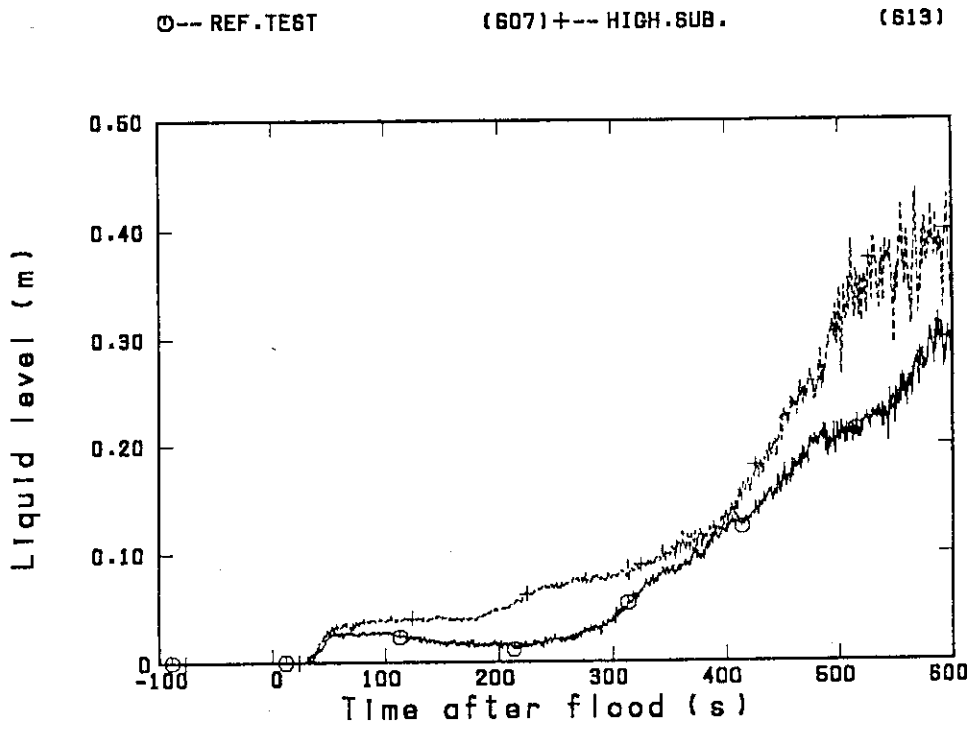

Fig.3.2.11 Comparison of radial difference of liquid level in upper plenum between above bundles 8 and 1

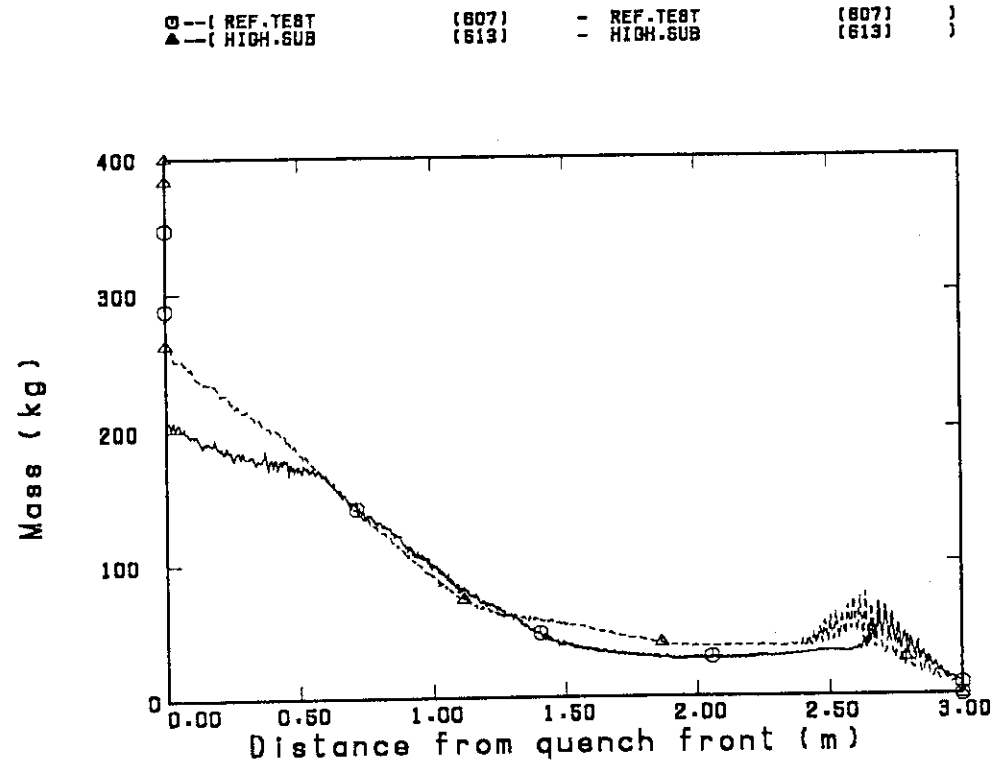

Fig.3.2.12 Comparison of upper plenum mass

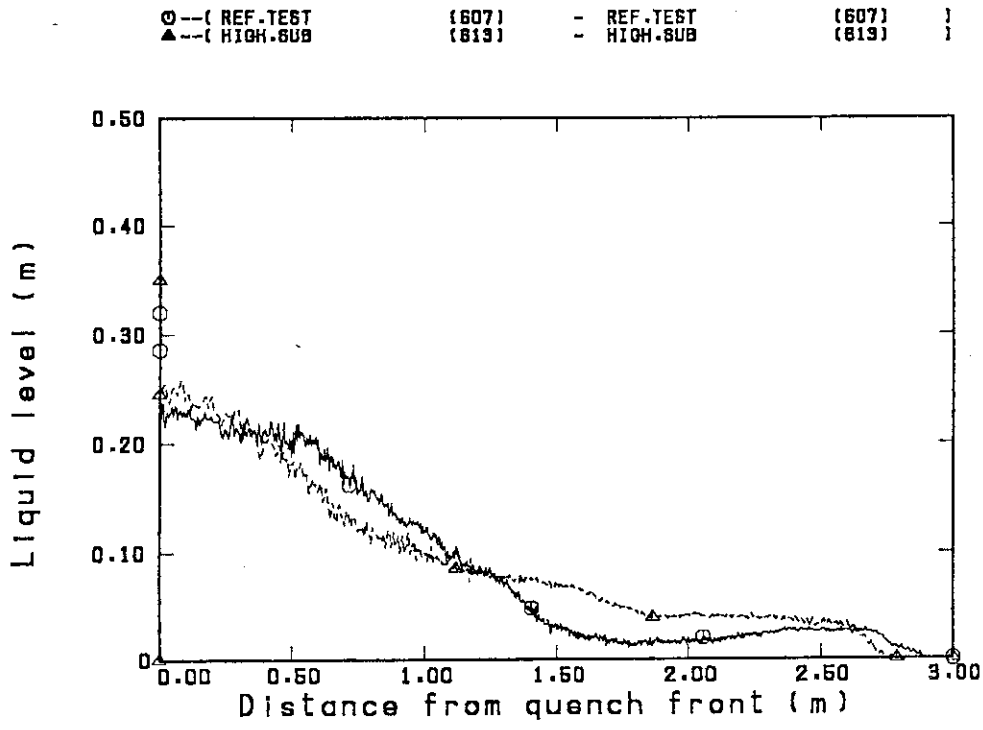

Fig.3.2.13 Comparison of radial difference of liquid level in upper plenum between above bundles 8 and 1

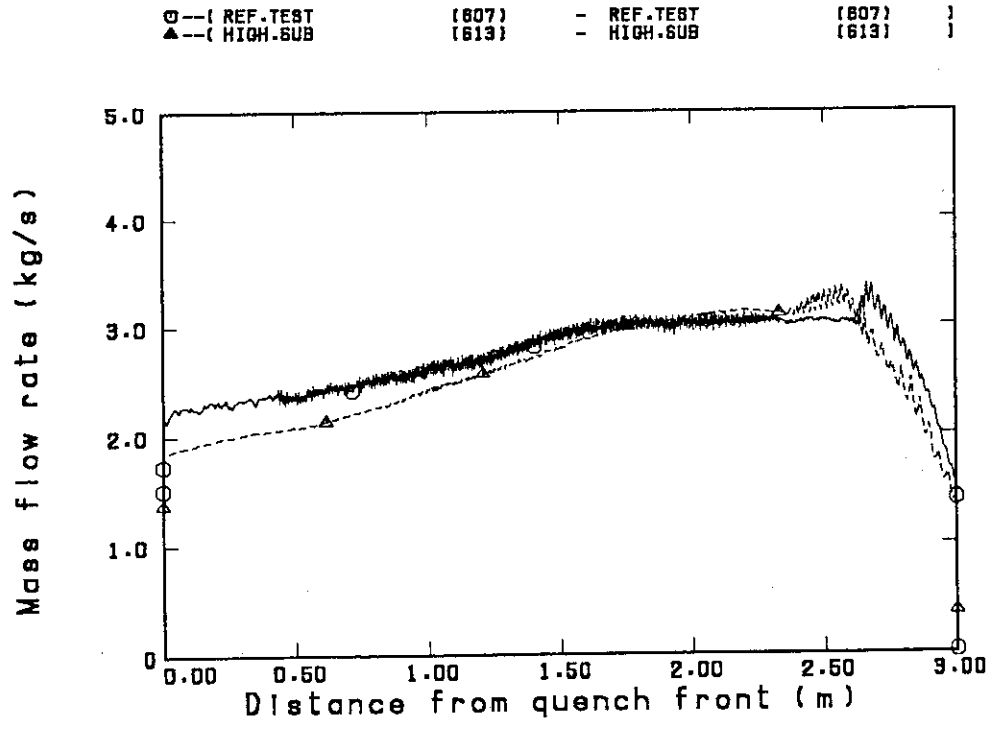

Fig.3.2.14 Comparison of steam mass flow rate generated in core

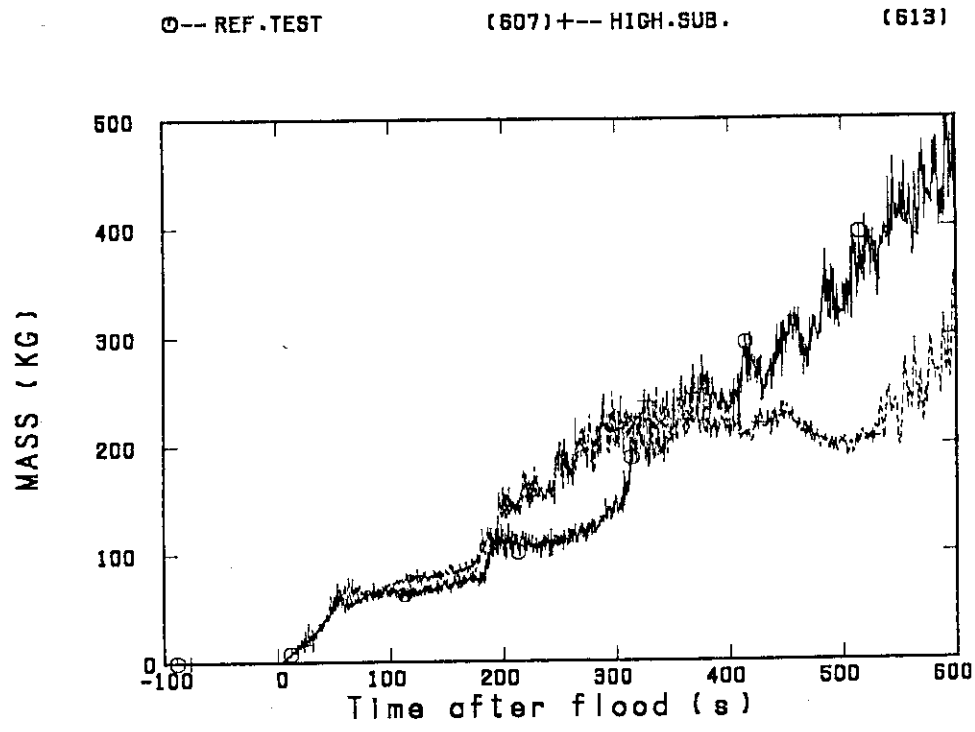

Fig.3.2.15 Comparison of carry-over mass at inlet of hot leg

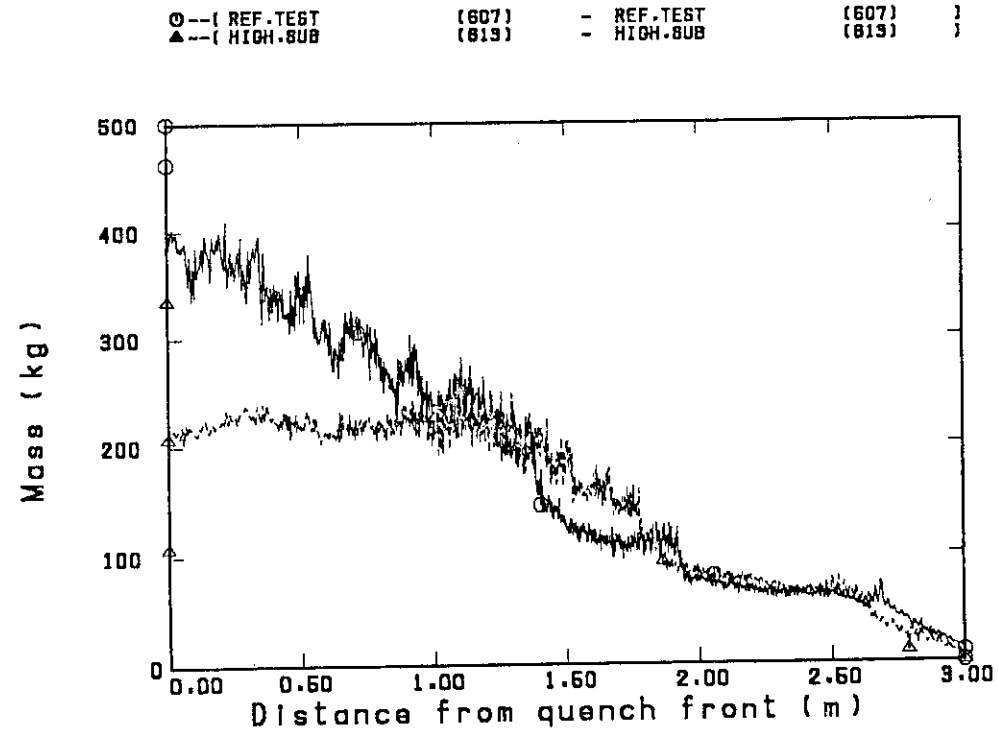

Fig.3.2.16 Comparison of carry-over mass at inlet of hot leg

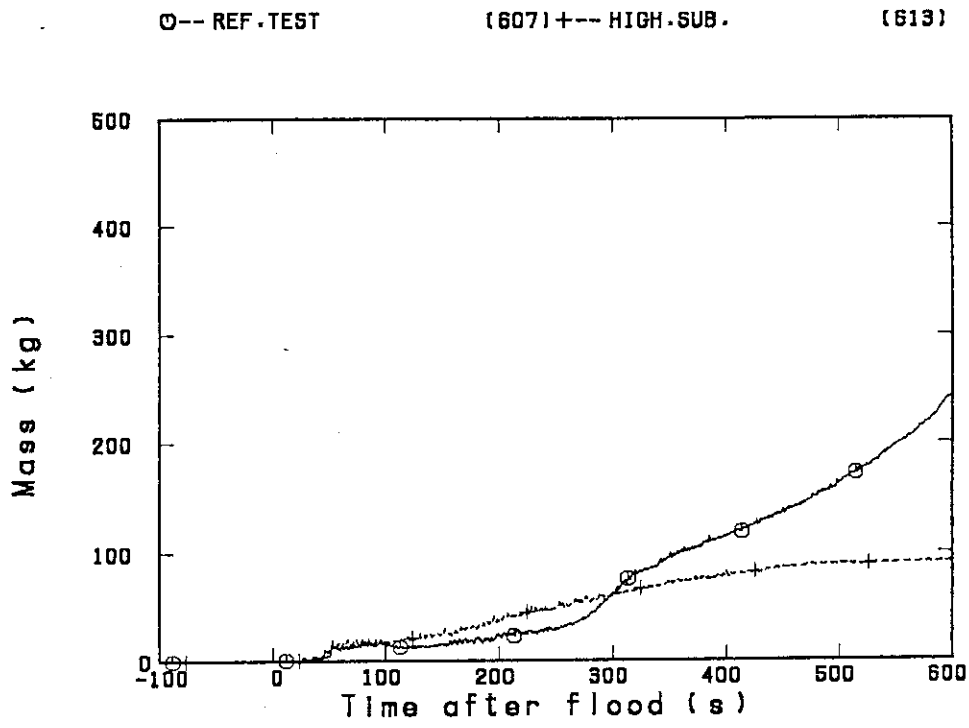

Fig.3.2.17 Comparison of carry-over mass at S/W separator

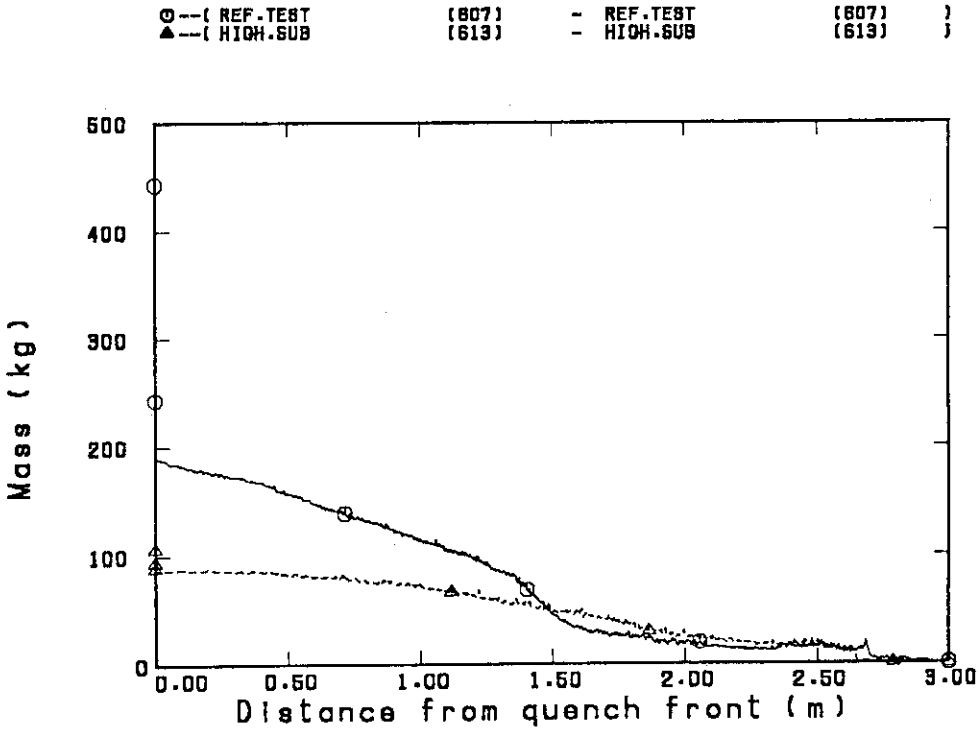

Fig.3.2.18 Comparison of carry-over mass at S/W separator

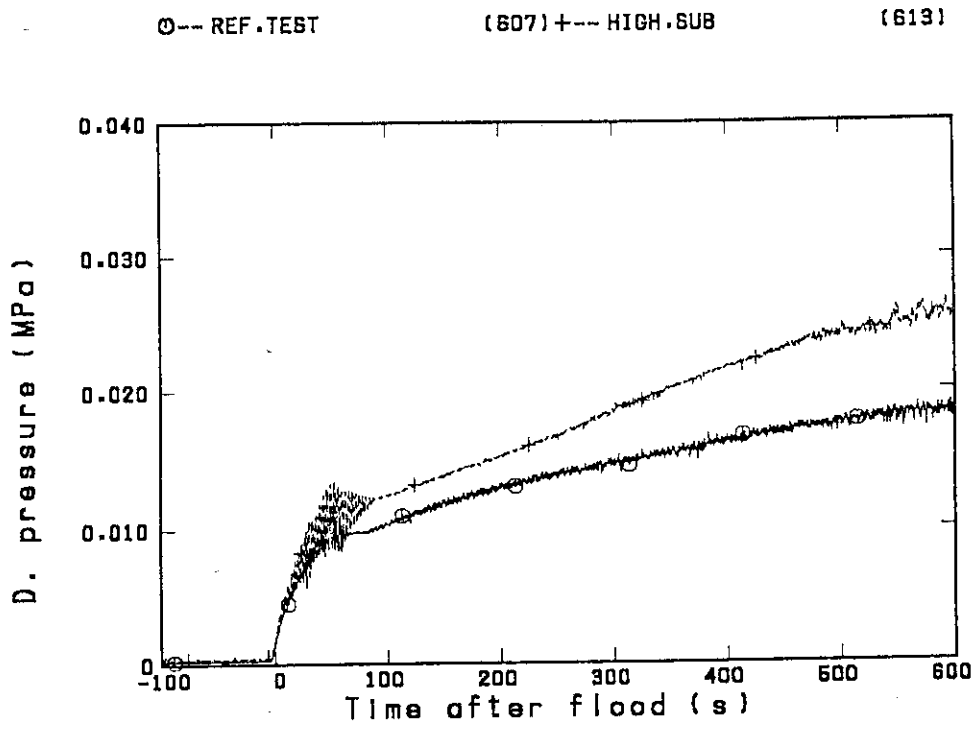

Fig.3.3.1 Comparison of differential pressure of core full height at bundle 4

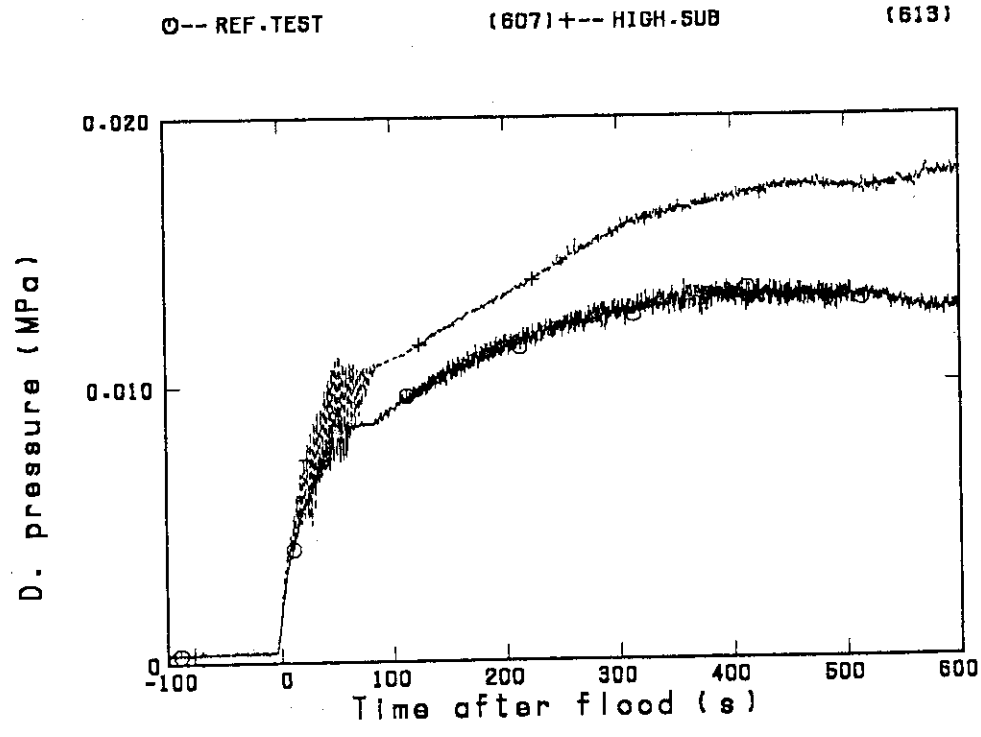

Fig.3.3.2(1) Comparison of differential pressure of core lower half at bundle 4

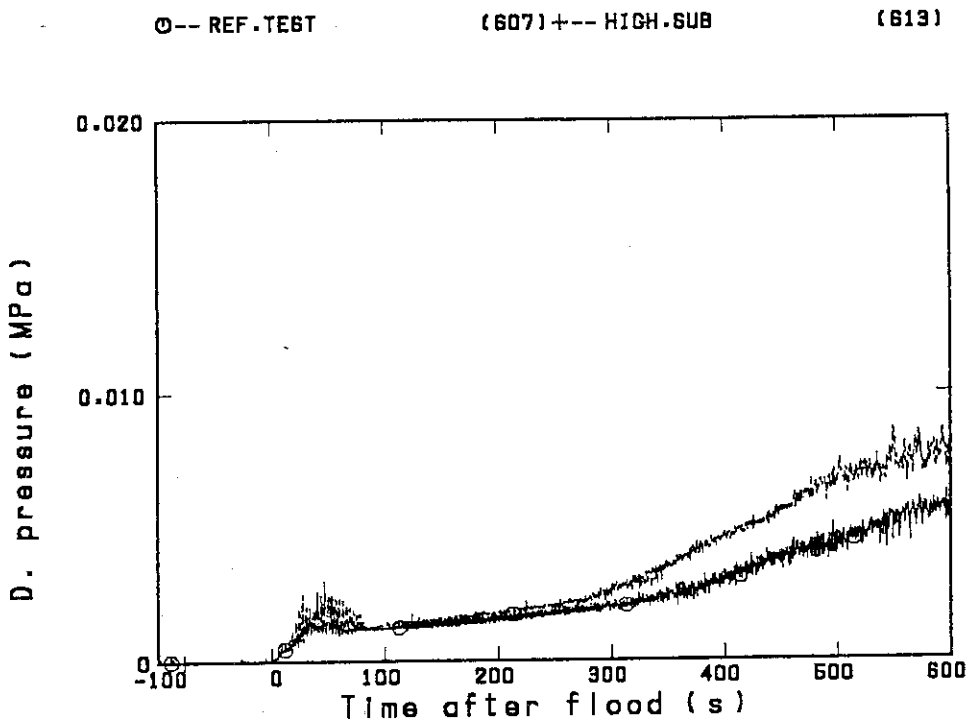

Fig.3.3.2(2) Comparison of differential pressure of core upper half at bundle 4

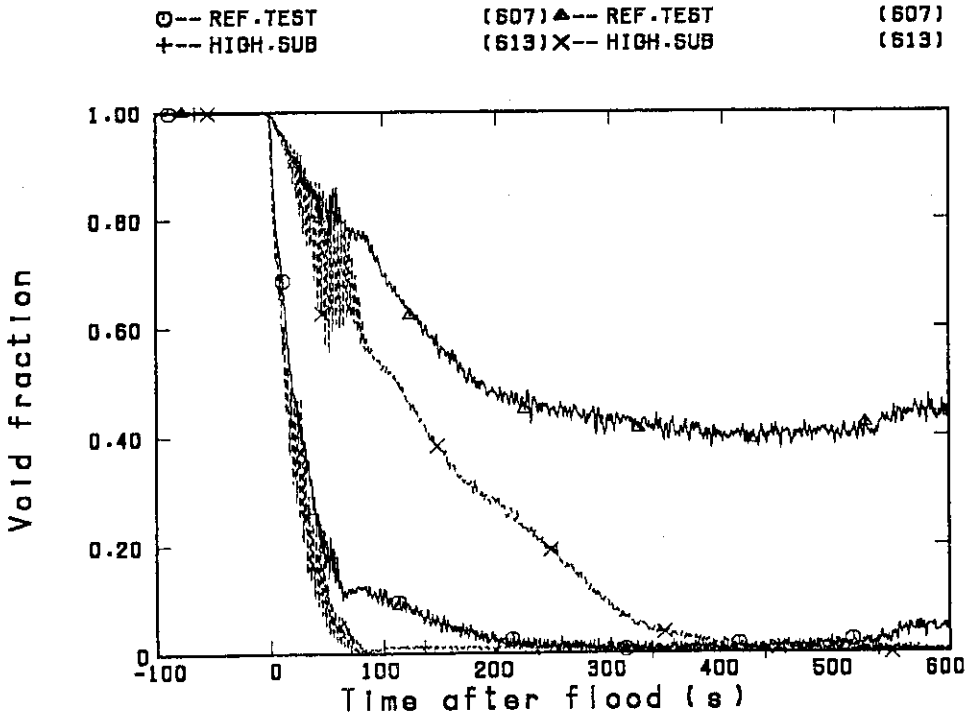

Fig.3.3.3(1) Comparison of sectional void fraction at 0.085-0.7m and 0.7-1.365m in bundle 4

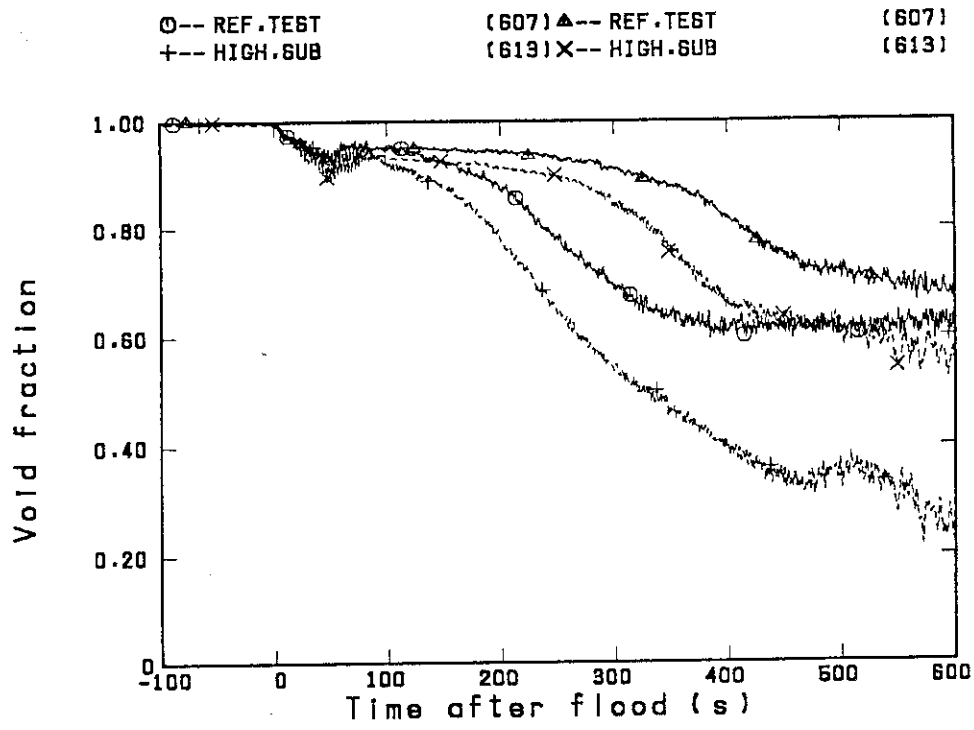

Fig.3.3.3(2) Comparison of sectional void fraction at 1.365-1.905m and 2.03-2.57m in bundle 4

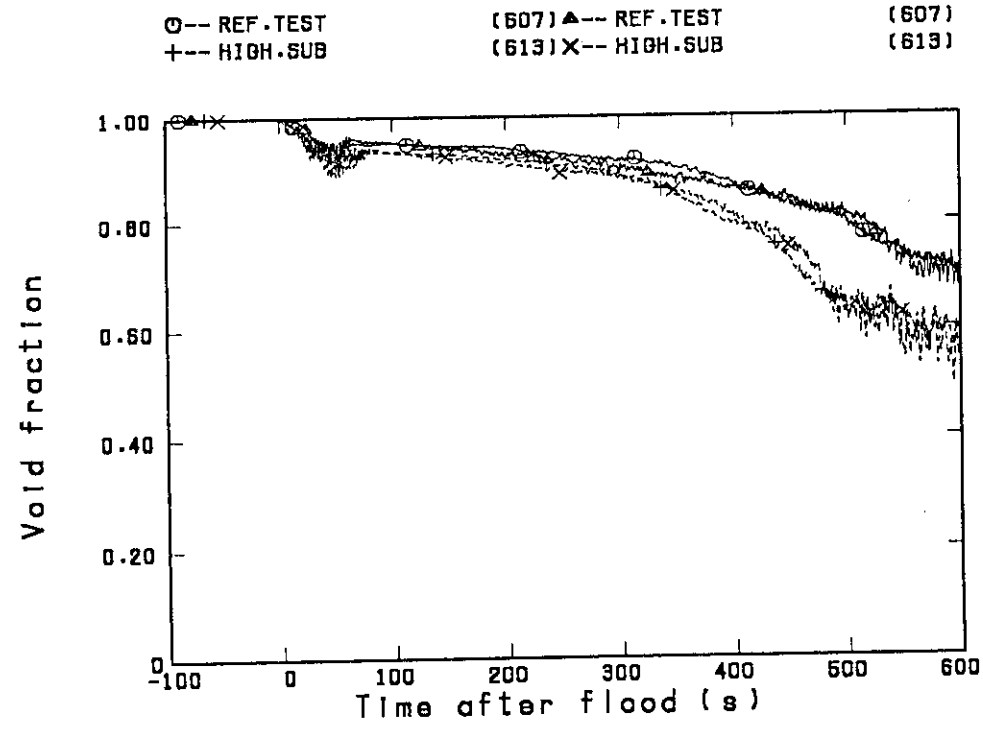

Fig.3.3.3(3) Comparison of sectional void fraction at 2.695-3.235m and 3.36-3.685m in bundle 4

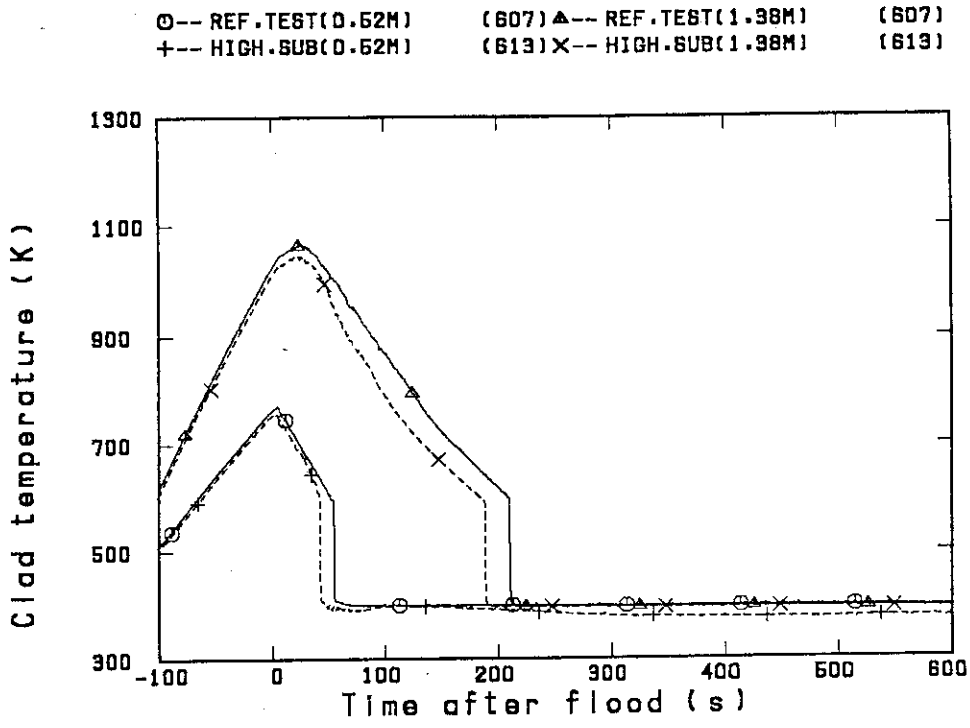

Fig.3.3.4(1) Comparison of clad temperature at 0.52m and 1.38m in bundle 4

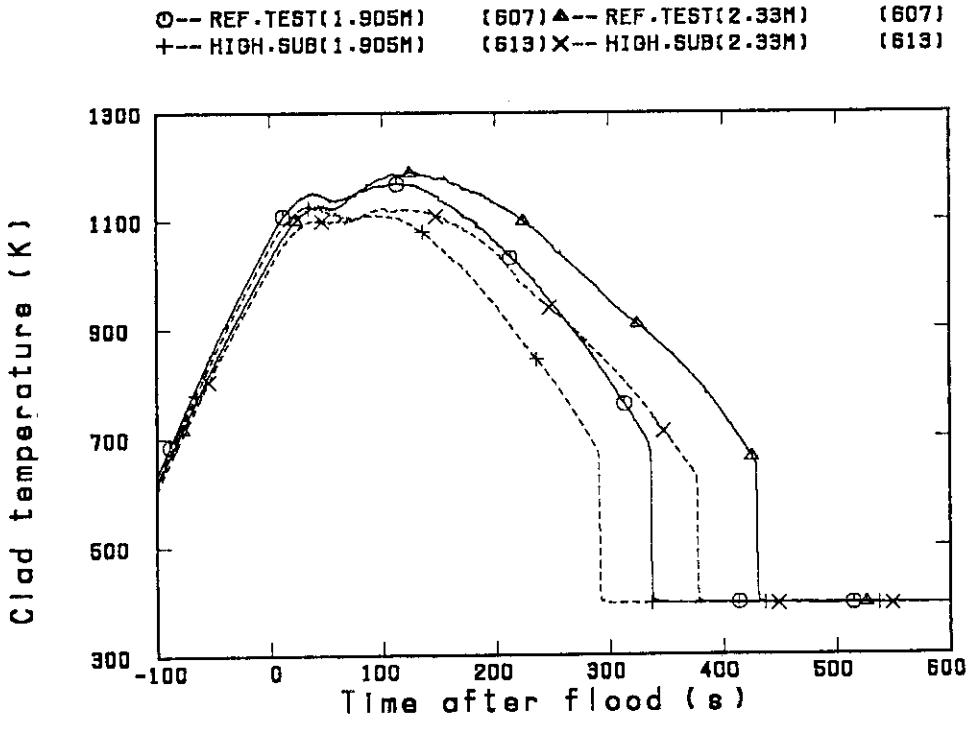

Fig.3.3.4(2) Comparison of clad temperature at 1.905m and 2.33m in bundle 4

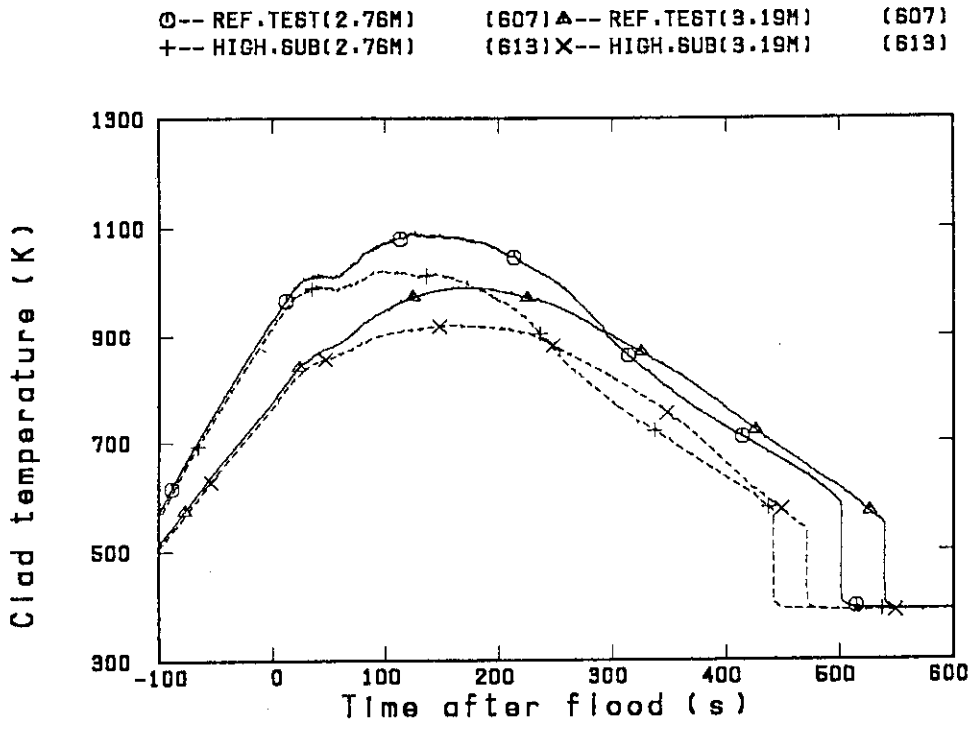

Fig.3.3.4(3) Comparison of clad temperature at 2.76m and 3.19m in bundle 4

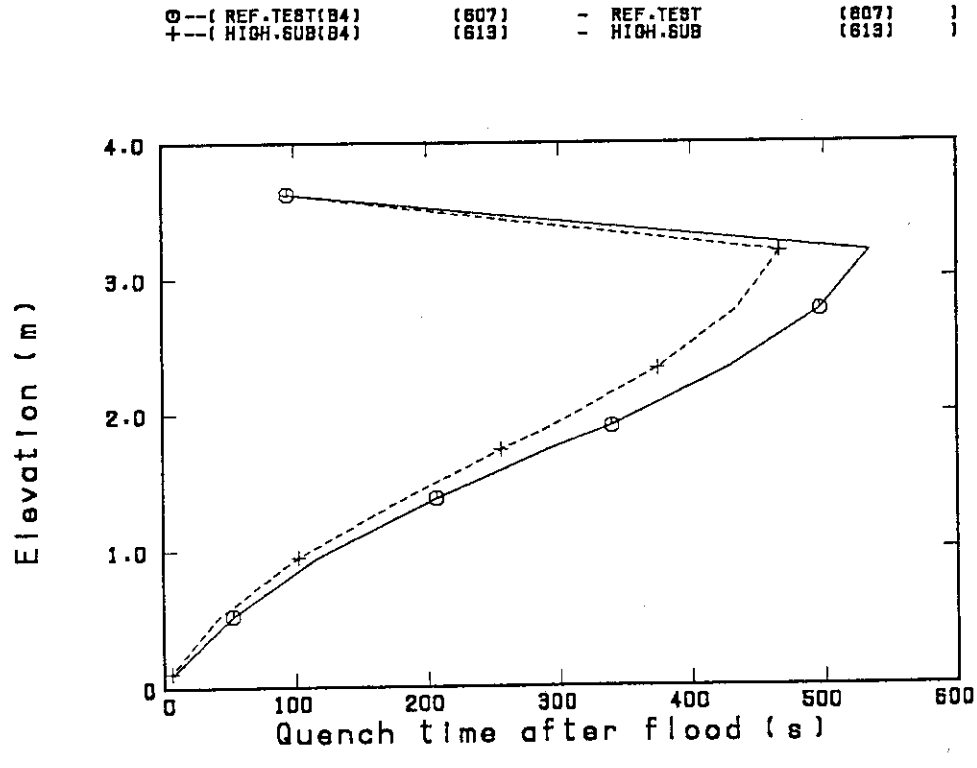

Fig.3.3.5 Comparison of quench time in bundle 4

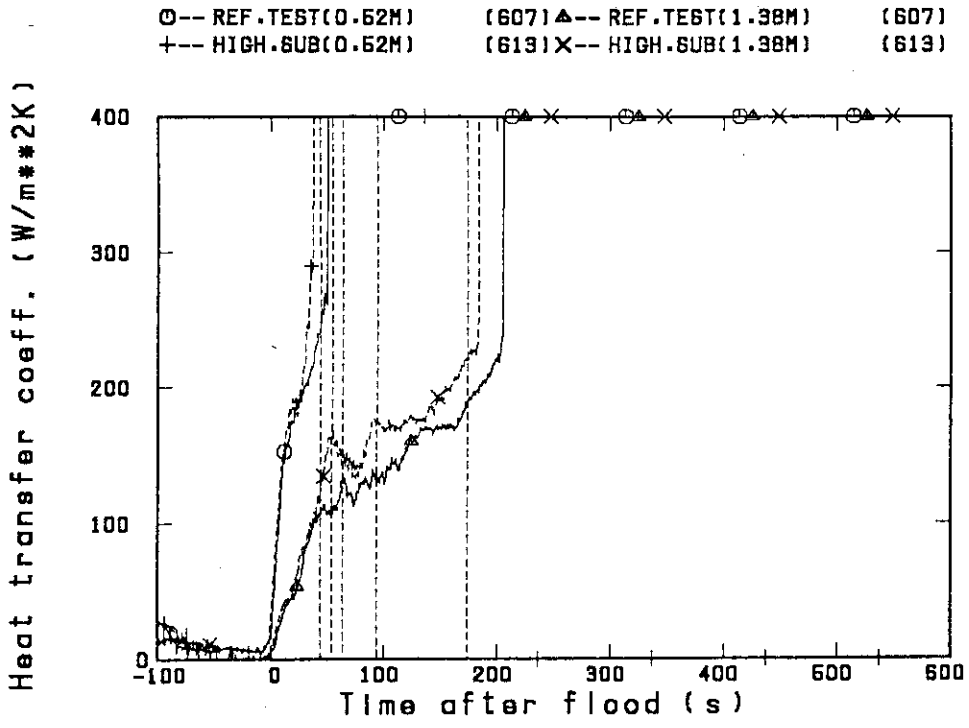

Fig.3.3.6(1) Comparison of heat transfer coefficient at 0.52m and 1.38m in bundle 4

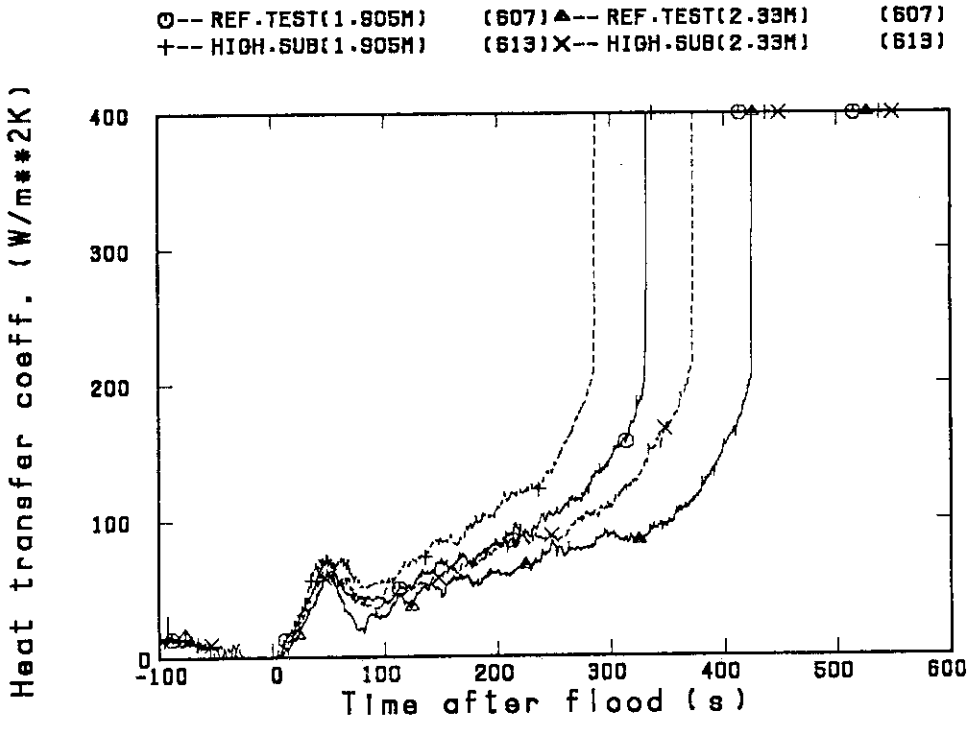

Fig.3.3.6(2) Comparison of heat transfer coefficient at 1.905m and 2.33m in bundle 4

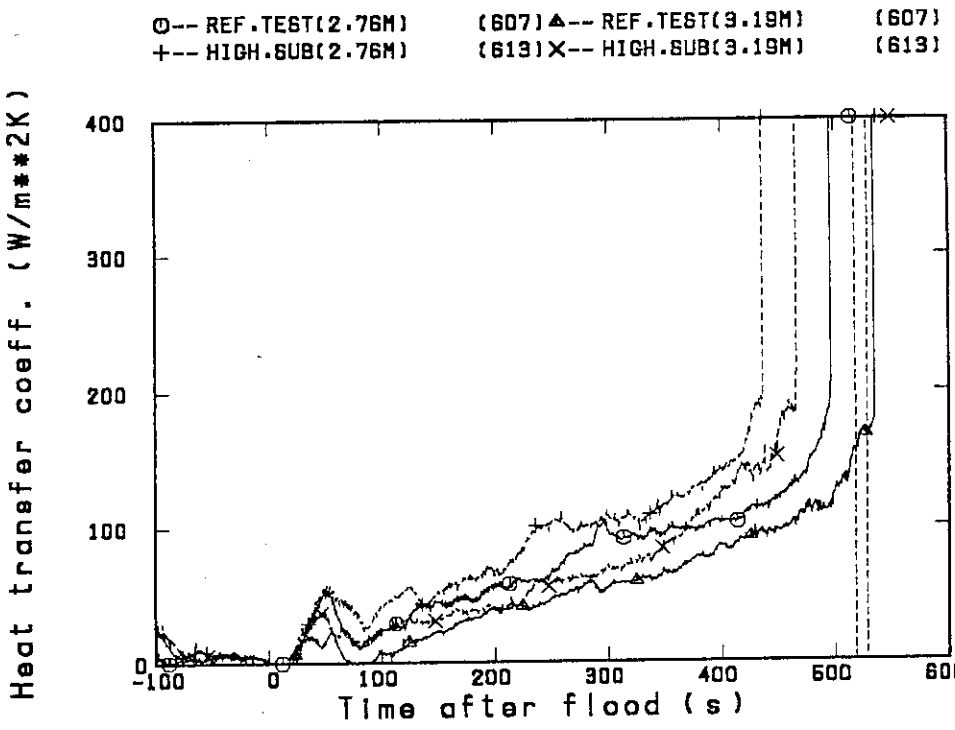

Fig.3.3.6(3) Comparison of heat transfer coefficient at 2.76m and 3.19m in bundle 4

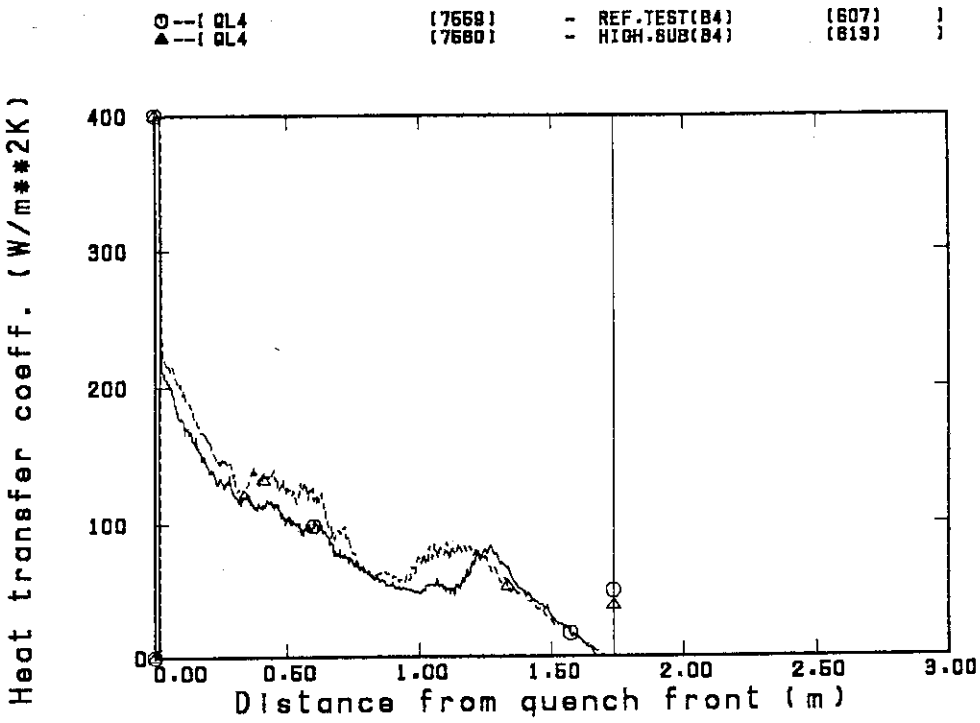

Fig.3.3.7(1) Comparison of heat transfer coefficient at 1.735m in bundle 4

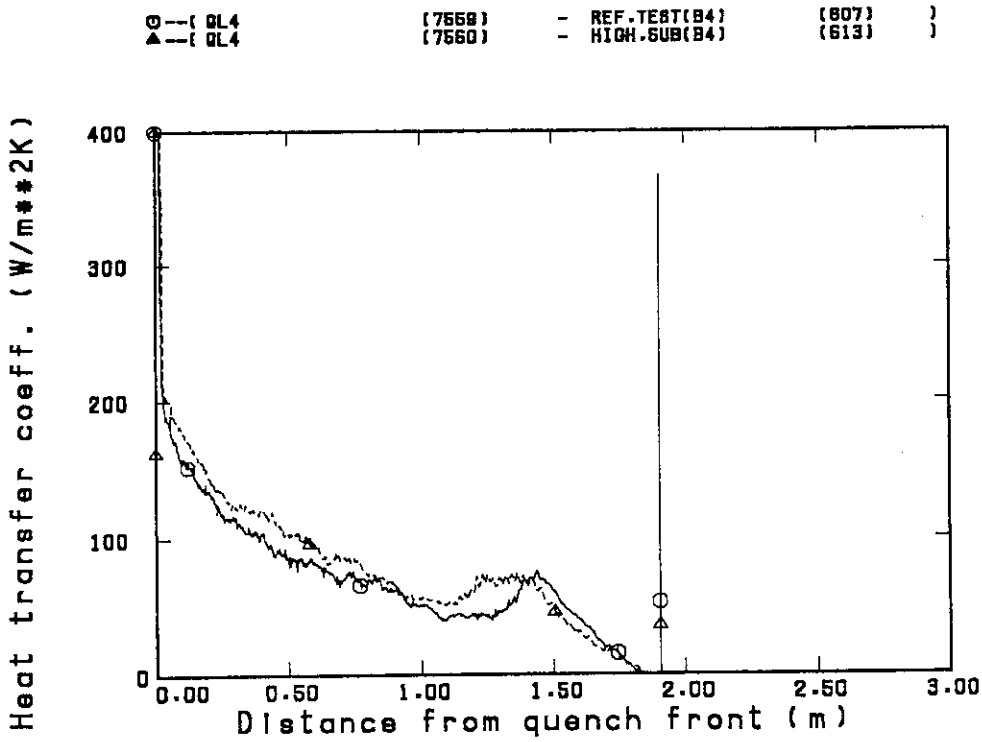

Fig.3.3.7(2) Comparison of heat transfer coefficient at 1.905m in bundle 4

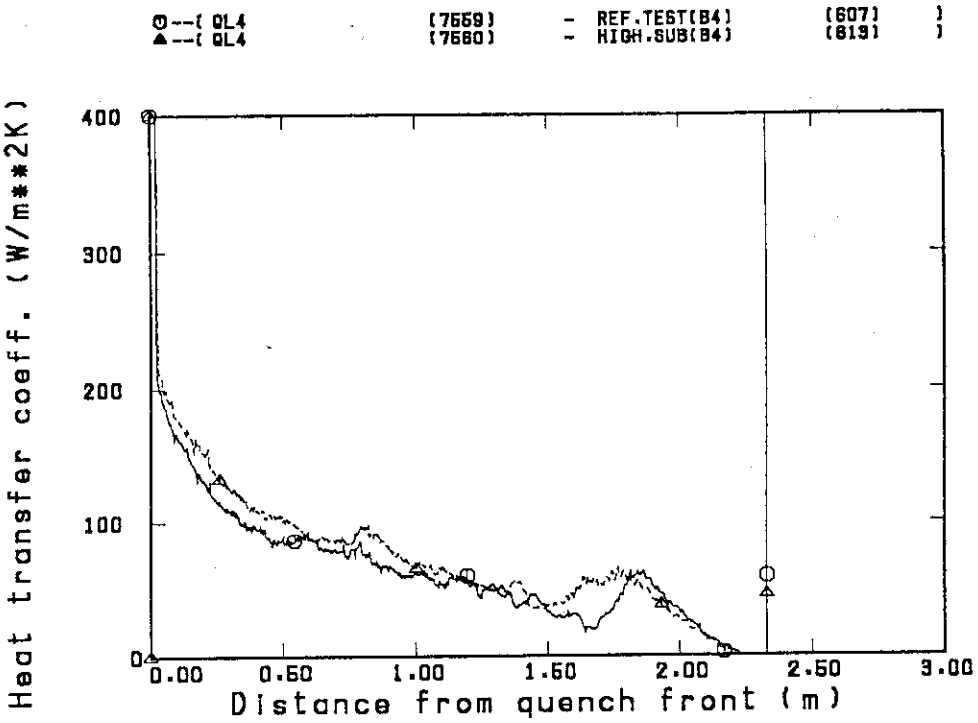

Fig.3.3.7(3) Comparison of heat transfer coefficient at 2.33m in bundle 4

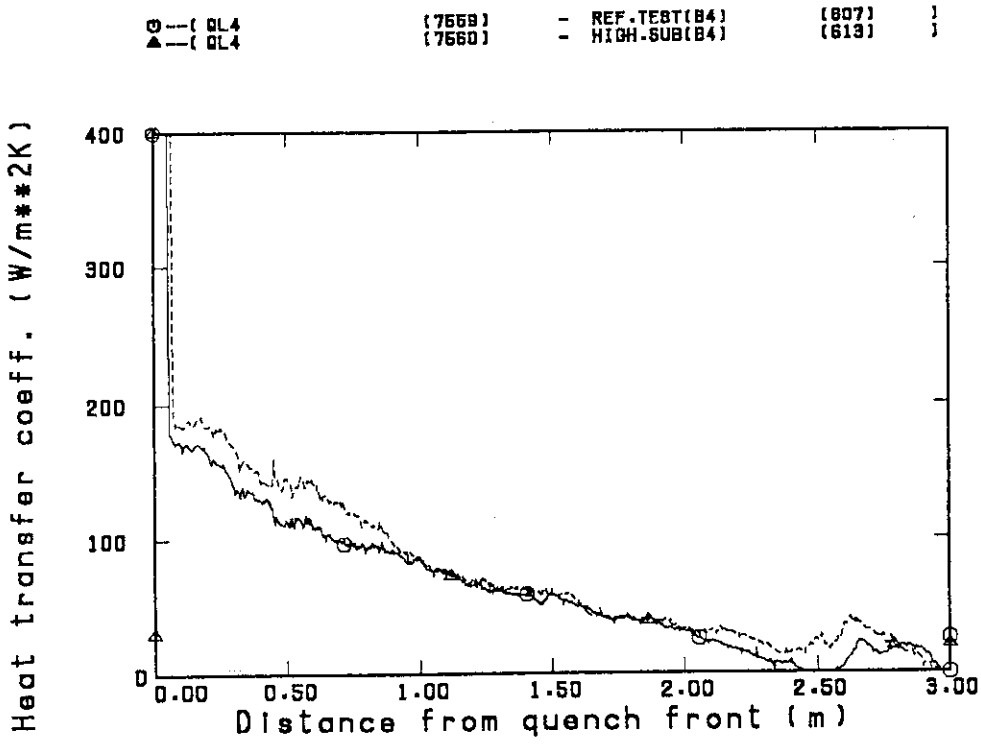

Fig.3.3.7(4) Comparison of heat transfer coefficient at 3.19m in bundle 4

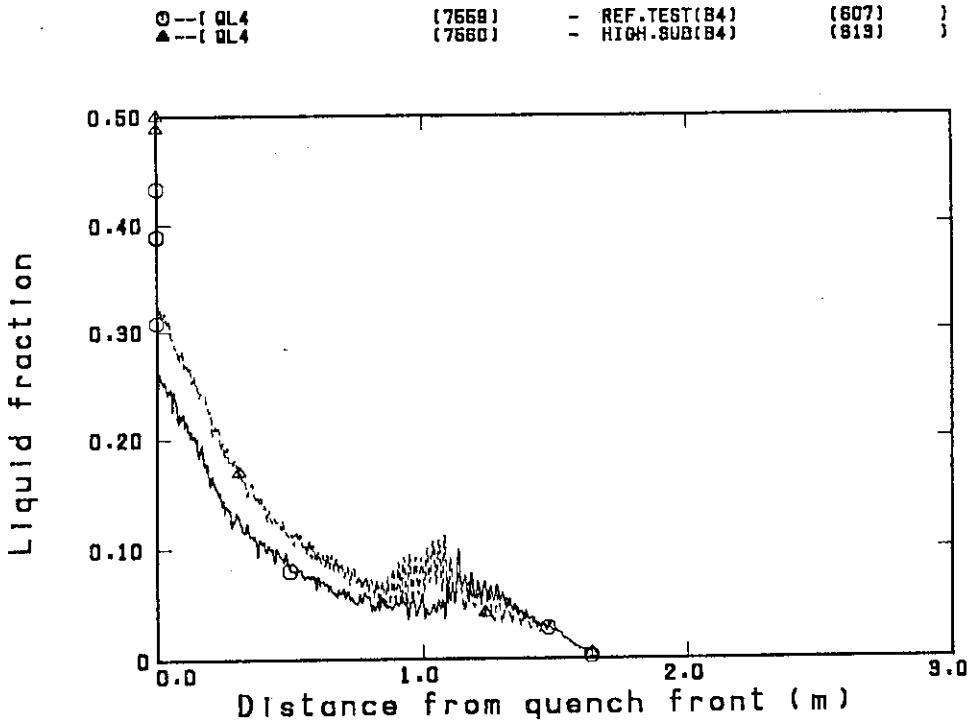

Fig.3.3.8(1) Comparison of liquid fraction in bundle 4 at 1.365-1.905m

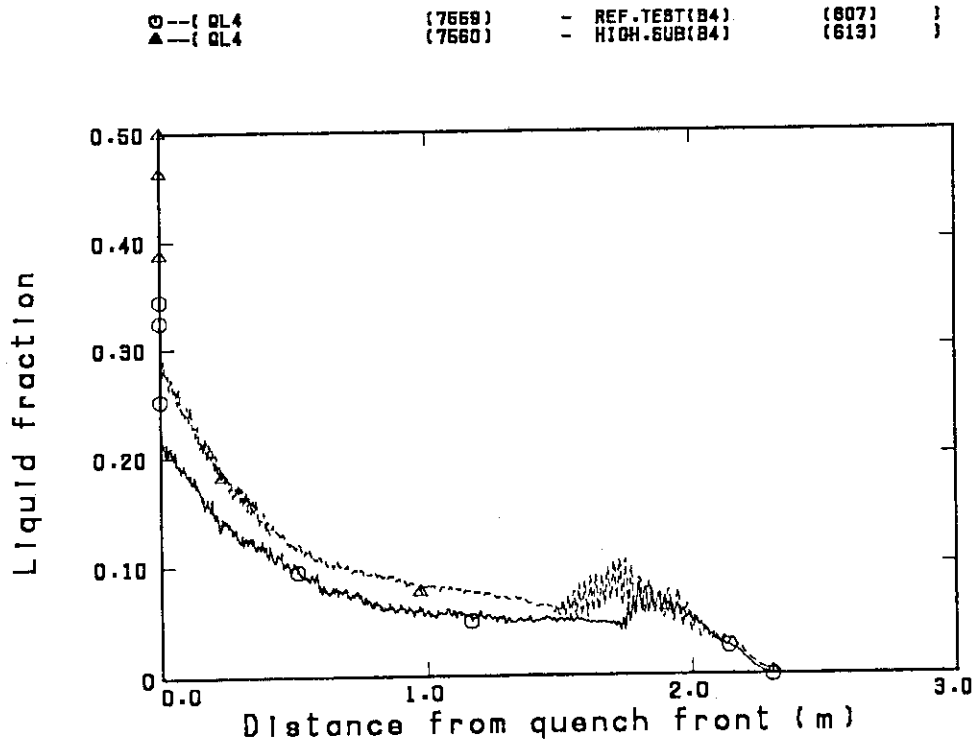

Fig.3.3.8(2) Comparison of liquid fraction in bundle 4 at 2.03-2.57m

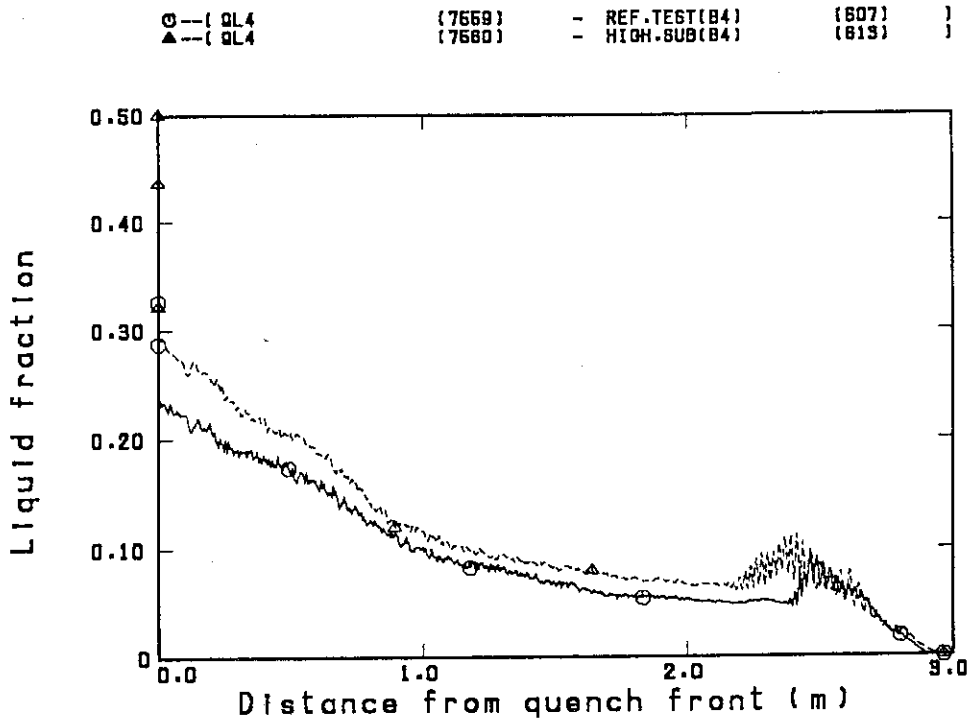

Fig.3.3.8(3) Comparison of liquid fraction in bundle 4 at 2.695-3.235m

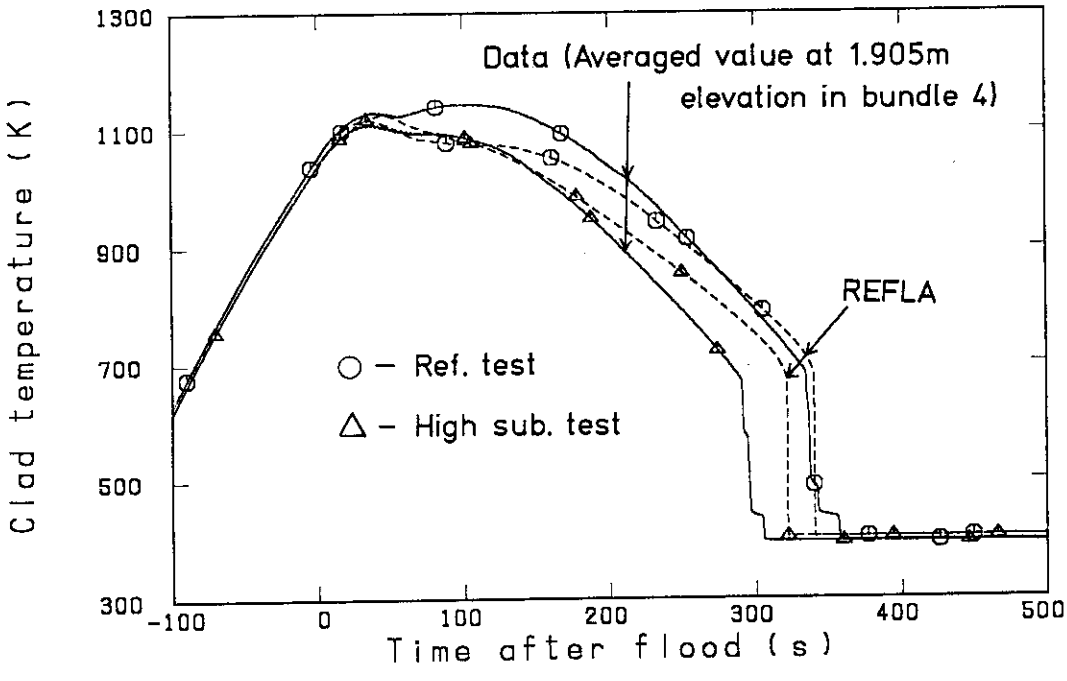

Fig.3.3.9 Comparison between data and predictions with REFLA code on clad surface temperature at 1.905m elevation in bundle 4

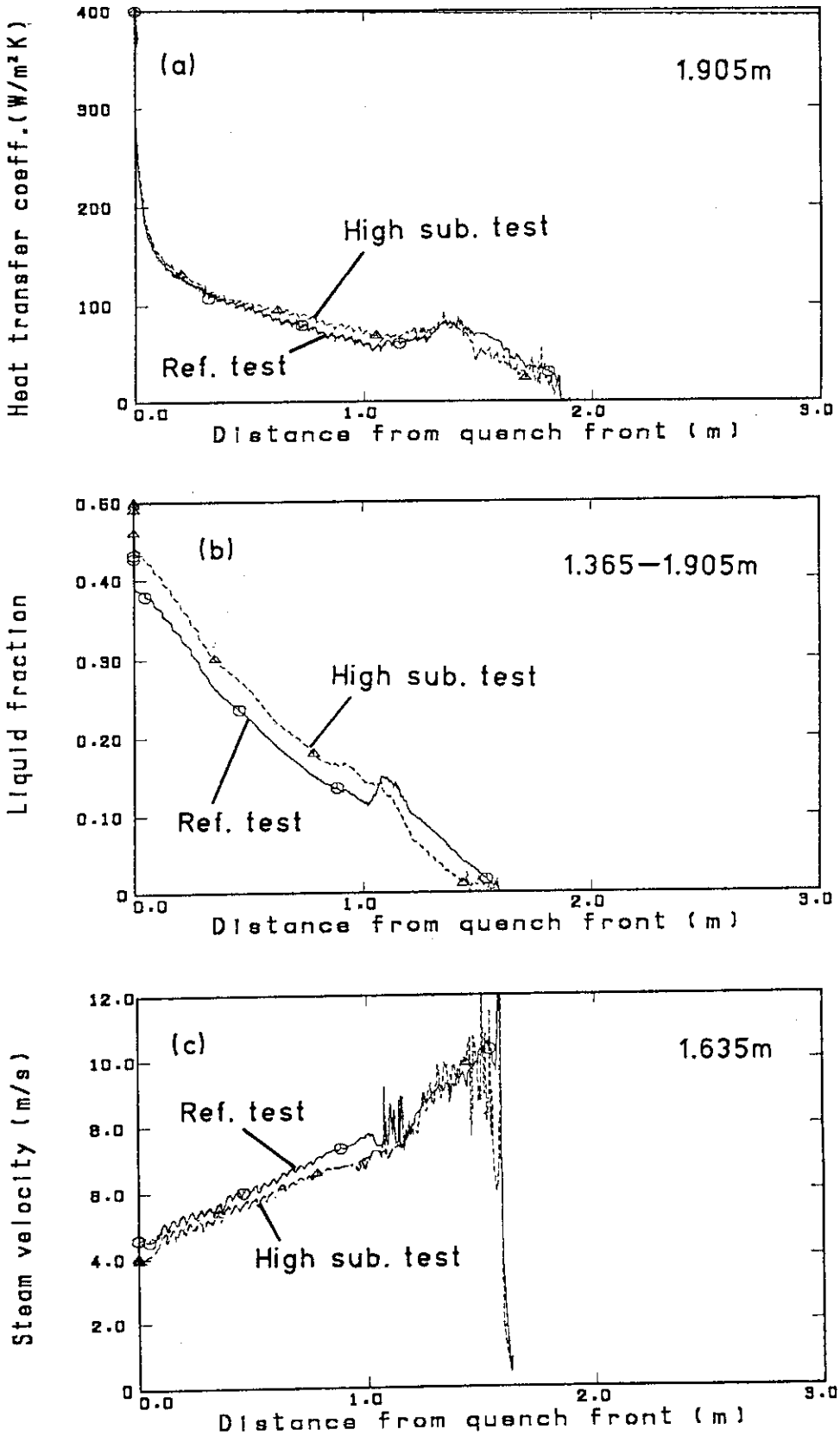

Fig.3.3.10 Comparison of the following values predicted with REFLA code: (a)Heat transfer coefficient, (b)Liquid fraction and (c)Steam velocity

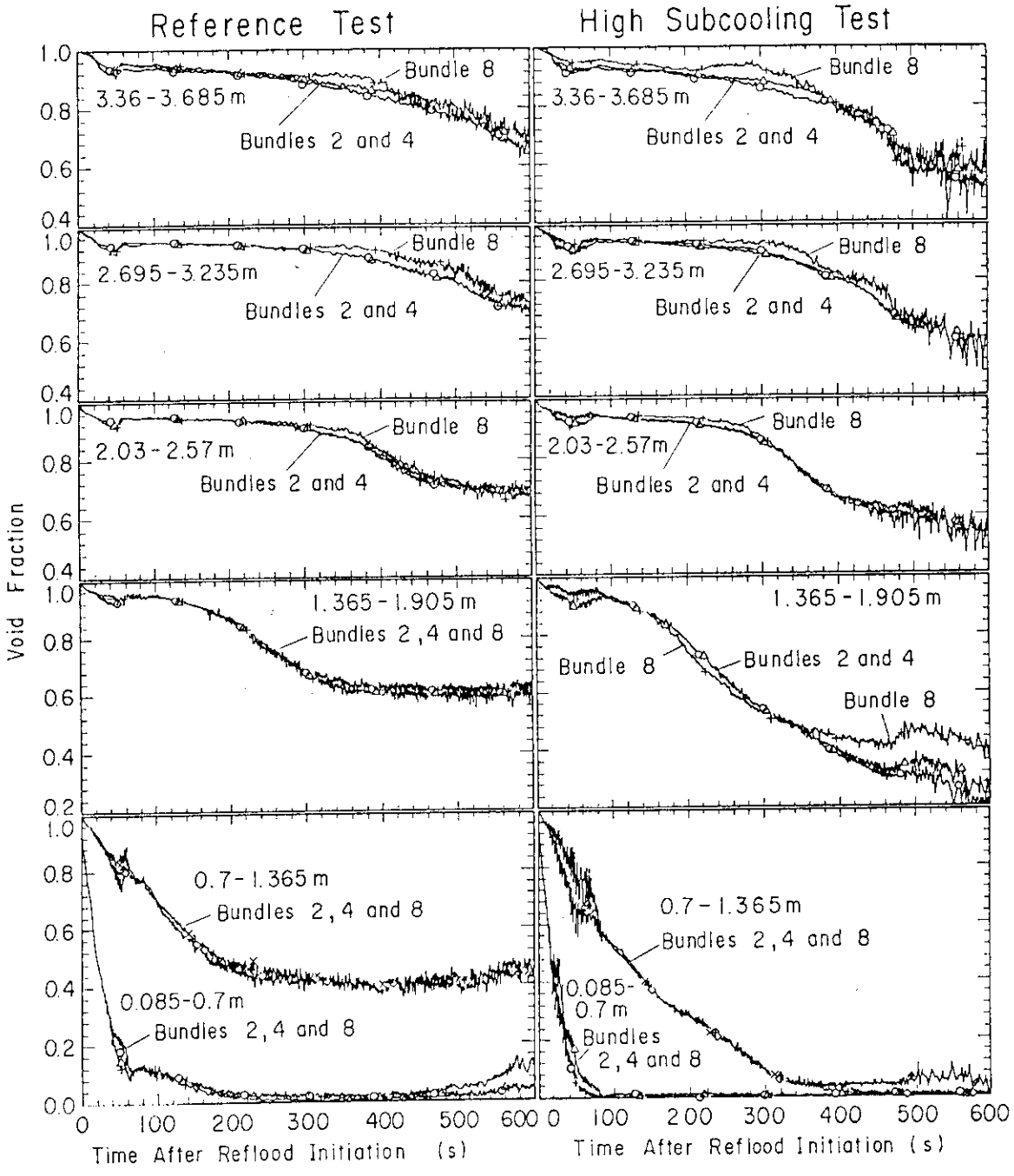

Fig.3.4.1 Comparison of radial distribution of sectional void fraction

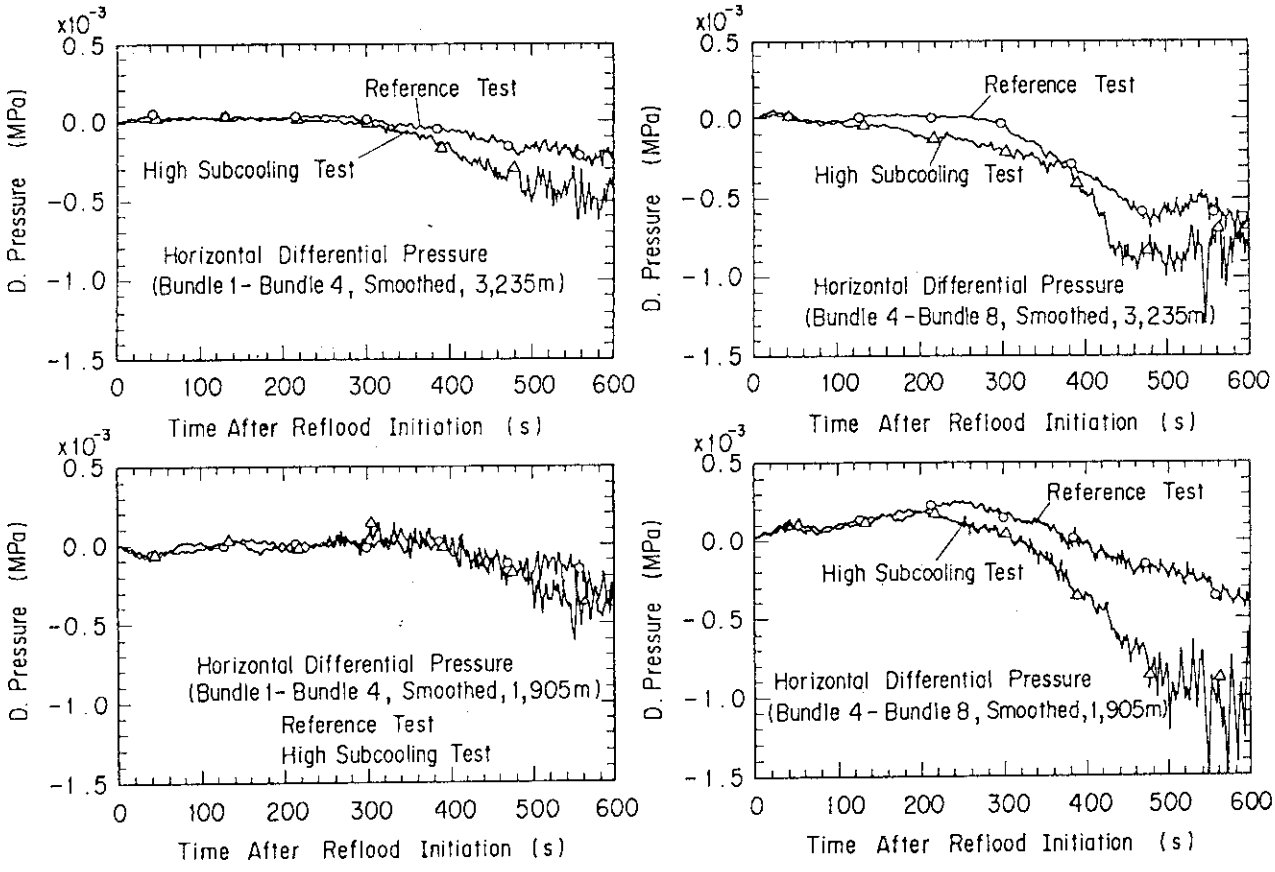

Fig.3.4.2 Comparison of horizontal differential pressure in core

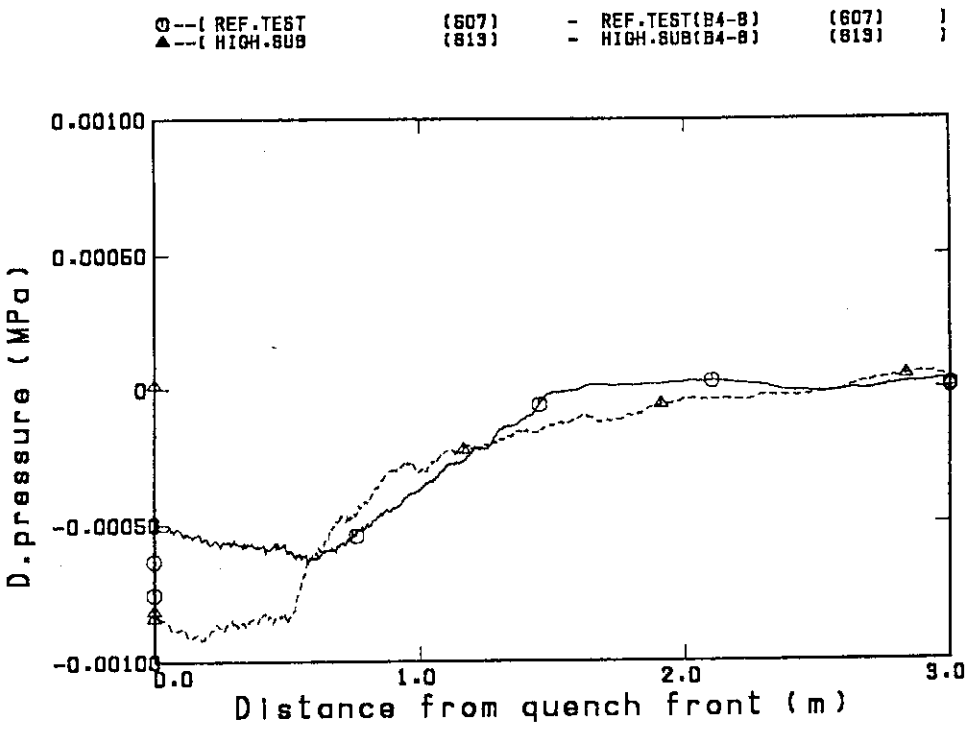

Fig.3.4.3(1) Comparison of horizontal differential pressure at 3.235m

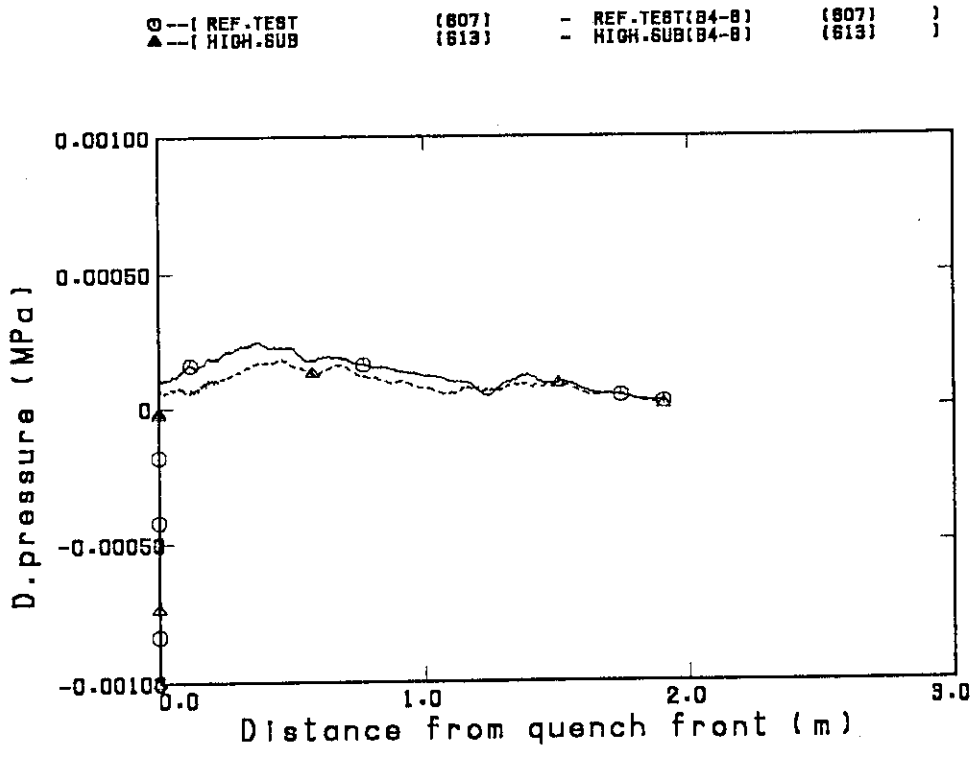

Fig.3.4.3(2) Comparison of horizontal differential pressure at 1.905m

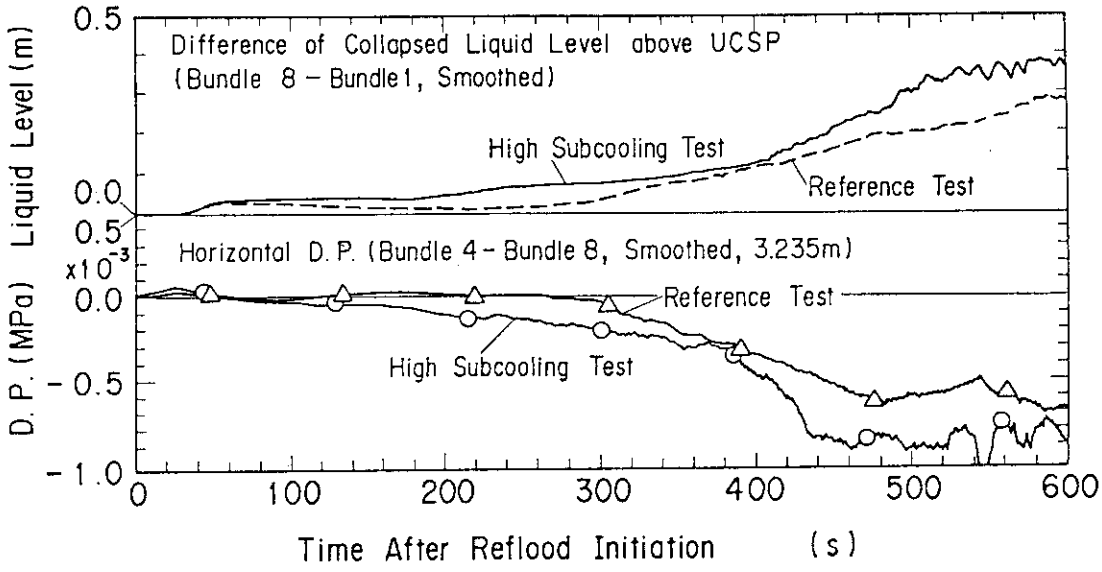

Fig.3.4.3(3) Comparison of radial difference of liquid level in upper plenum with horizontal differential pressure

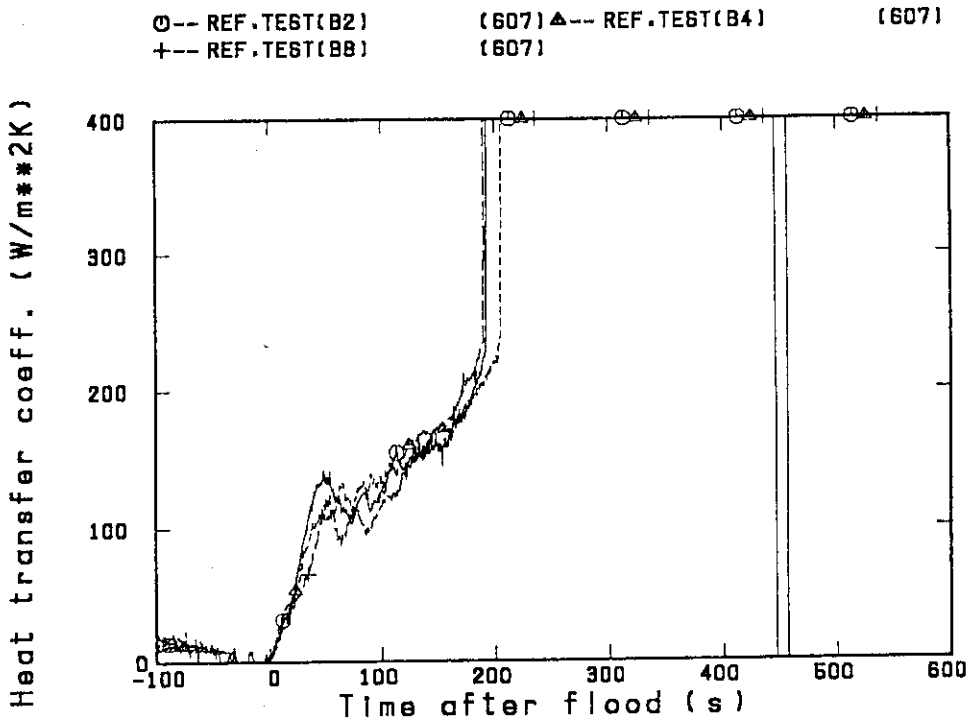

Fig.3.4.4(1) Radial comparison of heat transfer coefficient at 1.38m in reference test

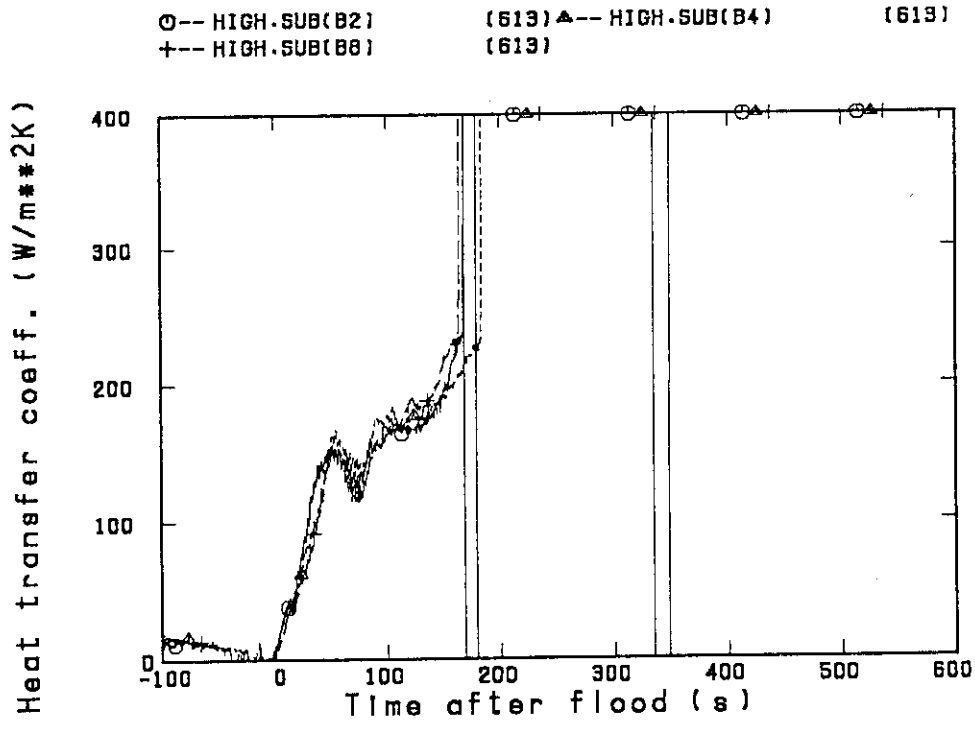

Fig.3.4.4(2) Radial comparison of heat transfer coefficient at 1.38m in high sub. test

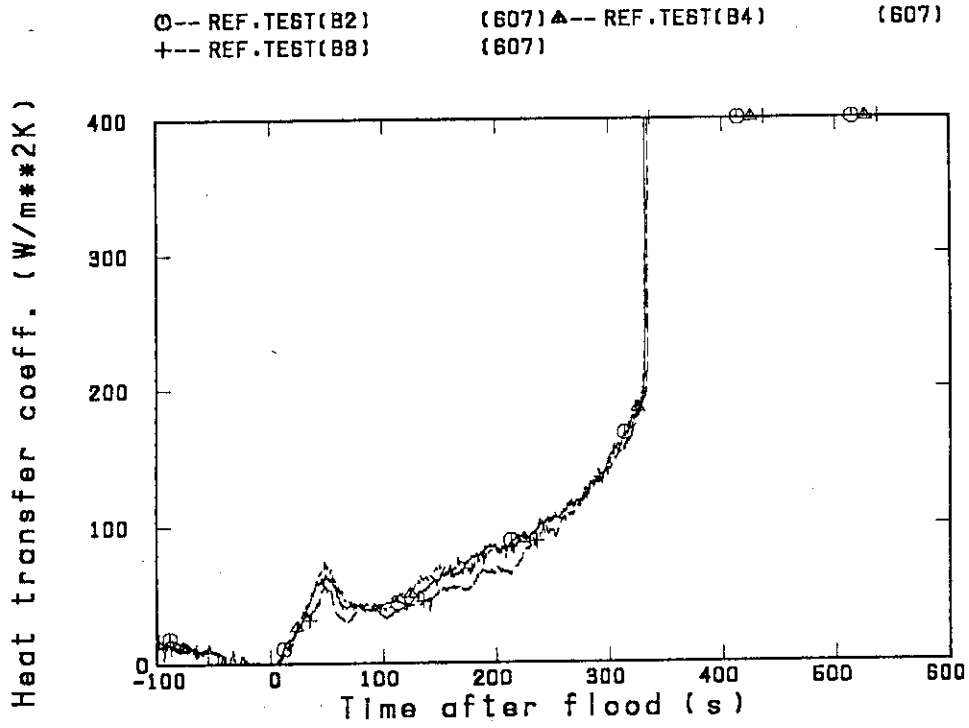

Fig.3.4.4(3) Radial comparison of heat transfer coefficient at 1.905m in reference test.

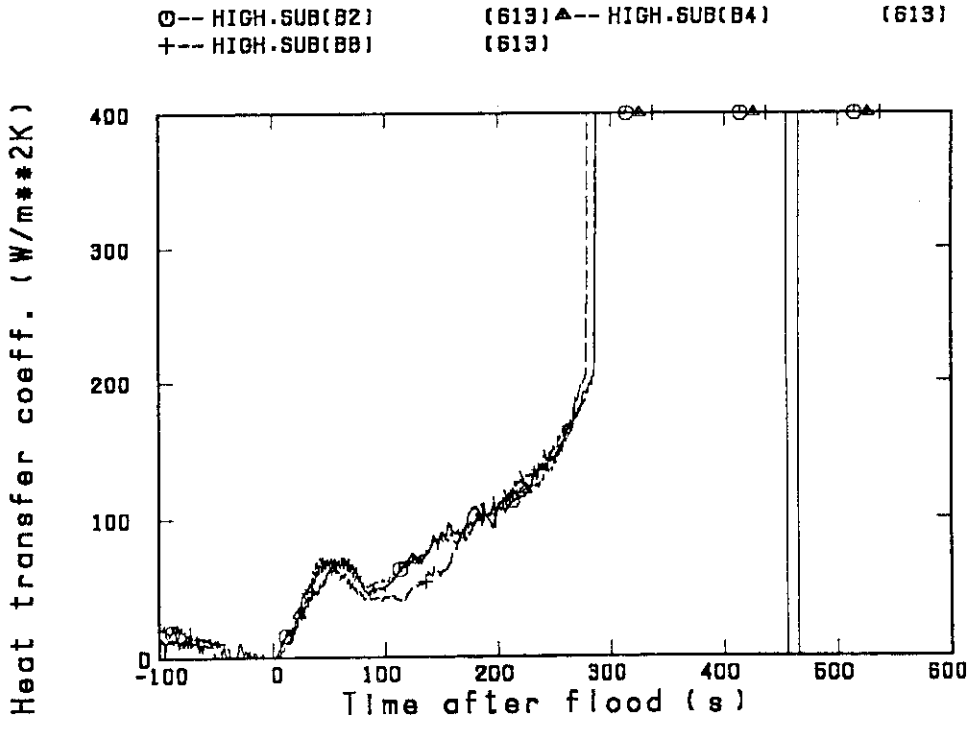

Fig.3.4.4(4) Radial comparison of heat transfer coefficient at 1.905m in high sub. test

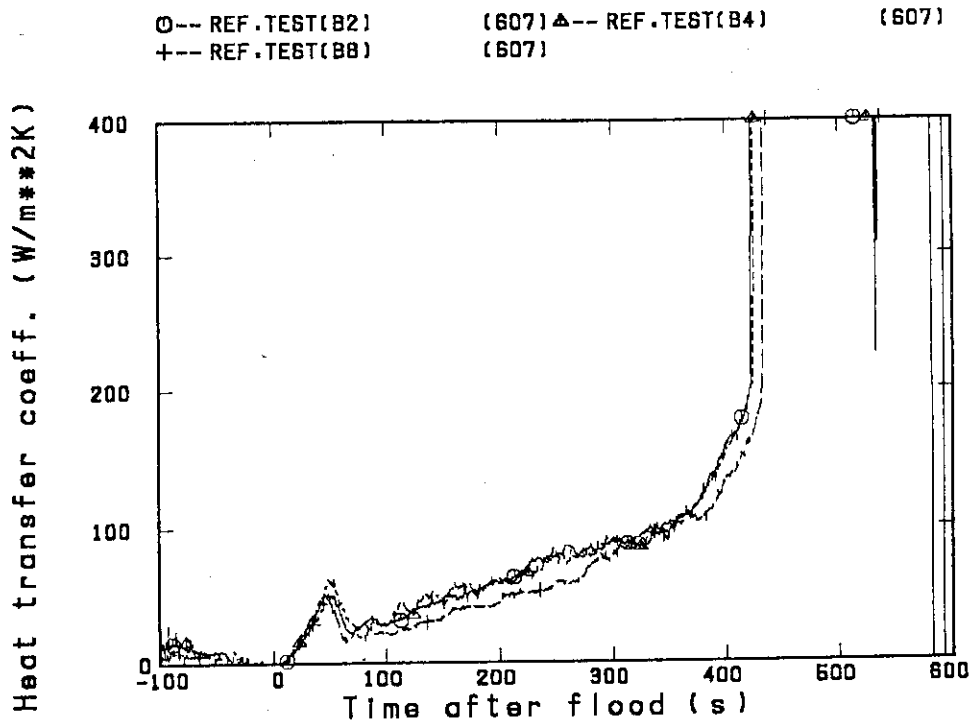

Fig.3.4.4(5) Radial comparison of heat transfer coefficient at 2.33 in reference test

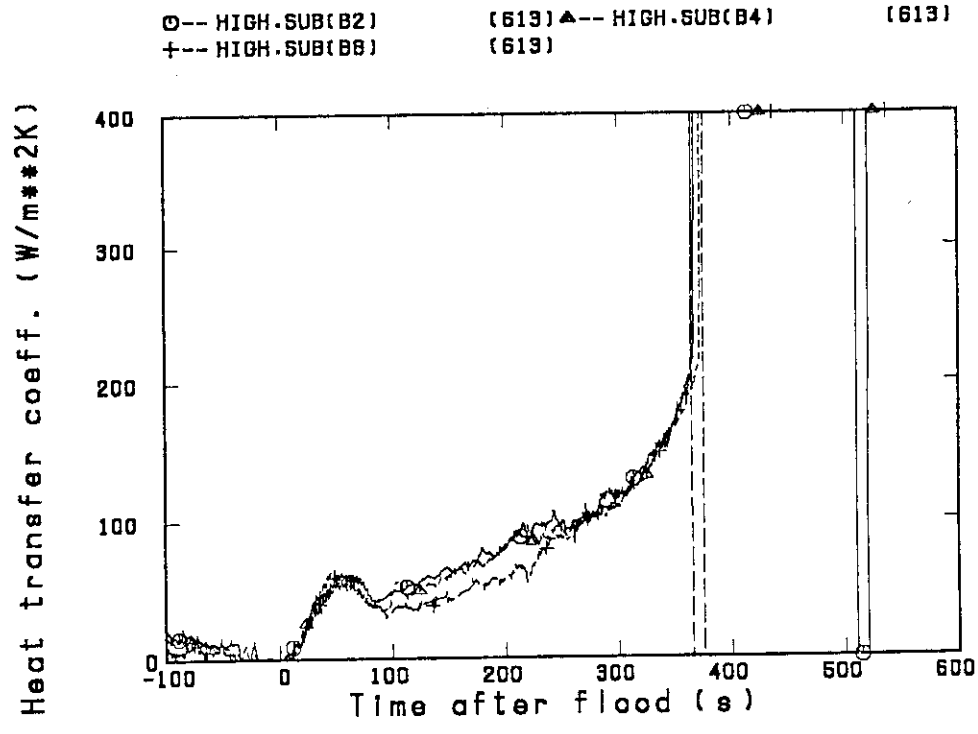

Fig.3.4.4(6) Radial comparison of heat transfer coefficient at 2.33m in high sub. test

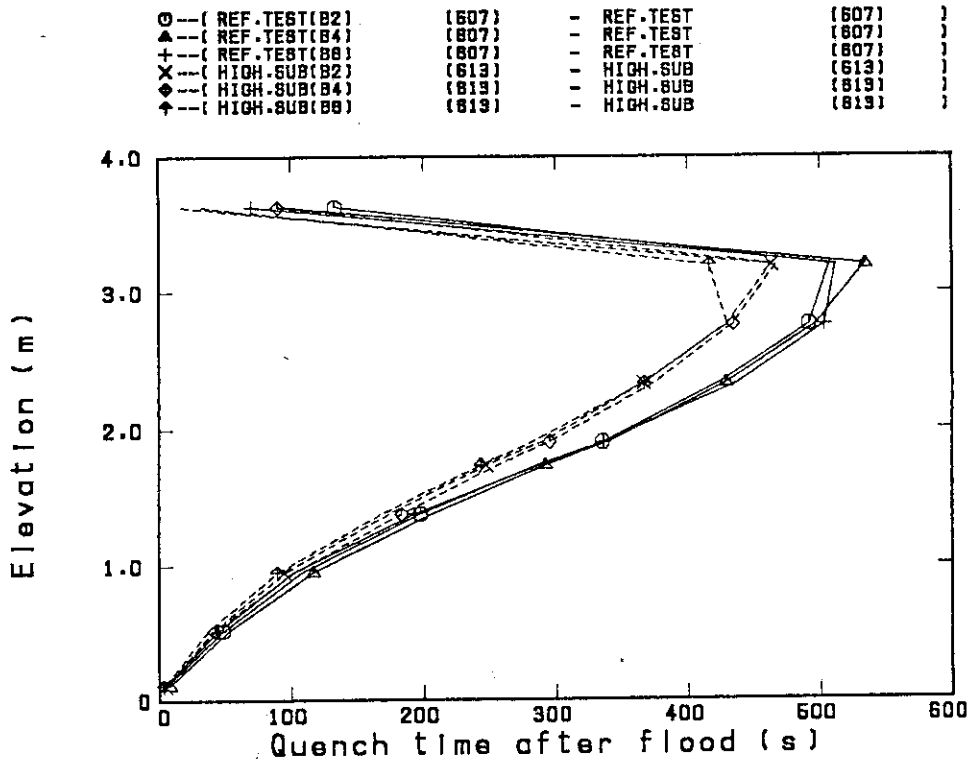

Fig.3.4.5 Comparison of quench time in bundles 2, 4 and 8

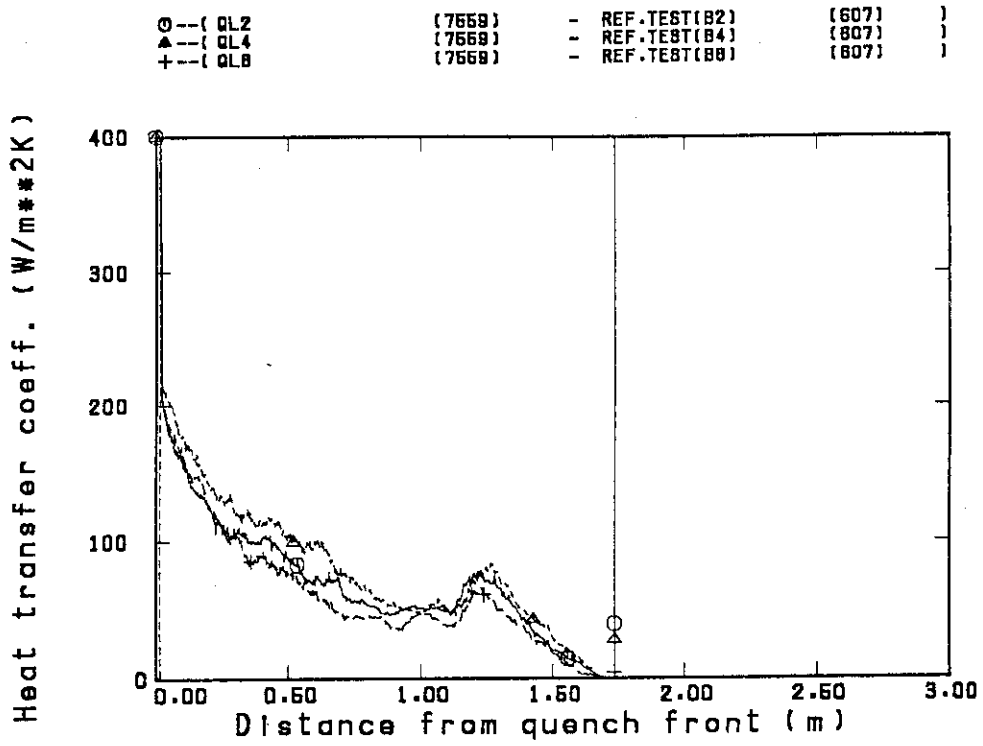

Fig.3.4.6(1) Radial comparison of heat transfer coefficient at 1.735m in reference test

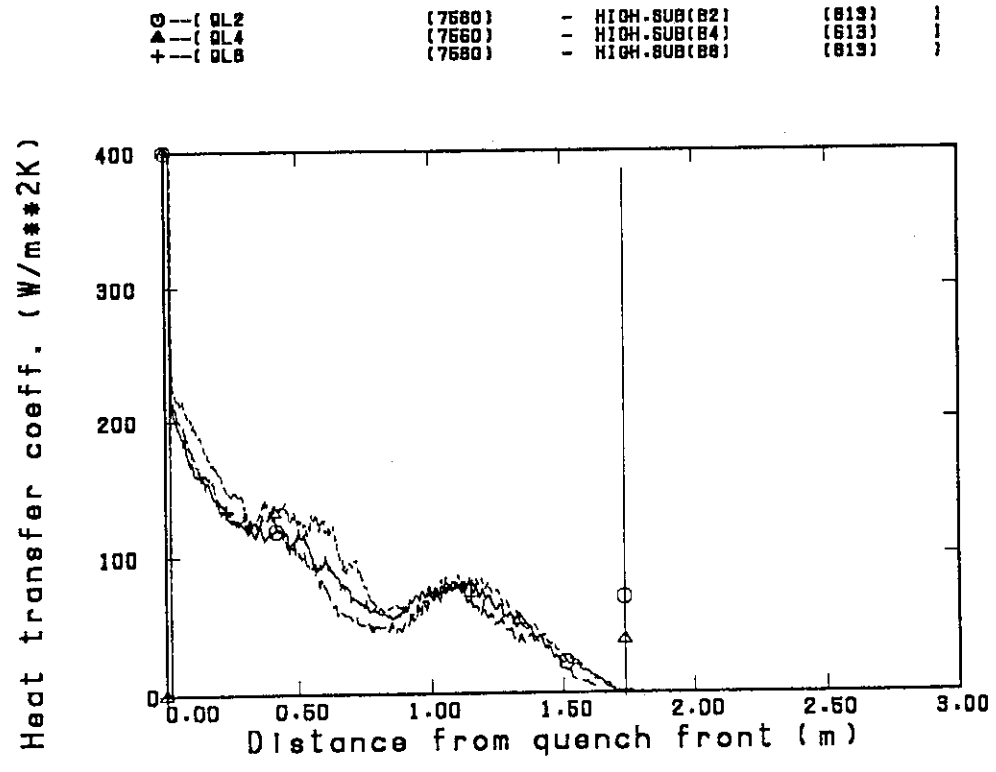

Fig.3.4.6(2) Radial comparison of heat transfer coefficient at 1.735m in high sub. test

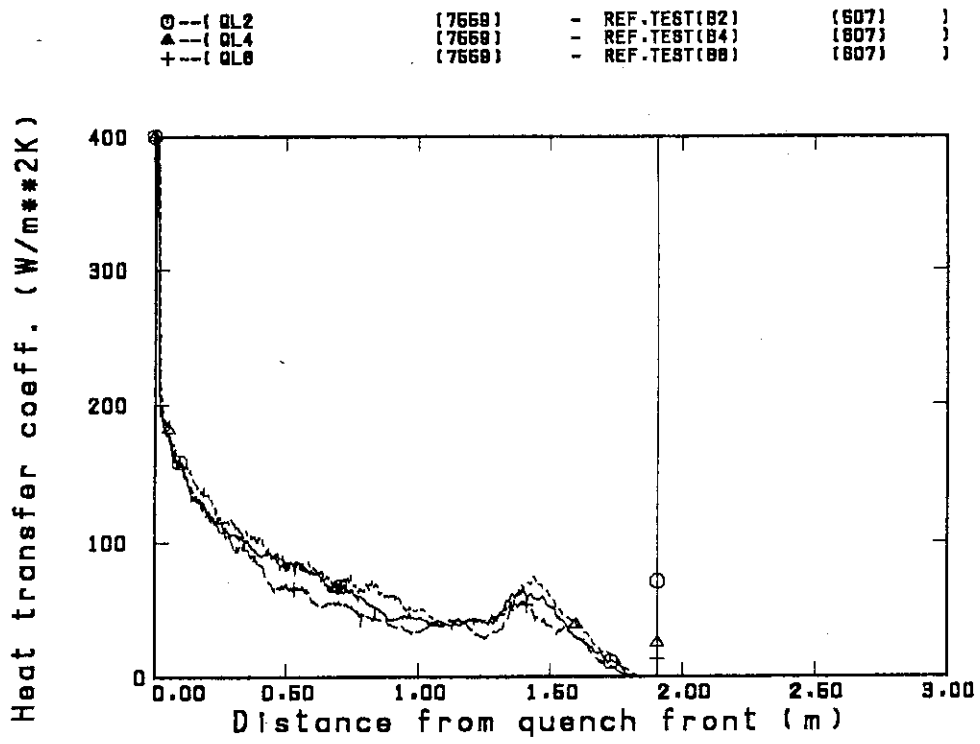

Fig.3.4.6(3) Radial comparison of heat transfer coefficient at 1.905m in reference test

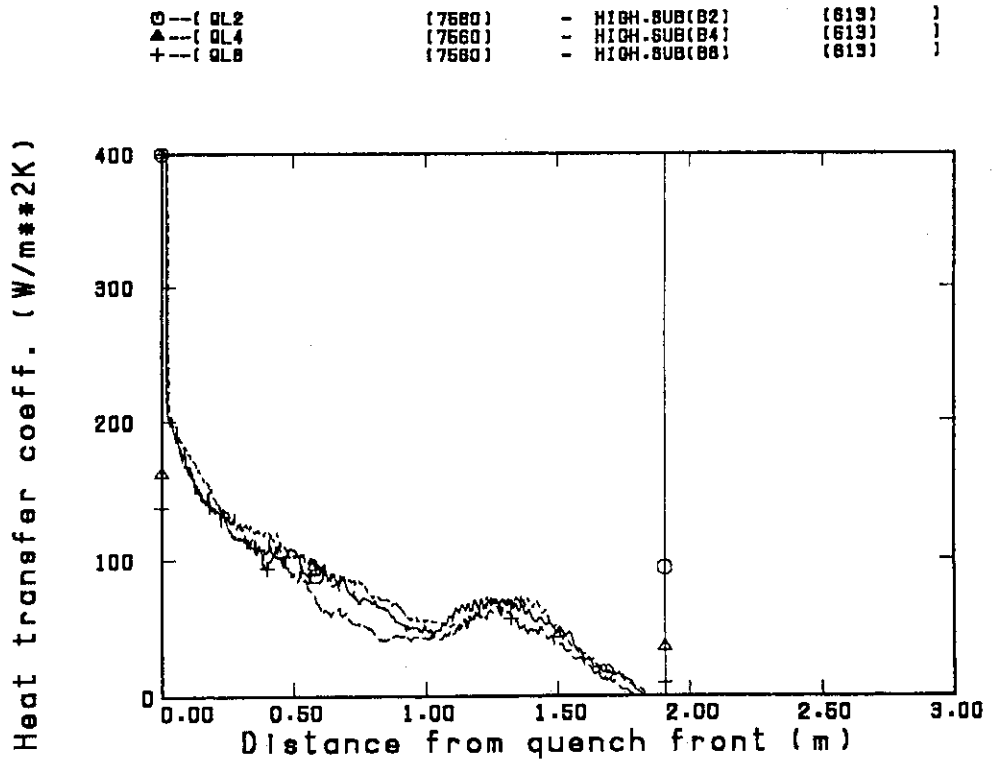

Fig.3.4.6(4) Radial comparison of heat transfer coefficient at 1.905m in high sub. test

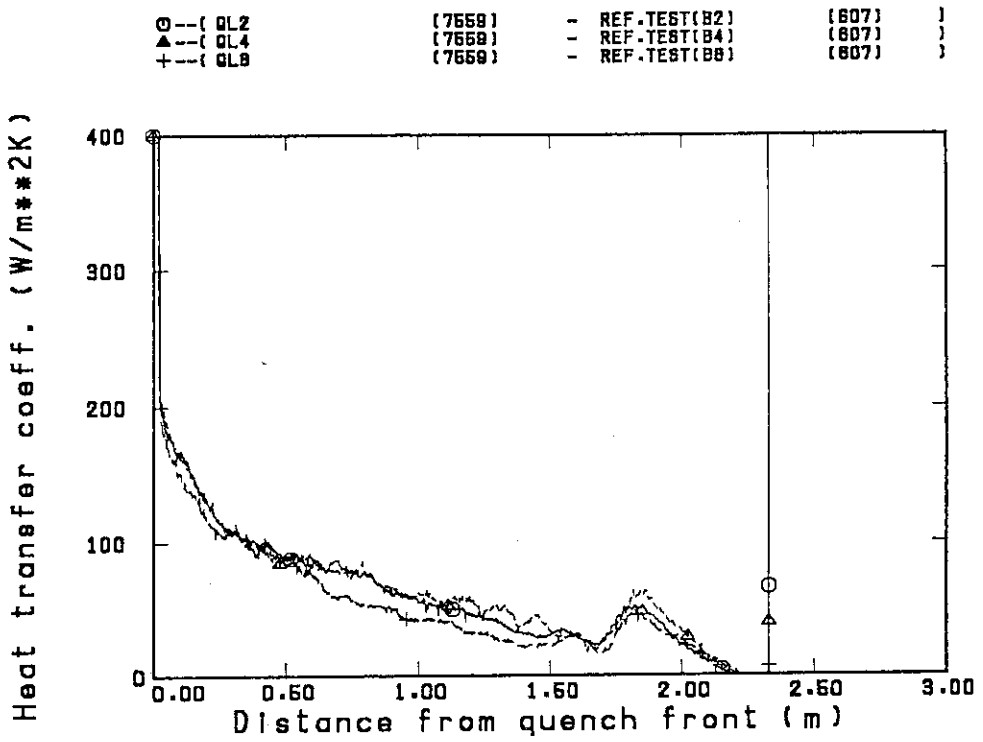

Fig.3.4.6(5) Radial comparison of heat transfer coefficient at 2.33m in reference test

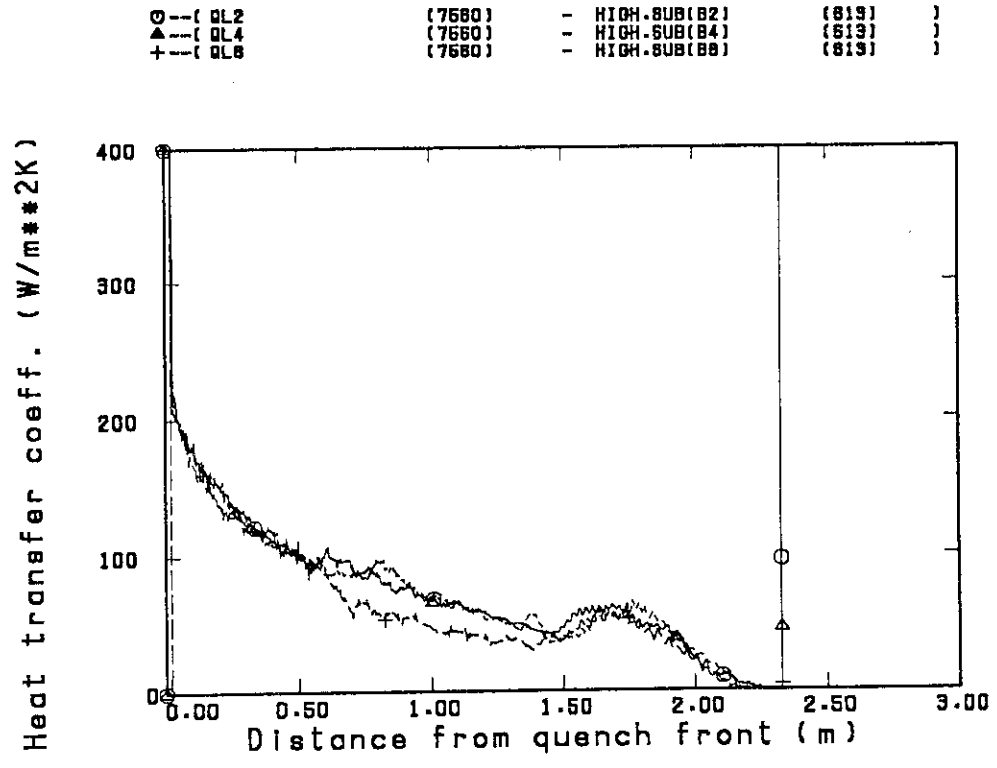

Fig.3.4.6(6) Radial comparison of heat transfer coefficient at 2.33m in high sub. test

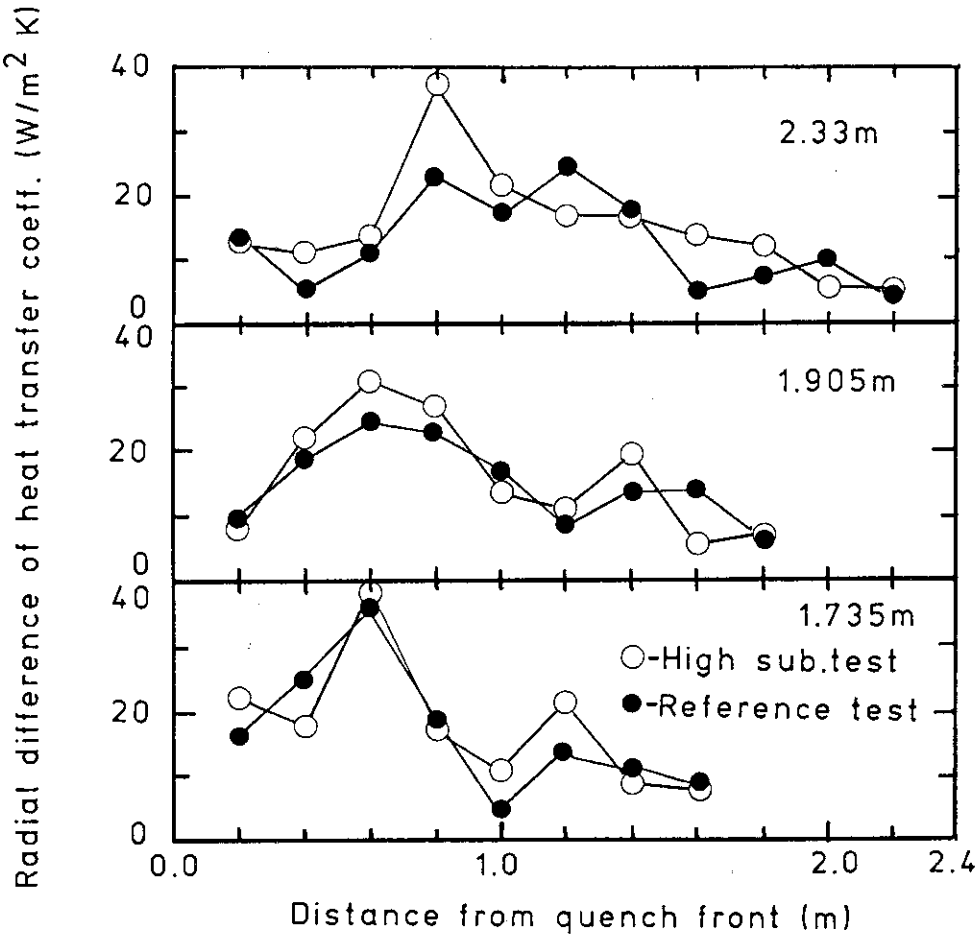

Fig.3.4.7 Comparison of radial difference of heat transfer coefficient

Appendix

Selected Data of Test S2-08

Locations of selected data in this appendix are shown in the following figures,

Fig. A-1 Thermocouple Locations of Heater Rod Surface Temperature Measurements,

Fig. A-2 Thermocouple Locations of Fluid Temperature Measurement just above and below End Box Tie Plate,

Fig. A-3 Thermocouple Locations of Fluid Temperature Measurements at Core Inlet,

Fig. A-4 Locations of Differential Pressure Measurements across End Box Tie Plate and Liquid Level Measurements above UCSP and End Box Tie Plate,

Fig. A-5 Locations of Hot Leg Instruments,

Fig. A-6 Locations of Vertical Differential Pressure Measurements in Core and

Fig. A-7 Measurement Locations of Horizontal Differential Pressures in Core and Differential Pressures in Upper Plenum.

List of figures for selected data

Figs. A-8~A-15	Heater rod temperature
Figs. A-16 and A-17	Fluid temperature just above end box tie plate
Figs. A-18 and A-19	Fluid temperature at core inlet
Figs. A-20 and A-21	Liquid level above UCSP
Figs. A-22	Liquid level in hot leg
Figs. A-23 and A-24	Differential pressure of core full height
Figs. A-25 and A-26	Differential pressure across end box tie plate
Figs. A-27~A-29	Horizontal differential pressure in core

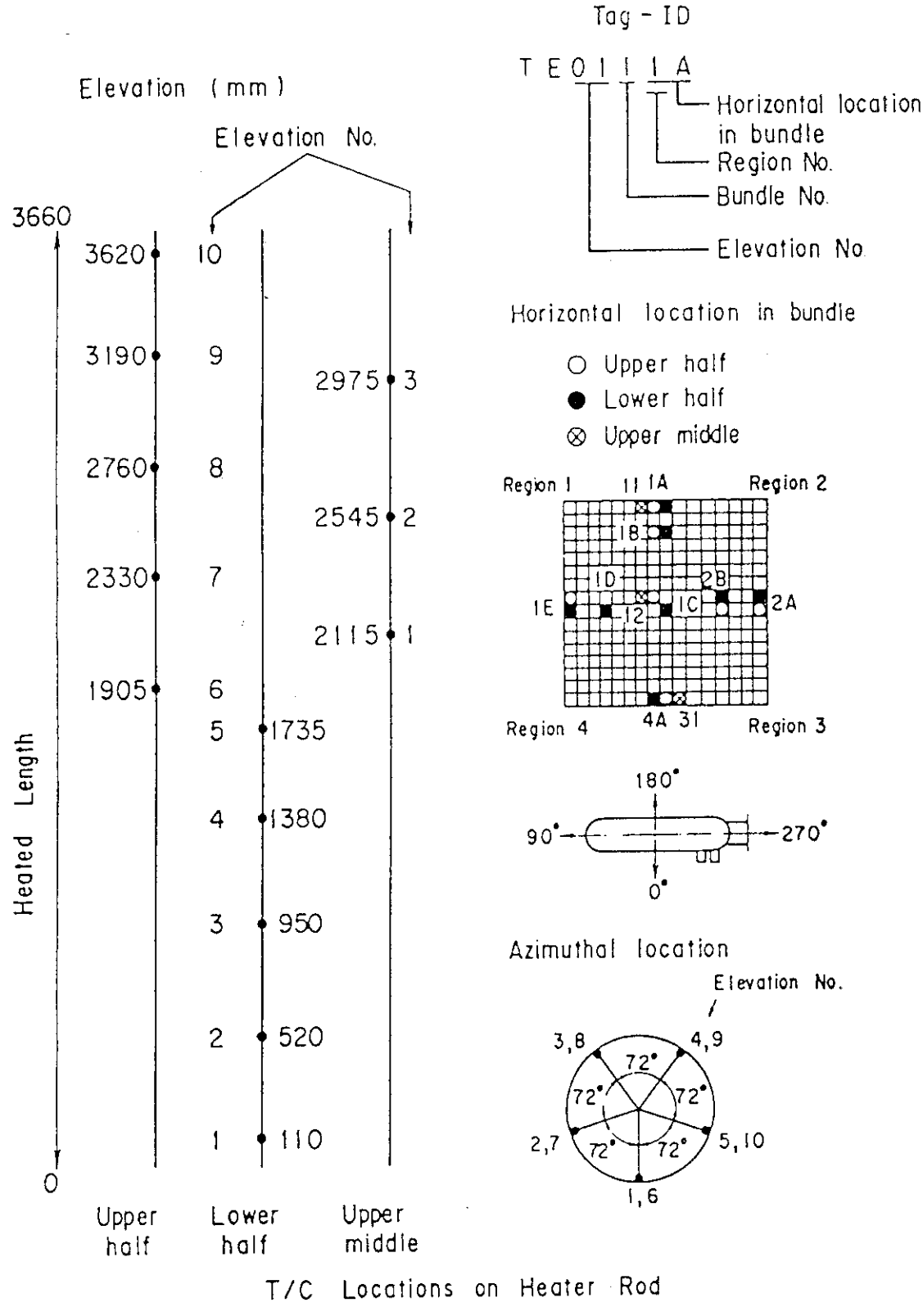

Fig. A-1 Thermocouple Locations of Heater Rod Surface Temperature Measurements,

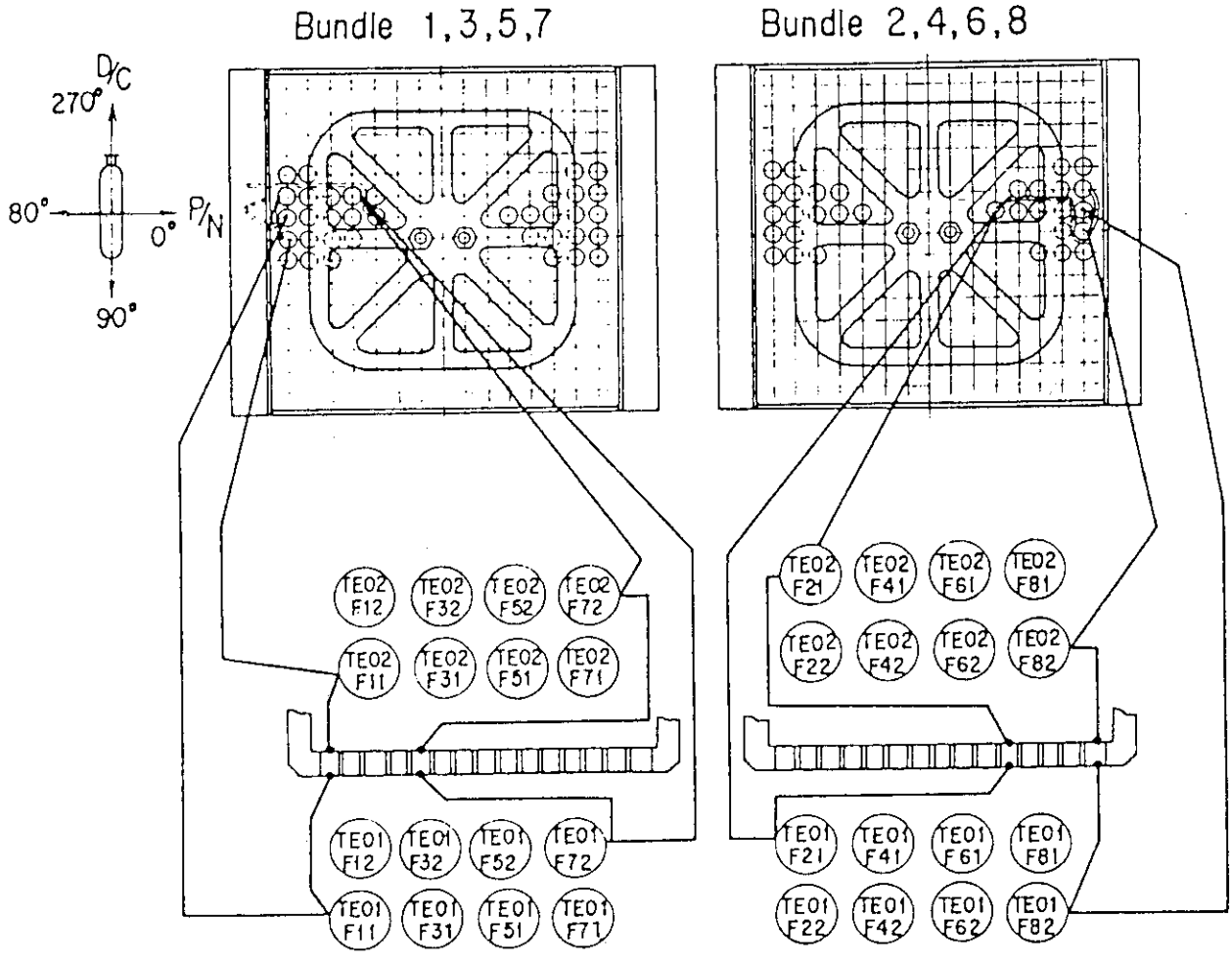

Fig. A-2 Thermocouple Locations of Fluid Temperature Measurement just above and below End Box Tie Plate,

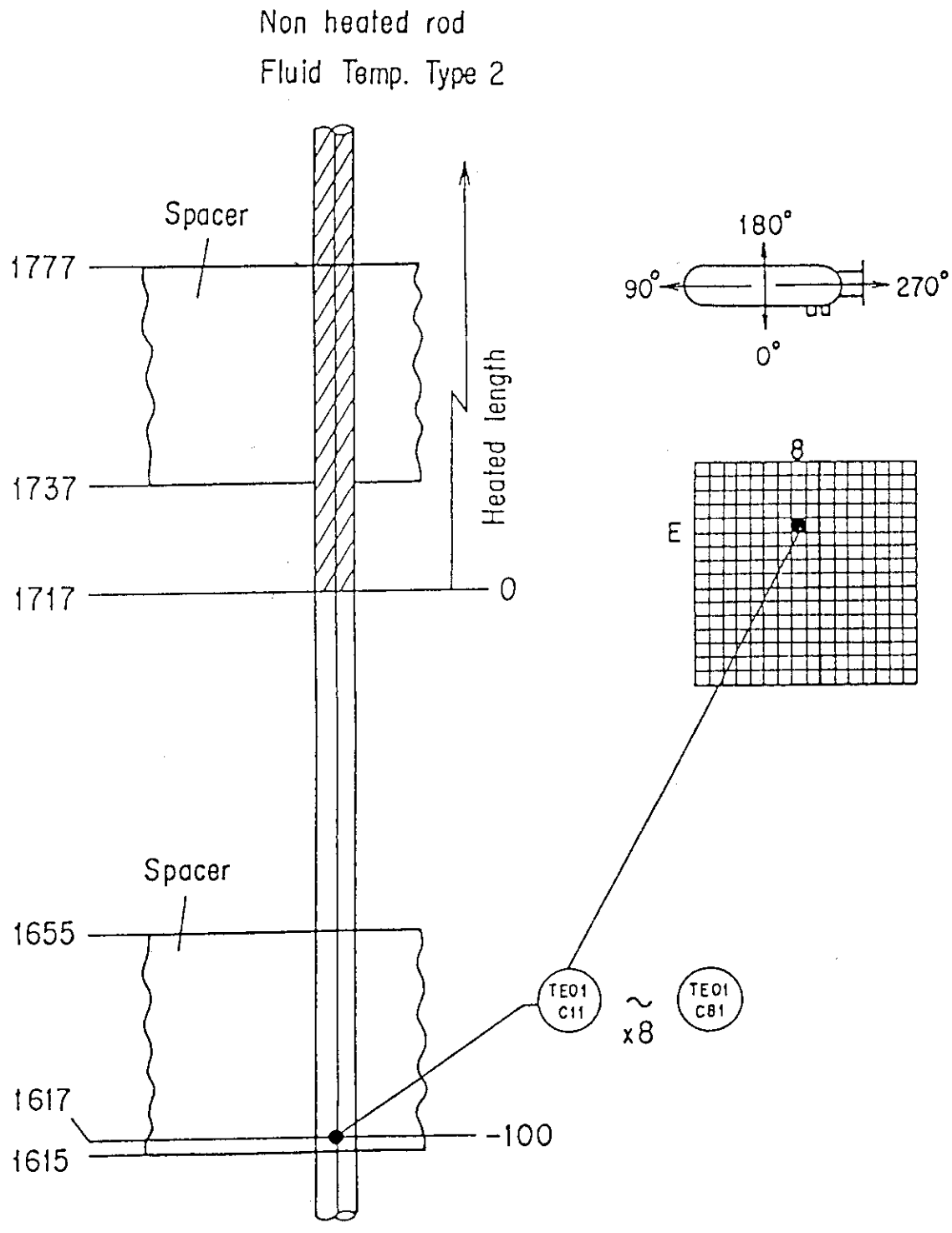

Fig. A-3 Thermocouple Locations of Fluid Temperature Measurements at Core Inlet,

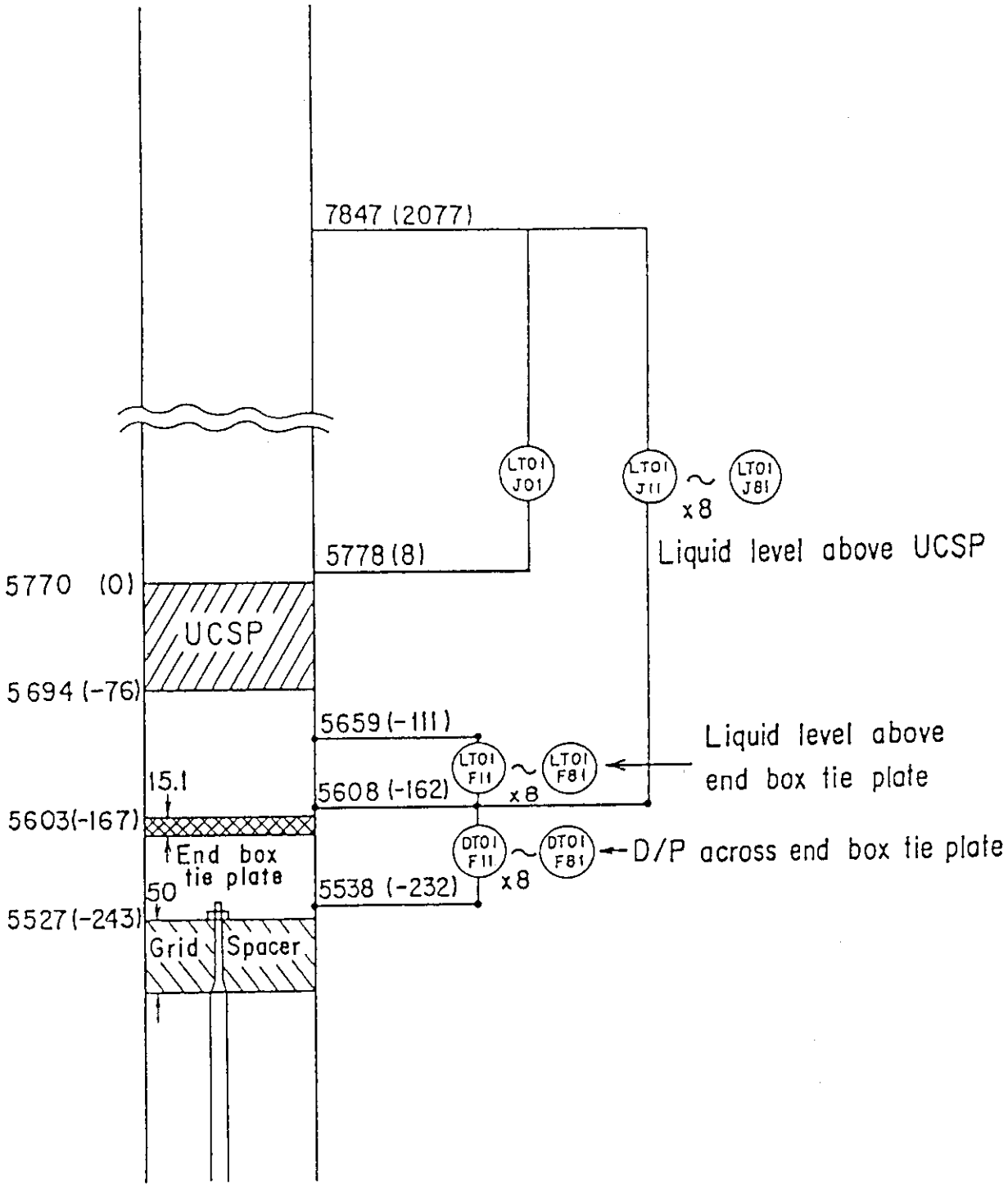

Fig. A-4 Locations of Differential Pressure Measurements across End Box Tie Plate and Liquid Level Measurements above UCSP and End Box Tie Plate,

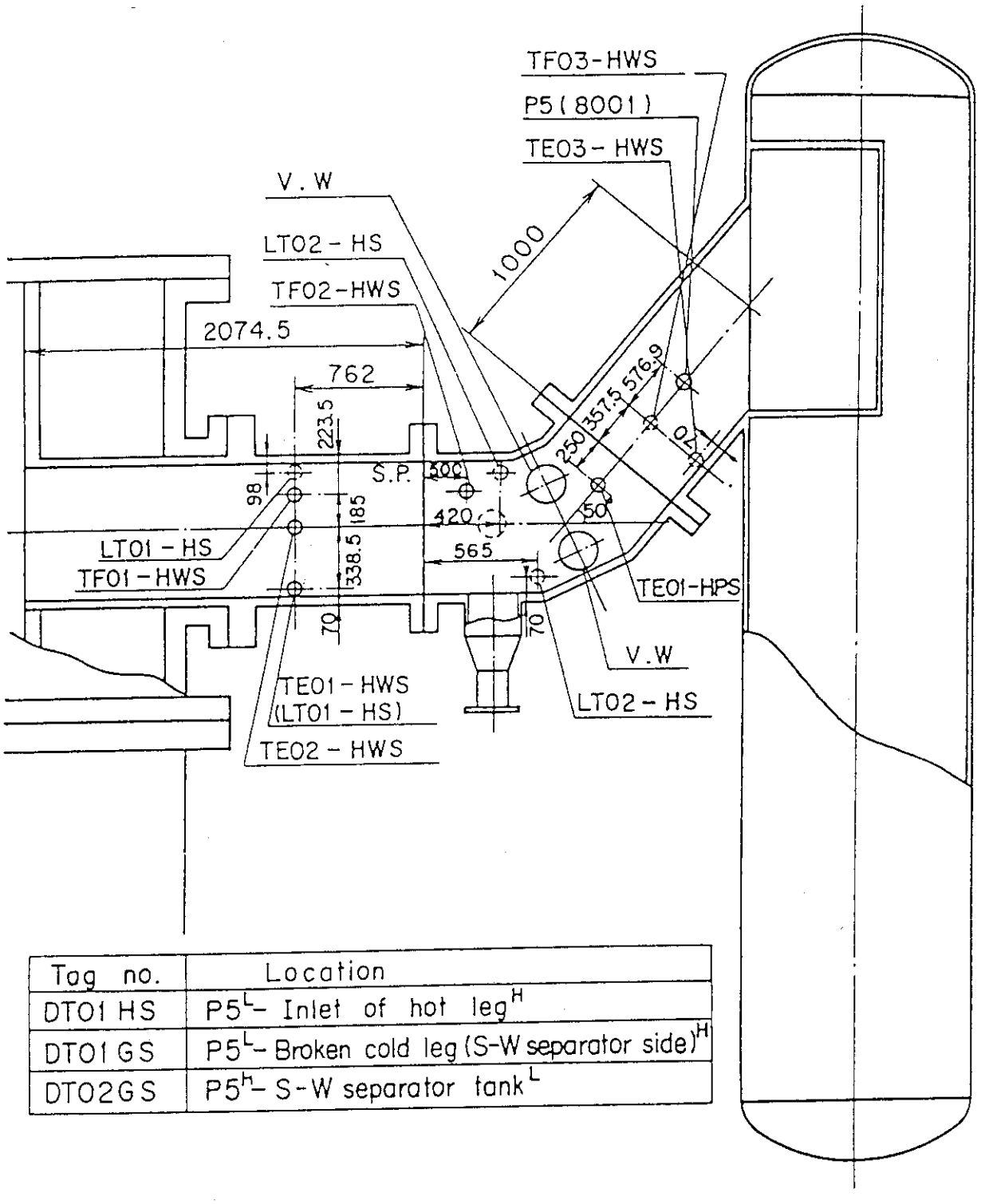

Tag no.	Location
DT01HS	P5[L]－Inlet of hot leg[H]
DT01GS	P5[L]－Broken cold leg (S-W separator side)[H]
DT02GS	P5[H]－S-W separator tank[L]

Fig. A-5 Locations of Hot Leg Instruments,

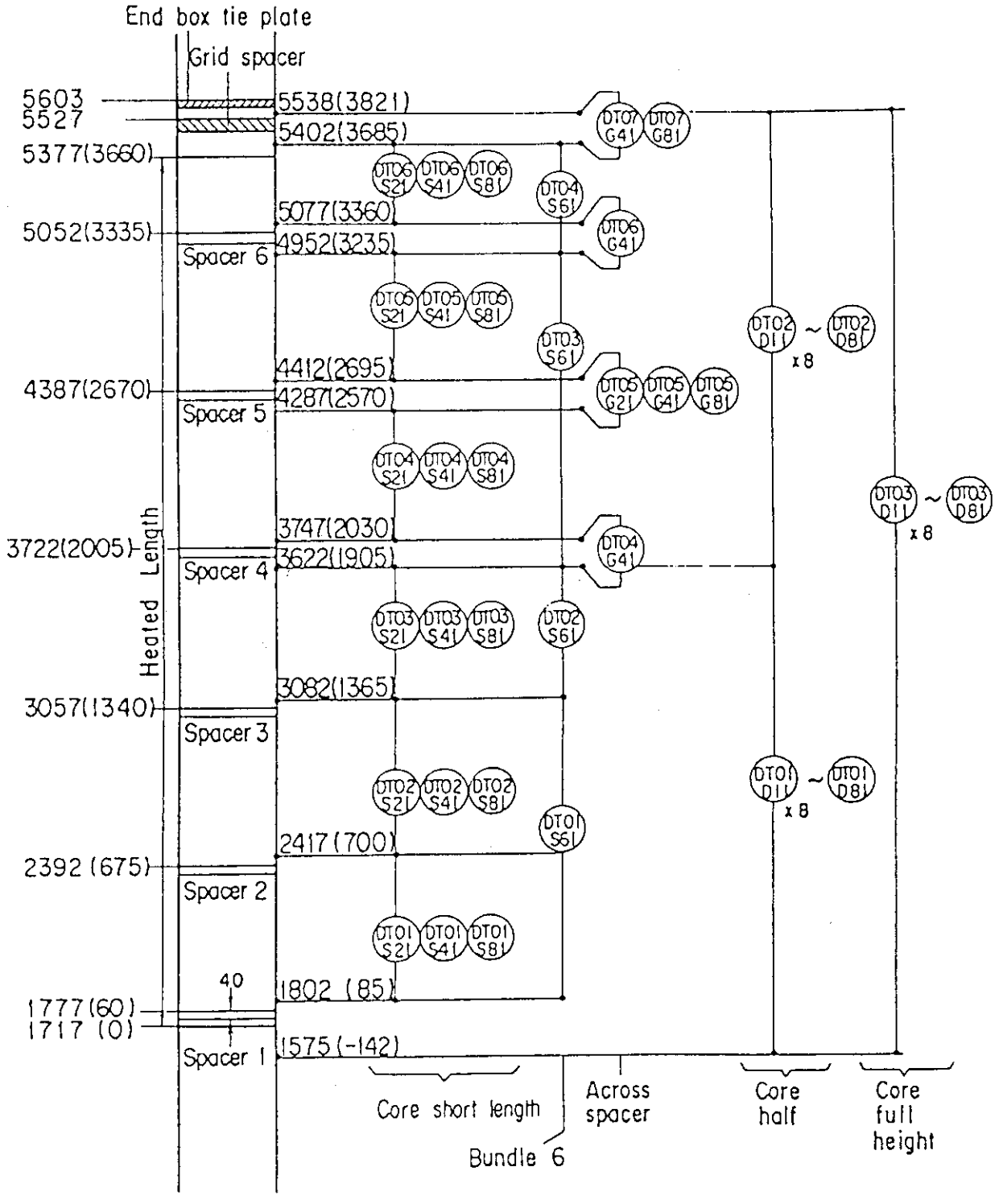

Fig. A-6 Locations of Vertical Differential Pressure Measurements in Core

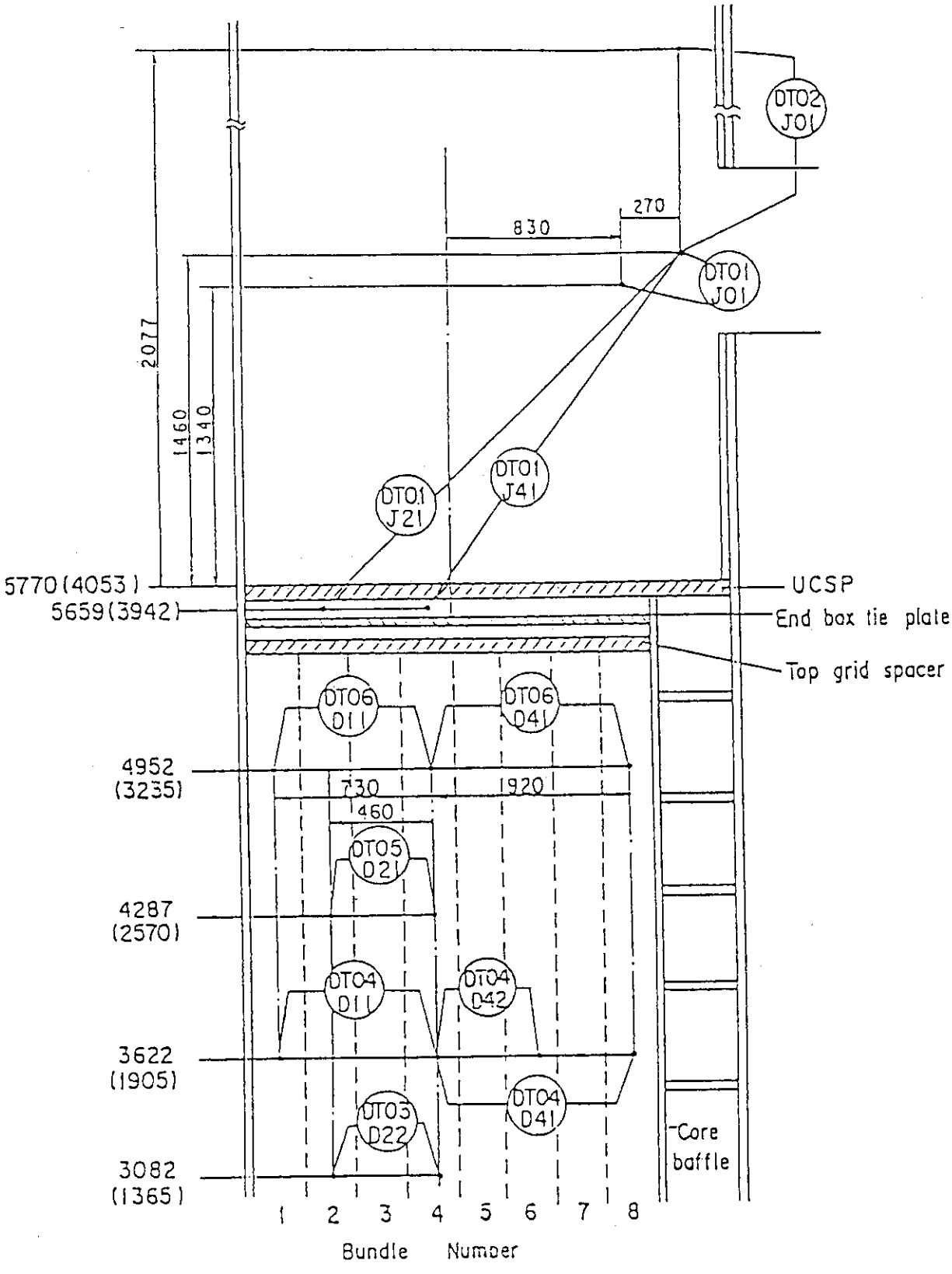

Fig. A-7 Measurement Locations of Horizontal Differential Pressures in Core and Differential Pressures in Upper Plenum.

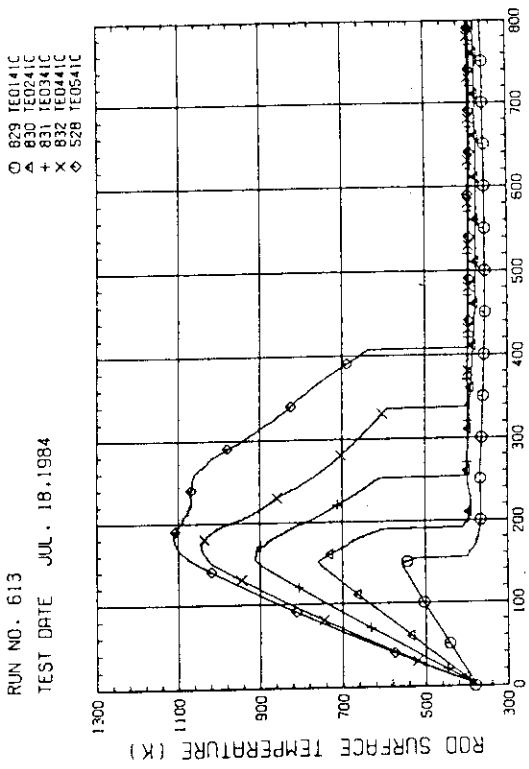

Fig. A－10 HEATER ROD TEMPERATURE (BUNDLE 4-1C, LOWER HALF)

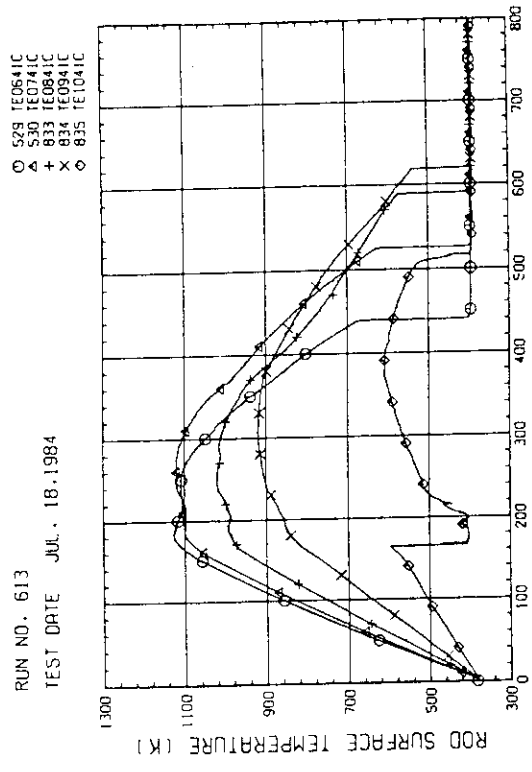

Fig. A－11 HEATER ROD TEMPERATURE (BUNDLE 4-1C, UPPER HALF)

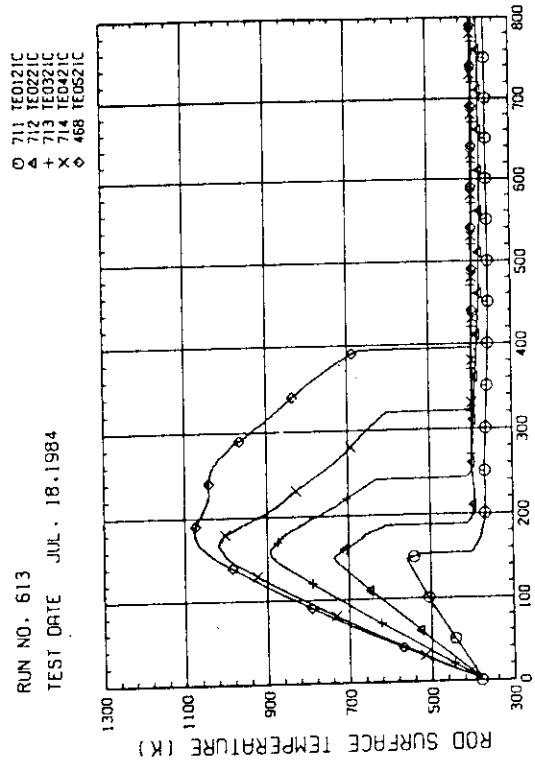

Fig. A－8 HEATER ROD TEMPERATURE (BUNDLE 2-1C, LOWER HALF)

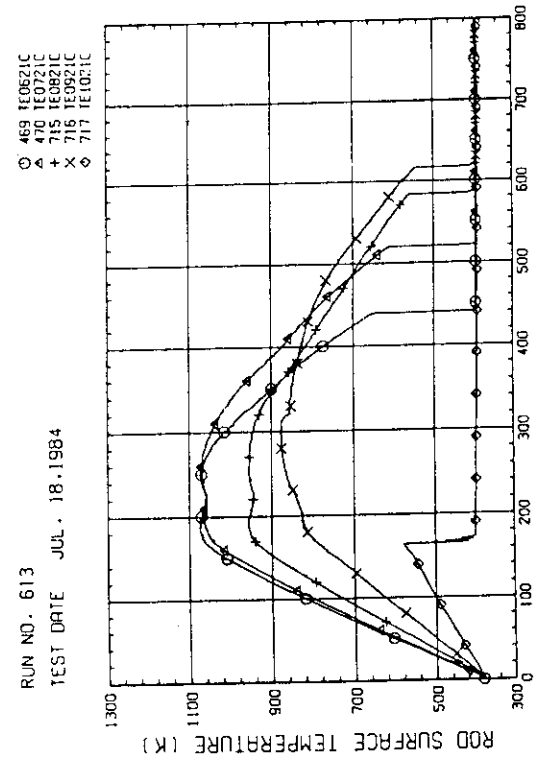

Fig. A－9 HEATER ROD TEMPERATURE (BUNDLE 2-1C, UPPER HALF)

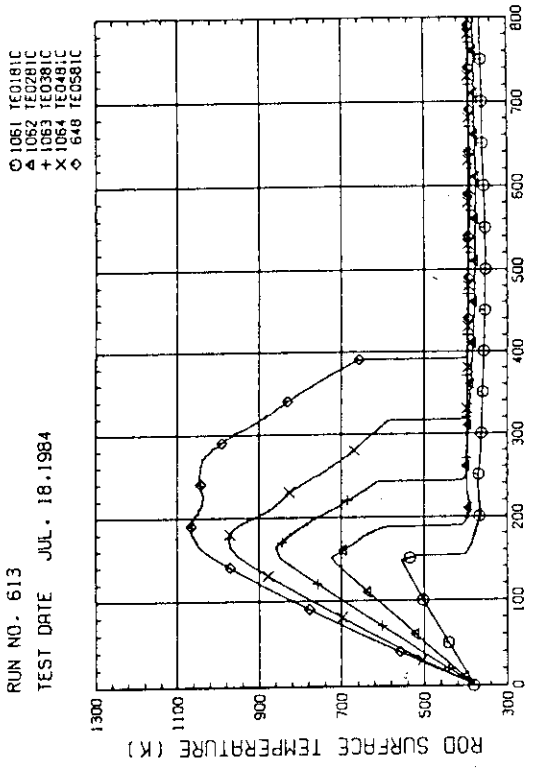

Fig. A－12 HEATER ROD TEMPERATURE (BUNDLE 6-IC, LOWER HALF)

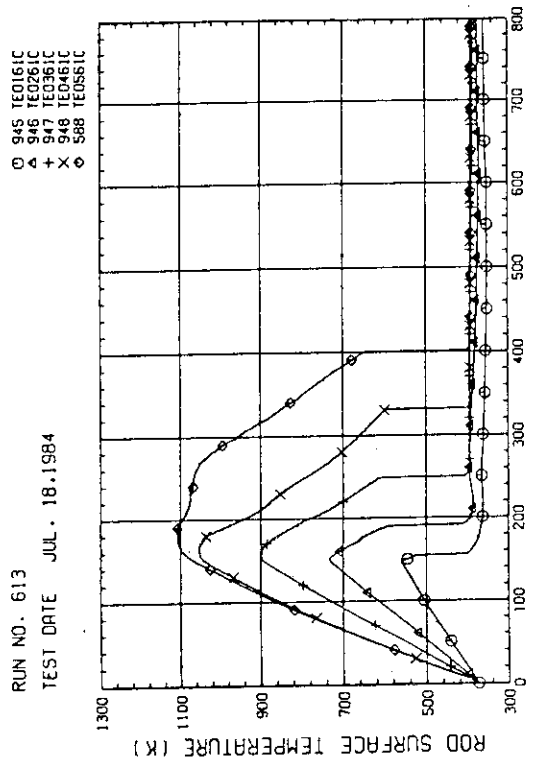

Fig. A－13 HEATER ROD TEMPERATURE (BUNDLE 6-IC, UPPER HALF)

Fig. A－14 HEATER ROD TEMPERATURE (BUNDLE 8-IC, LOWER HALF)

Fig. A－15 HEATER ROD TEMPERATURE (BUNDLE 8-IC, UPPER HALF)

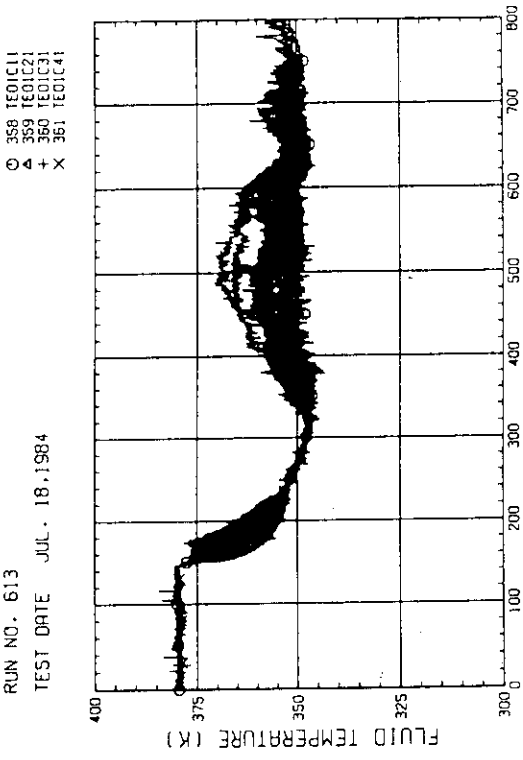

Fig. A－18 FLUID TEMPERATURE AT CORE INLET (BUNDLE 1.2.3.4. 100MM BELOW HEATED PART)

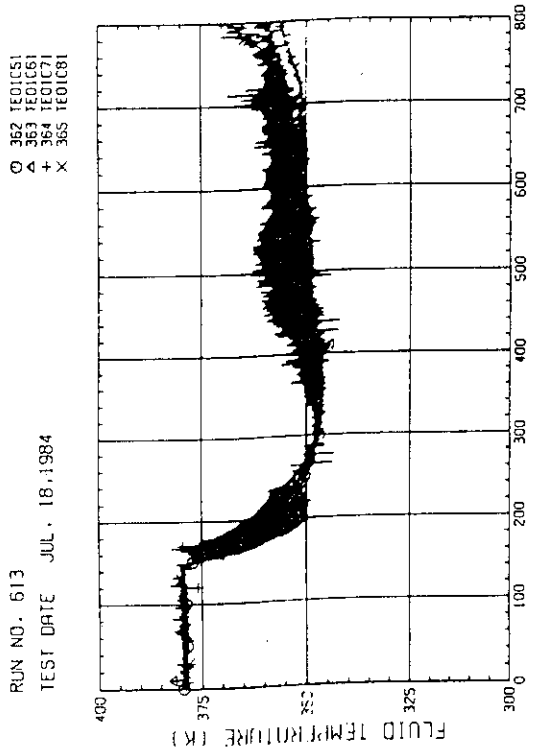

Fig. A－19 FLUID TEMPERATURE AT CORE INLET (BUNDLE 5.6.7.8. 100MM BELOW HEATED PART)

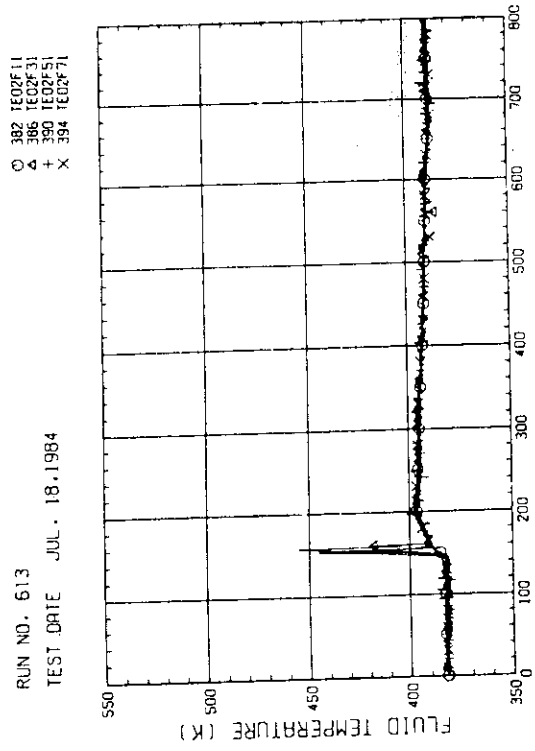

Fig. A－16 FLUID TEMPERATURE JUST ABOVE END BOX TIE PLATE (BUNDLE 1.3.5.7. OPPOSITE SIDE OF COLD LEG. OUTER)

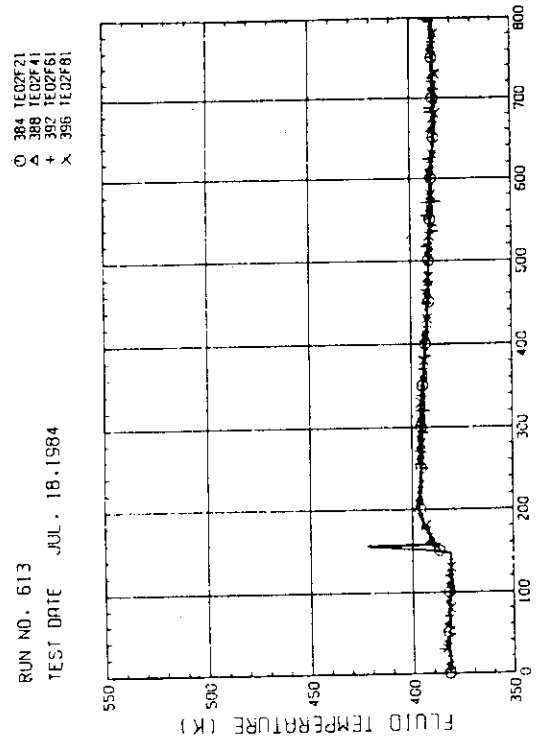

Fig. A－17 FLUID TEMPERATURE JUST ABOVE END BOX TIE PLATE (BUNDLE 2.4.6.8. COLD LEG SIDE. INNER)

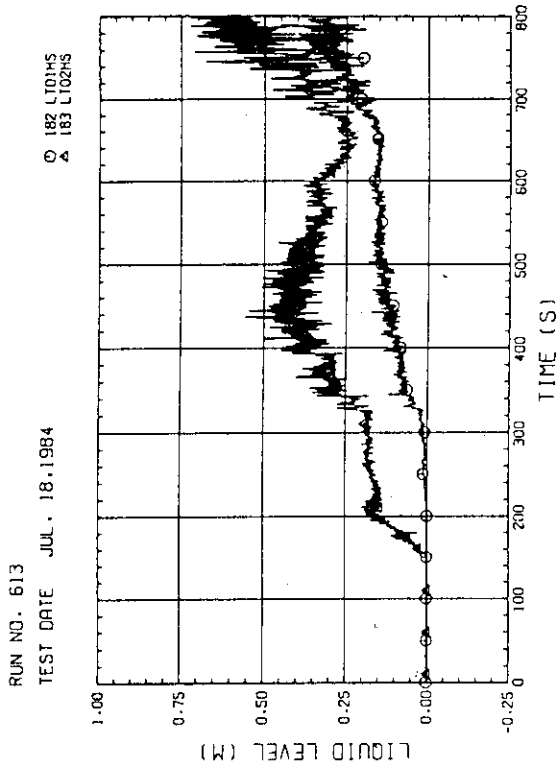

Fig. A－22 LIQUID LEVEL IN HOT LEG
(O1HS - PV SIDE, O2HS - STEAM/WATER SEPARATOR SIDE)

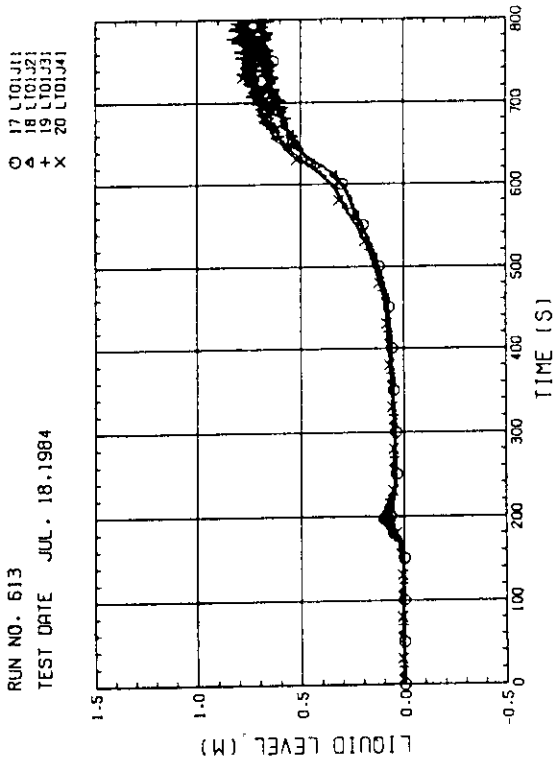

Fig. A－20 LIQUID LEVEL ABOVE UCSP
(BUNDLE 1.2.3.4)

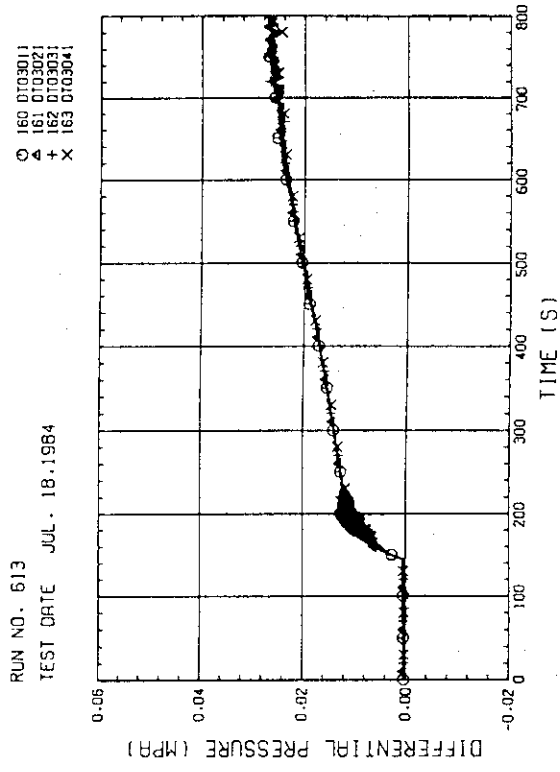

Fig. A－23 DIFFERENTIAL PRESSURE OF CORE FULL HIGHT
(BUNDLE 1.2.3.4)

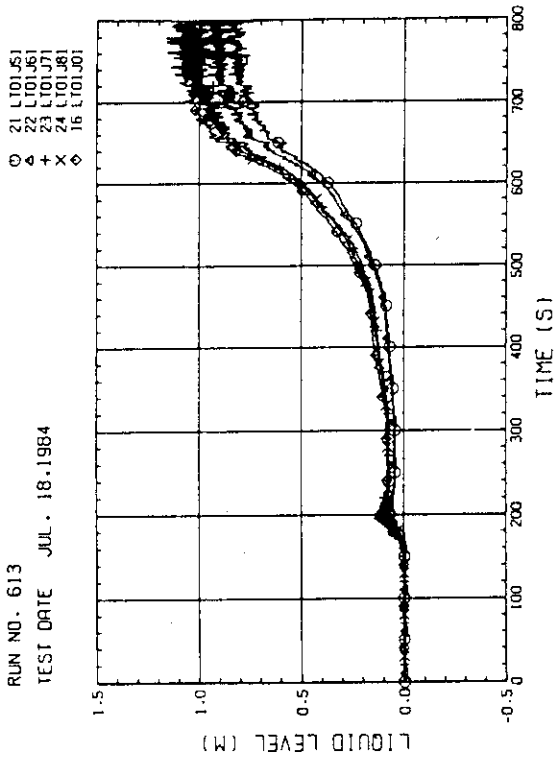

Fig. A－21 LIQUID LEVEL ABOVE UCSP
(BUNDLE 5.6.7.8 AND CORE BAFFLE)

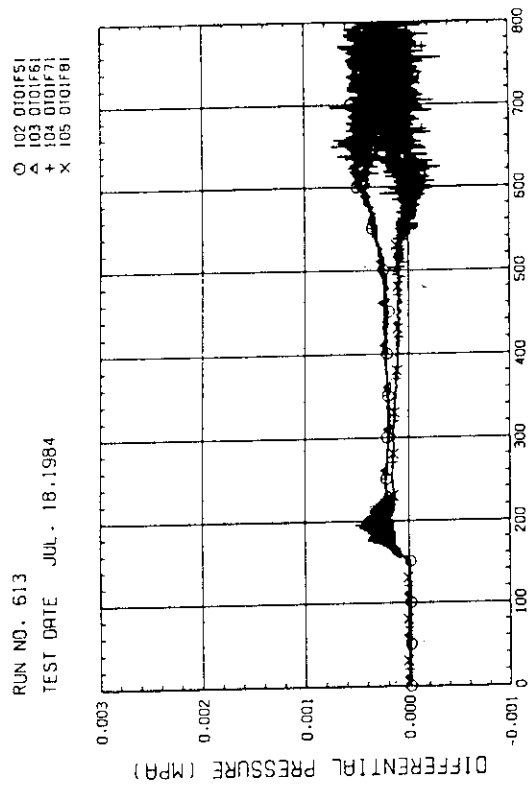

Fig. A－26 DIFFERENTIAL PRESSURE ACROSS END BOX TIE PLATE (BUNDLE 5.6.7.8)

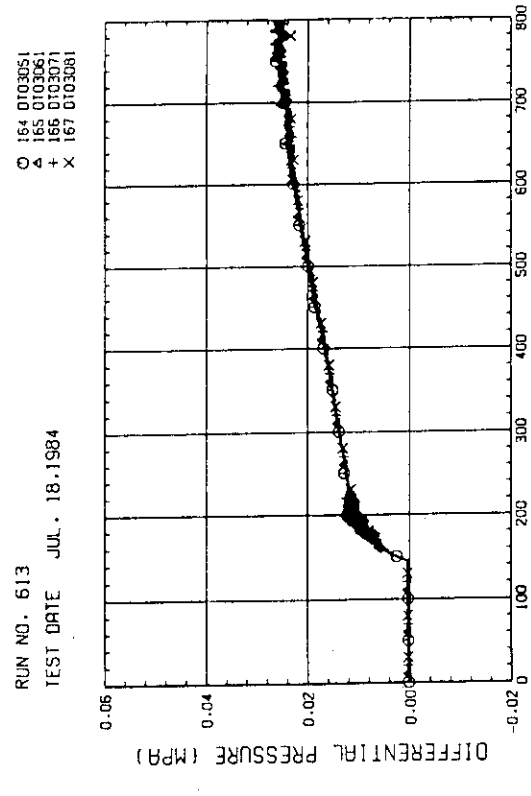

Fig. A－24 DIFFERENTIAL PRESSURE OF CORE FULL HEIGHT (BUNDLE 5.6.7.8)

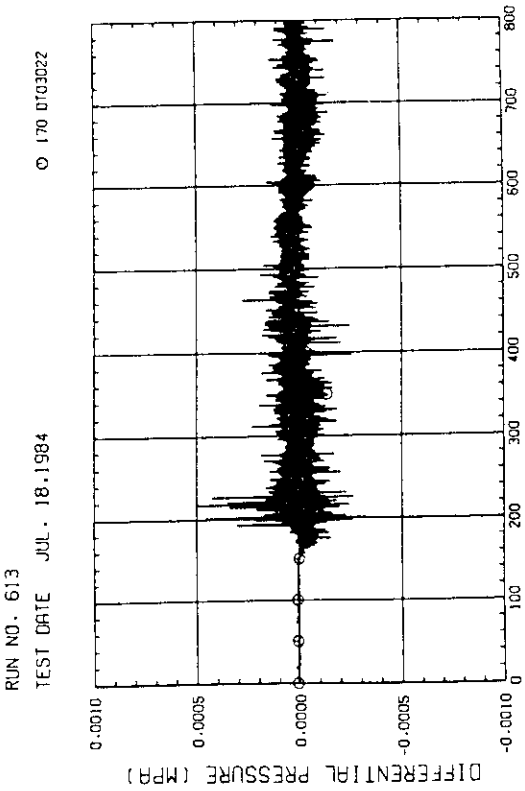

Fig. A－27 DIFFERENTIAL PRESSURE, HORIZONTAL AT 1365 MM (BUNDLE 2-4)

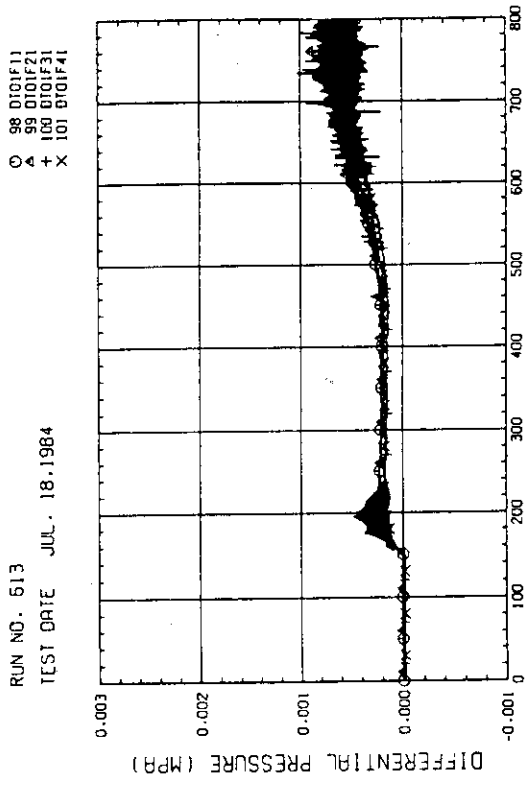

Fig. A－25 DIFFERENTIAL PRESSURE ACROSS END BOX TIE PLATE (BUNDLE 1.2.3.4)

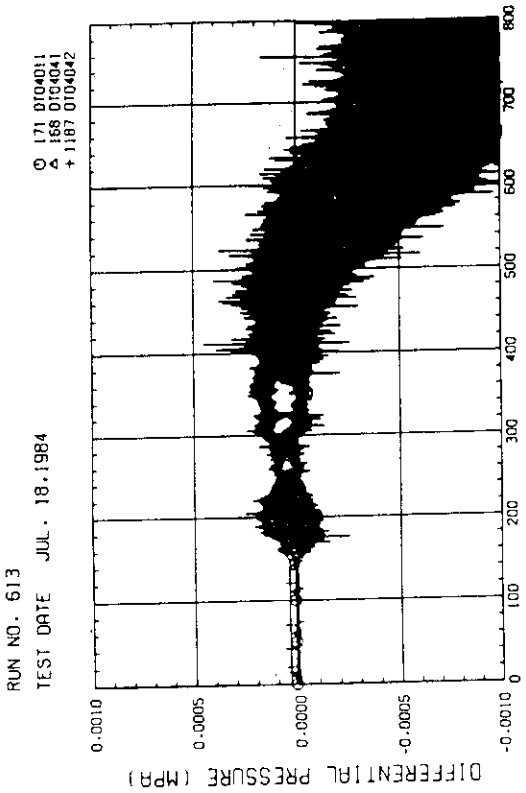

Fig. A－28 DIFFERENTIAL PRESSURE, HORIZONTAL AT 1905 MM
(1)-BUNDLE 1-4, 41-BUNDLE 4-8, 42-BUNDLE 4-6)

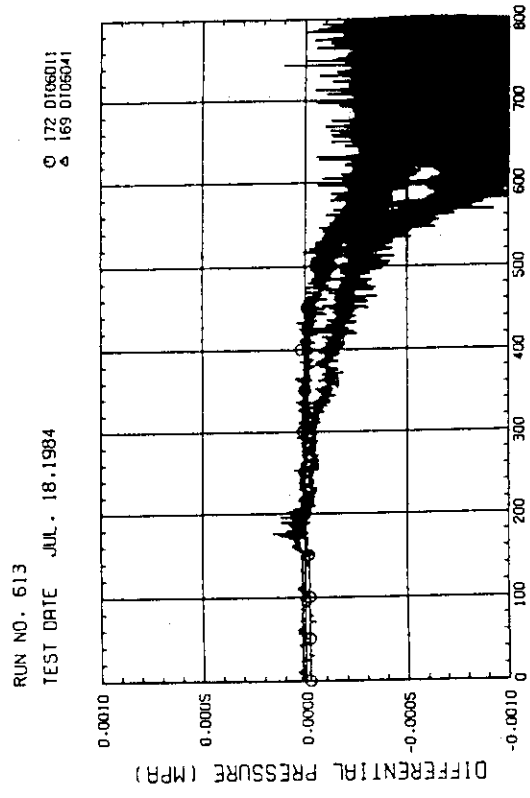

Fig. A－29 DIFFERENTIAL PRESSURE, HORIZONTAL AT 3235 MM
(11-BUNDLE 1-4, 41-BUNDLE 4-8)